DRYING OF LIQUID FOOD DROPLETS
Enzyme Inactivation and Multicomponent Diffusion

Ontvangen

0 9 SEP 1998

UB-CARDEX

Promotoren: dr. ir. K. van 't Riet
hoogleraar in de levensmiddelenproceskunde

dr. ir. P.J.A.M. Kerkhof
hoogleraar in de fysische technologie, Technische Universiteit Eindhoven

G. Meerdink

DRYING OF LIQUID FOOD DROPLETS
Enzyme Inactivation and Multicomponent Diffusion

STELLINGEN

1   Blijkbaar is de fysische juistheid van modellen voor de beschrijving van de droogkinetiek niet altijd relevant, gelet op de positieve conclusies omtrent de geschiktheid van fysisch onjuiste modellen in het kader van geavanceerde procescontrole systemen.

Zaror, C.A. and Pérez-Correa, J.R. (1991). Model based control of centrifugal atomizer spray-drying. Food Control, 2, 170-75.

Clement, K.H., Hallström, A., Dich, H.C., Le, C.M., Mortensen, J. and Thomsen , H.A. (1991). On the dynamic behaviour of spray dryers. Trans IChemE, 69, Part A, 245-52.

2   Het is op z'n minst verbazingwekkend dat Masters in zijn Spray Drying Handbook slechts summiere informatie verstrekt over de droogkinetiek van druppels en evenmin verwijst naar recente-literatuur over dit onderwerp.

Masters, K. (1991). Spray Drying Handbook. Longman Scientific & Technical, Harlow, England.

3   In de meeste hoofdstukken over drogen in studie- en handboeken op het gebied van de (levensmiddelen-) proceskunde is weinig bruikbare informatie over droogkinetiek en drogerontwerp te vinden.

4   In de literatuur worden voor de beschrijving van de droogkinetiek van agrarische produkten veelal de 'thin layer equations' gebruikt. Het in plaats daarvan toepassen van de 'short cut calculation method' zal het fysisch realiteitsgehalte van de geschatte modelparameters sterk verhogen en het inzicht in de optredende transportprocessen vergroten, zonder dat dit leidt tot rekentechnische complicaties.

Coumans, W.J. (1987). Power law diffusion in drying processes. PhD. thesis, Technical University Eindhoven, The Netherlands.

5   In veel studie- en handboeken over moleculaire scheidingsprocessen en fasenevenwichten wordt bij de beschrijving van het fasenevenwicht gebruik gemaakt van het begrip fugaciteit in plaats van chemische potentiaal. Deze gewoonte draagt niet bij tot het vergroten van het inzicht bij de studenten, en is thermodynamisch gezien ook niet noodzakelijk.
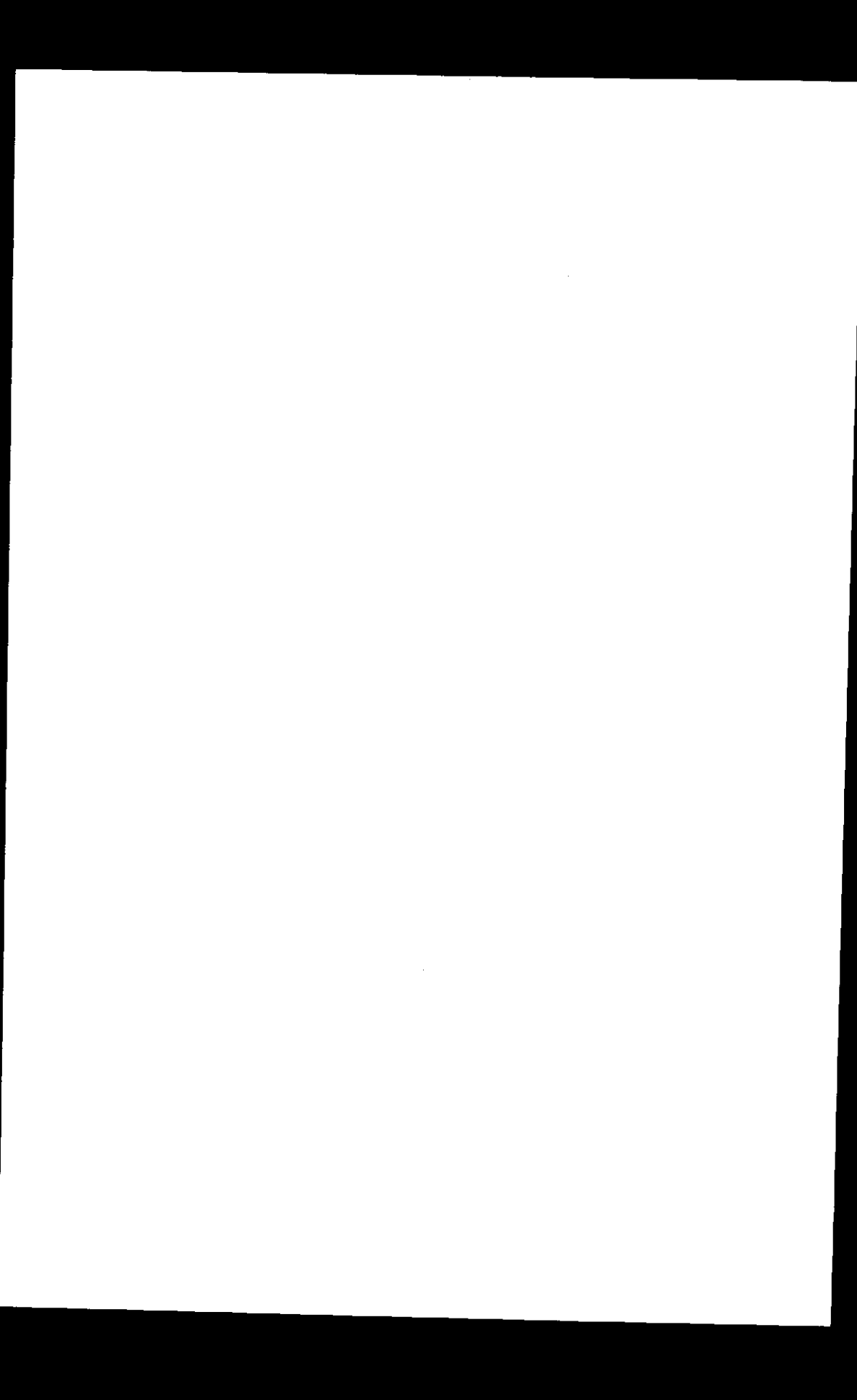
6. Docenten in de procestechnologie zouden zich meer moeten realiseren dat het behandelen van gecompliceerde stofoverdrachtsproblemen weinig zinvol is zolang slechts een beperkt aantal studenten de basisconcepten voor de beschrijving van stofoverdracht werkelijk doorgrondt.

7. Indien de Landbouwuniversiteit blijft vasthouden aan de gedachte dat alle studies in de eerste en tweede fase gelijk van opzet en lengte moeten zijn, zal dat leiden tot een ernstige verzwakking van de positie van de technologische studierichtingen ten opzichte van 'concurrende' opleidingen aan andere universiteiten.

8. Het grote belang dat de centrale beleidsorganen van de Landbouwuniversiteit aan de verbetering van de kwaliteit van de onderwijspraktijk zeggen te hechten, heeft tot nu toe weinig uitwerking gekregen in daadwerkelijk beleid, inclusief de daarbij behorende wijzingen in de verdeling van middelen en mankracht.

9. Het grote aantal onzinnige of verwerpelijke uitspraken en maatregelen als gevolg van de heersende 'law and order' manie is verontrustend.

10. Indien de PvdA blijft vasthouden aan opvattingen omtrent de taak van de overheid die 25-50 jaar geleden nuttig en goed waren, zal zij elke politieke invloed verliezen en vele potentiële kiezers blijvend van zich vervreemden.

Stellingen behorende bij het proefschrift "Drying of liquid food droplets".

G. Meerdink
Wageningen, 22 september 1993
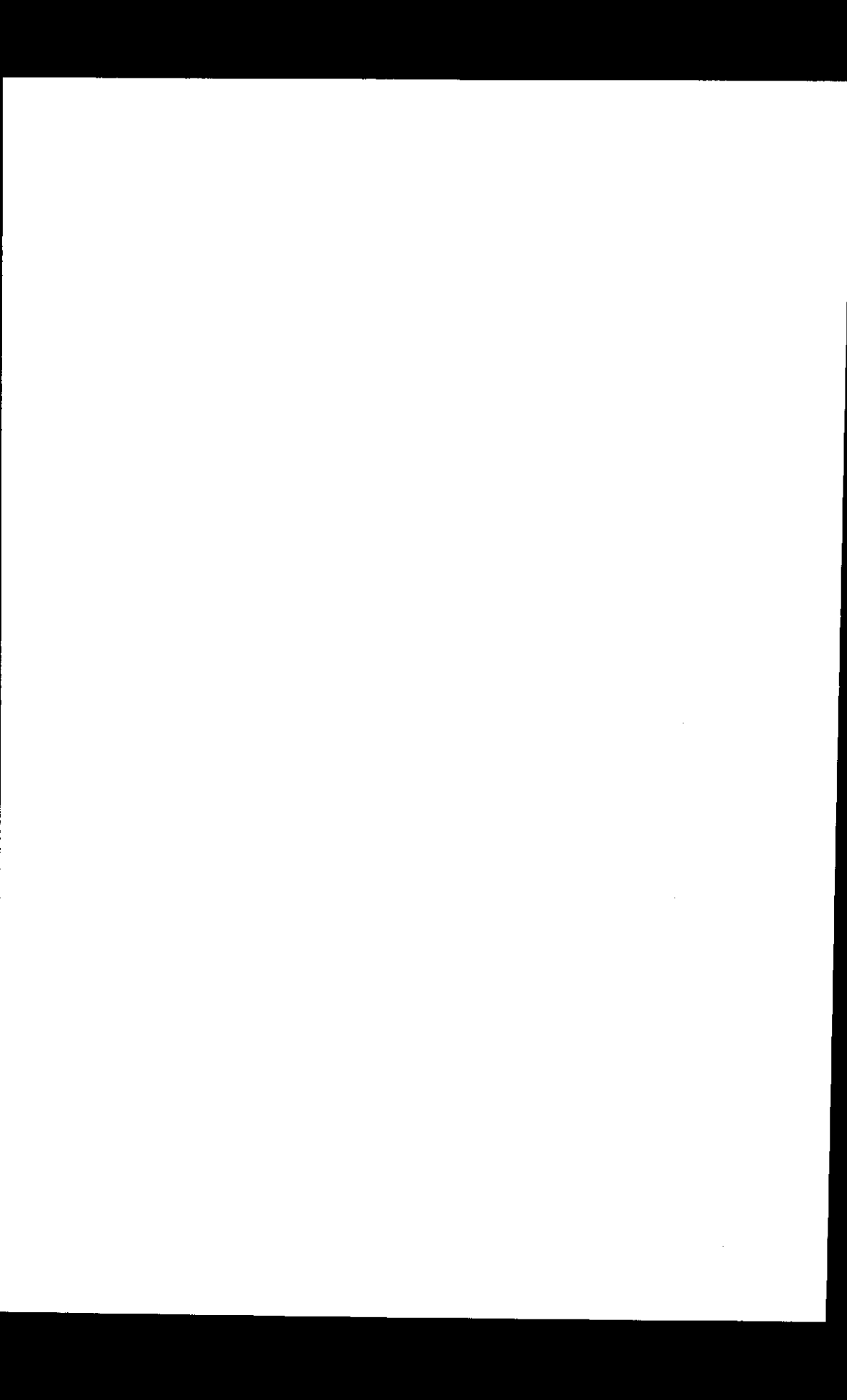
ABSTRACT

In this thesis the drying of liquid food droplets is studied from three different points of view: drying kinetics, enzyme inactivation and multicomponent diffusion. Mathematical models are developed and validated experimentally.

Drying experiments are performed with suspended droplets and with free falling droplets under spray-drying conditions. The experiments with the free falling droplets are performed in a specially designed drying tower using a resonance nozzle. The resonance nozzle is capable of producing equally sized droplets.

Thermal enzyme inactivation kinetics are determined at different water concentrations in separate experiments. The inactivation kinetics can be described by a first order Arrhenius-type model.

A mathematical model based on the binary diffusion equation and the inactivation kinetics is developed that describes the drying kinetics of the droplets as well as the enzyme inactivation. The significance of the spray-air mixing pattern on enzyme inactivation is examined using the developed model.

Slab drying experiments are performed with a ternary food model system. All experiments show that segregation of the dissolved solids can occur. This segregation cannot be described by a binary diffusion equation. Therefore the Maxwell-Stefan multicomponent diffusion equations are applied. Model simulations are used to examine the extent of segregation during spray-drying.
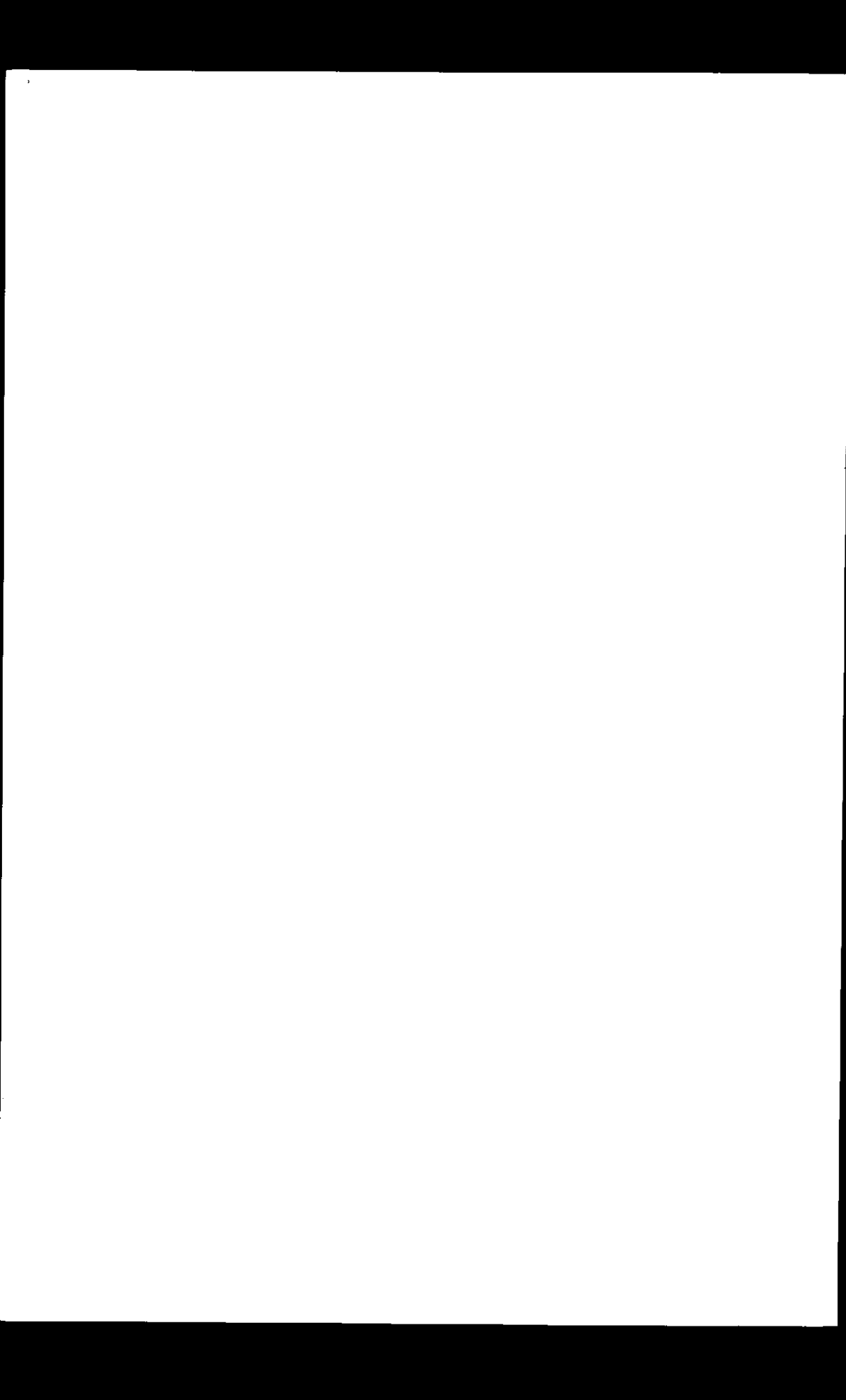
ter herinnering aan mijn vader

VOORWOORD

Het is nu tien jaar geleden dat ik door Klaas van 't Riet bij de Sectie Proceskunde werd aangesteld. Ik heb daar tot nu toe met plezier gewerkt. De Sectie Proceskunde is een leuke groep, terwijl daarnaast het afwisselende karakter van het werk mij zeer aanspreekt. Gedurende deze tijd heeft het nu voorliggende proefschrift langzamerhand zijn vorm en inhoud gekregen. Dit was echter niet gelukt zonder de steun van een aantal mensen die ik met name wil bedanken.

Klaas van 't Riet: de wijze waarop jij je mensen de vrijheid geeft, maar 'sturend' als jij dat noodzakelijk vindt, resulteert in een goed werkklimaat en is tegelijkertijd stimulerend. En wat het onderzoek betreft: je wordt pas 'echt' enthousiast als de experimentele data niet overeenkomen met de (model-) verwachtingen, dan komt een stroom van mogelijke verklaringen en slimme proefjes op gang.

Piet Kerkhof: ik vind het erg leuk dat je nu als promotor bij de afronding van dit onderzoek betrokken bent. Jouw kennis, enthousiasme en inzet hebben een grote rol gespeeld bij de start van het onderzoek en hebben mijn interesse in de procestechnologie vergroot.

Bert Gundlach: zonder jouw bijdrage zou het experimentele werk minder snel en minder goed verlopen zijn. Daarnaast heeft je optimistische en enthousiaste karakter de moed er bij mij en onze studenten in gehouden als het weer eens niet verliep zoals gepland was.

Gerrit Heida: je bent een prima kamergenoot. Het is aan jou te danken dat een computeranalfabeet als ik toch zo nu en dan iets zinnigs uit deze apparaten krijg.

Wim Beverloo: het doet er niet toe met welk proceskundig probleem ik bij je aanklop, steeds ben je bereid om ernaar te luisteren en elke keer lukt het je weer om mij wijzer weg te laten gaan.

Studenten: jullie inzet is op vrijwel elke bladzijde van dit proefschrift terug te vinden. Al is het misschien frustrerend te ontdekken dat het werk van maanden zo nu en dan slechts in

een paar regels is terug te vinden. Dit betekent echter niet dat het daarom minder belangrijk was.

Medewerkers Technische Dienst Biotechnion: ik sta er meestal niet zo bij stil, maar jullie bijdrage aan dit onderzoek in de vorm van tekeningen, apparaten en adviezen, moet toch al gauw meer dan 1 manjaar omvatten, met de droogtoren als opvallendste werkstuk. Mijn dank daarvoor.

Mijn ouders: dit proefschrift is indirect ook een resultaat van jullie voortdurende inzet en betrokkenheid tijdens mijn opleiding en werk.

Verder gaat mijn dank uit naar Dr. ir. T.H.M. Snoeren voor de suggestie om het optreden van segregatie tijdens drogen eens nader te bestuderen; naar Giovanna Ferrari voor het werk aan de droogkinetiek van melkdruppels; naar Anne Hulst en Jan Hunik voor het meedenken over het ontwerp van de resonantie-nozzle; en naar de collega's bij Proceskunde voor de prettige werksfeer en samenwerking.

José, de keuze voor de combinatie van werken, opleiding, krijgen en verzorgen van kinderen, en aandacht voor elkaar blijkt niet altijd gemakkelijk te zijn en is slechts met vallen en opstaan te leren. Toch zou ik het niet anders hebben gewild.

CONTENTS

Chapter 1

GENERAL INTRODUCTION

1.1 MAIN RESEARCH QUESTIONS IN THIS THESIS

Drying is a very important unit operation in the food industry; it is a concentration as well as a preservation method. The obtained dry product has a much longer shelflife at ambient temperature than the original 'fresh' product because of the decreased water activity. Drying processes are designed and operated in such a way that heat deterioration of the dried product is avoided as much as possible, while good rehydration and handling properties are aimed at.

The design and optimisation of drying apparatus is, despite their significance and extensive use, generally still based on qualitative insights in the importance of various drying and product parameters, empirical correlations and practical experience. The design and optimisation is based on 'trial and error' and empirical scale-up experiments. This is caused by the complicated relations between original product properties, drying process conditions and desired dried product characteristics. Moreover, (validated) mathematical drying models based on fundamental drying parameters (e.g. water diffusion coefficients and water sorption isotherms) and product properties (e.g. reaction kinetics of heat labile components) are scarce.

The existence of drying models, describing parts of or the entire drying process, will facilitate design procedures and enhance the possibilities of improving process conditions regarding among other things product quality. Furthermore the number of large-scale experiments will be reduced and the understanding of the results of drying experiments will be improved.

An important group of food materials that are being dried, are liquid foods such as dairy products, fruit juices, and carbohydrate solutions. Liquid foods are commonly dried in spray-dryers, in which the fluid is atomised and small free falling droplets (droplet diameter d_d is 10 - 300 μm) are formed. Spray-dryers are mostly operated in co-current mode to avoid thermal deterioration of the drying products. Spray-dryers are designed and optimised in an 'empirical' way. The development of an 'overall' dryer model is still in its first stage (Kerkhof and Coumans (1990), Lively *et al.* (1992)).

Essential parts of an 'overall' spray-dryer model are a kinetic model of a drying droplet and a model that predicts the final product properties using calculated internal water concentration profiles and droplet temperatures. In recent years droplet drying kinetics models are developed and validated experimentally. However, almost all experimental work on droplet drying kinetics is performed with 'large' suspended droplets ($d_d = 1-10\,\text{mm}$). No studies have been published which deal extensively with the drying kinetics of small free-falling droplets under spray-drying conditions. In a few publications the relations between droplet drying kinetics and product quality are explicitly taken into consideration, but the empirical evidence for the proposed mathematical relations is limited and absent on the level of small free falling droplets.

In almost all (droplet) drying models (liquid) foods are considered as binary systems, with water and dry solids as the two components. Foods are, however, multicomponent systems and as a consequence segregation during drying can occur of the dissolved solids. In the literature no attention is paid to the occurrence and possible consequences of segregation for drying kinetics and product quality.

The starting point of this thesis was the conviction that the kinetics of a drying droplet of liquid food material can be predicted using an existing model and consequently no new model had to be developed. The main questions raised in this thesis are therefore:

1. Is the droplet drying model that is developed and validated for 'large' suspended liquid food droplets, appropriate also for describing the drying kinetics of 'small' free falling droplets under spray-drying conditions?

2. Is it possible to predict a (bio-) chemical product quality change during drying by integrating the droplet drying model with a kinetics model that describes the reaction rate as a function of water concentration and temperature? Or, more specific, can the inactivation of the enzyme α-amylase during drying be predicted?

3. Is it necessary to develop a droplet drying model which takes into account the multicomponent nature of liquid foods? Or, more specific, can segregation of solutes during drying be measured and modelled?

In this thesis the (existing) droplet drying model is adapted and extended to include reaction rates and multicomponent diffusion. The drying experiments and/or model

simulations are performed always on two levels, on the level of 'large' suspended droplets or layers ($d_d \approx 10\,\text{mm}$) and on the level of 'small' free falling droplets ($d_d \approx 0.2\,\text{mm}$) under spray-drying conditions.

1.2 DROPLET DRYING KINETICS

The drying kinetics of liquid food droplets has been studied experimentally and or theoretically by several authors (Ranz and Marshall (1952), Charlesworth and Marshall (1960), Trommelen and Crosby (1970), Kerkhof and Schoeber (1974), van der Lijn (1976), Schoeber (1976), Toei *et al.* (1978), Liou (1982), Sano and Keey (1982), Furuta *et al.* (1985), Yamamoto *et al.* (1985), Coumans (1987)). The proposed models are usually based on the 'effective-diffusivity' concept. In this concept the different internal mass transfer mechanisms are lumped by one parameter, the 'effective' water diffusion coefficient, which is regarded as the controlling factor in the drying process. This effective water diffusion coefficient is in general dependent on water concentration and temperature. In most studies, like in this thesis, it is assumed that no vacuole formation occurs during drying. The influence of vacuole formation on droplet drying kinetics is explicitly considered by Van der Lijn (1976), Wijlhuizen et al. (1979), Sano and Keey (1982), and Kerkhof and Coumans (1990).

The water concentration and temperature dependence of the effective diffusion coefficient can be determined in separate diffusion experiments (Schoeber (1976), Luyben *et al.* (1980), Furuta *et al.* (1984), Coumans (1987), Tong and Lund (1990)). The advantages of this modelling concept compared with other approaches (e.g.: 'curve-fitting' and 'complete modelling') are: the mathematical models obtained are not too complicated, the number of parameters to be determined (or estimated) is limited, the parameters have physical meaning, and water concentration profiles can be calculated. Moreover, water diffusion is the main internal mass transfer process in liquid foods for a large part of the drying process.

Droplet drying experiments, although limited in number, showed in general a good agreement between experimental and simulated drying kinetics (Liou (1982), Sano and Keey (1982), Yamamoto *et al.* (1985), Furuta *et al.* (1985)). Measured diffusion coefficients were used in the simulations. However, in the droplet drying experiments performed in literature, the drying conditions applied are quite different from the circumstances one encounters in a spray-dryer. In particular:

- the applied initial droplet diameter is 1 or 2 orders of magnitude larger than the droplet diameter ($d_d = 10\text{-}300\,\mu\text{m}$) in a spray-dryer.

- the droplets are attached to a support or suspended in an upward directed air stream, instead of free falling.
- the applied drying air temperatures are often lower than the inlet (150-250 °C) and outlet (70-120 °C) temperatures used in spray-drying of liquid foods.
- the initial and final moisture contents are often higher than in spray-drying. In spray-drying of liquid foods these values are 1 à 2 kg H_2O(kg ds)$^{-1}$ and 0.01 à 0.05 kg H_2O(kg ds)$^{-1}$, respectively.
- the air velocities used in the experiments (about 1 ms^{-1}) are much smaller than the initial droplet velocities in a spray-dryer (about 100 ms^{-1}).

As a consequence the initial droplet drying flux in spray-drying is 10^2 - 10^3 times larger than in the experiments with the suspended droplets and the characteristic drying times are 10^4 - 10^6 times smaller.

This means that although there is experimental evidence that the proposed mathematical models are applicable in describing the drying kinetics of single droplets, it is still uncertain if the models are appropriate under spray-drying conditions. This leaves the question whether they can be used in the design or optimisation of spray-drying processes. Validating these models in spray-drying experiments is, however, extremely difficult. This is caused by the non-uniform conditions within the drying chamber, the existence of a droplet size distribution and different droplet trajectories. Furthermore it is very difficult, not to say impossible, to perform controlled experiments in a spray-dryer in such a way that only a single parameter is changed at a time.

In literature a few experiments are described in which the drying behaviour of free falling equally sized (uniform) droplets under relatively constant external drying conditions was studied (Hendricks and Babil (1972), Büttiker (1978), Greenwald (1980), Alexander (1983), El-Sayed (1987), Wallack (1988), Flick *et al.* (1988), El-Sayed *et al.* (1990), and Wallack *et al.* (1990)). The conditions used in these experiments were better comparable with the conditions one finds during spray-drying. A special atomisation device was used in these experiments for the production of uniform droplets. The experiments were, moreover, performed always in a drying tower in which the drying conditions were controlled. In this way problems were avoided related to the drop size distribution and the non-uniformity of the drying conditions during spray-drying as well as to the limitations of experiments with suspended droplets. In table 1.1 an overview of the different studies is presented concerning the products dried, the drying conditions applied and the main aims of the study performed.

Table 1.1 Overview of studies on the drying behaviour of free-falling uniform droplets.

Author(s)	Product(s)	Drying conditions[1]	Aim of the study
Hendricks and Babil (1972)	aqueous and non-aq. inorganic salts, liquid foods and polymers	$d_d = 10 - 40 \mu m$ $T = 25 - 330\ ^\circ C$ $m_{ds} = 0.01 - 10\%$	uniformity and morphology
Büttiker (1978)	aqueous $CaCO_3$ solutions	$d_d = 300 - 800 \mu m$ $T = 190\ ^\circ C$ $m_{ds} = 10 - 55\%$	morphology and drying kinetics
Greenwald (1980)	liquid foods	$d_d = 80 - 240 \mu m$ $T = 30 - 170\ ^\circ C$ $m_{ds} = 10 - 40\%$	morphology
Alexander (1983)	liquid foods	$d_d = 180 - 300 \mu m$ $T = 75 - 275\ ^\circ C$ $m_{ds} = 10 - 40\%$	morphology and surface folding
El-Sayed (1987), El-Sayed *et al.* (1990)	liquid foods	$d_d = 200 - 350 \mu m$ $T = 175 - 225\ ^\circ C$ $m_{ds} = 10 - 40\%$	morphology and drying kinetics
Wallack (1988), Wallack *et al.* (1990)	liquid foods	$d_d = 180 - 250 \mu m$ $T = 100 - 250\ ^\circ C$ $m_{ds} = 30\%$	morphology and drying kinetics
Flick *et al.* (1988)	skim-milk	$d_d = 200 - 400 \mu m$ $T = 80 - 180\ ^\circ C$ $m_{ds} = 24 - 31\%$	morphology and drying kinetics

1) m_{ds} = dry solids content on total basis

Most experiments were performed at the University of California in Berkeley (Greenwald (1980), Alexander (1983), El-Sayed (1987), Wallack (1988), El-Sayed *et al.* (1990), Wallack *et al.* (1990)). At this university a small drying tower (diameter ≈ 0.08 m, length ≈ 2.5 m) was build and different droplet producing devices were used. Different liquid foods were studied in the experiments. Most experiments were performed at high drying air temperatures ($T_g \approx 175\ ^\circ C$). In almost all studies listed in table 1.1, mainly changes were

investigated in the morphology of the product. From table 1.1 it can be seen that there have been four (limited) attempts to determine the drying kinetics of the falling droplets and to compare experimental results with model simulations. Agreement between experiments and simulations was found only for the constant drying rate period (Büttiker (1978), El-Sayed (1987), Wallack (1988), El-Sayed *et al.* (1990), Wallack *et al.* (1990)) or in the onset of the falling drying rate period (Flick *et al.* (1988)). This is due to the complicated drying behaviour of the products studied (Büttiker (1978), El-Sayed (1987), Wallack (1988), El-Sayed *et al.* (1990), Wallack *et al.* (1990)) or to the limited length of the drying tower used by Flick *et al.* (1988). The drying air temperatures used by El-Sayed (1987), Wallack (1988), El-Sayed *et al.* (1990), and Wallack *et al.* (1990) were high (T ≈ 175 °C) and as a result water vapour bubbles were formed after a certain drying time and expansion of the droplets occurred. Moreover considerable axial air temperature gradients existed in the drying tower.

It can be concluded that, although some attempts have been made, the drying kinetics of 'small' free falling (liquid food) droplets is not yet studied in detail. Experimental evidence of the appropriateness of drying models, based on the 'effective-diffusivity' concept, is still lacking for spray-drying calculations.

The objectives of the drying experiments with the suspended droplets are:
- to validate the kinetics model for droplet drying before the experiments with the 'small' free falling droplets are started.
- to develop a validated model which can be used as starting point for the study on enzyme inactivation during drying.

The objective of the experiments with the free falling droplets is:
- to validate the developed droplet drying model under spray-drying conditions, without using a spray-dryer.

1.3 INACTIVATION OF α - AMYLASE DURING DRYING

Drying can profoundly alter the quality of a dried product after rehydration. In the literature numerous articles are published measuring and discussing the quality of dried products in relation to initial product qualities and applied drying process conditions. But in almost all these articles the drying process itself is considered as a 'black box' and no explicit mathematical models are developed in which the drying kinetics are related with changes in

(bio-) chemical or mechanical properties of the dried product. Consequently, the knowledge and understanding of the relations between drying conditions and product quality is at most of a qualitative character. Above that possibilities are limited of applying the obtained results in the design and optimisation of drying processes.

In this thesis the inactivation of enzymes, or more specific of α-amylase, during drying is studied as an interesting example of a biochemical quality parameter. Drying can significantly reduce the activity of enzymes after rehydration. This reduction is determined by the enzyme characteristics and by the drying process conditions. The determination of the optimal drying conditions is an important prerequisite for the successful production of active dried enzymes or alternatively, to inactivate the enzymes to avoid enzymatic deterioration of dried foods during storage or after rehydration.

In the literature there are only a few publications dealing systematically with the theoretical and/or experimental aspects of the inactivation behaviour of enzymes during drying. Almost no information is available describing the inactivation kinetics at water concentrations as low as found in drying processes. Kerkhof and Schoeber (1974), Wijlhuizen *et al.* (1979), Luyben *et al.* (1982) and Kerkhof and Coumans (1990) have described the inactivation of enzymes during (spray-) drying theoretically. The inactivation kinetics used were based on sparse literature data, mainly from Verhey (1973), Daemen (1981, 1983) and Daemen and Van der Stege (1982), who studied experimentally the inactivation behaviour of several enzymes during the spray-drying of milk. The inactivation of enzymes in single droplets was studied theoretically and experimentally by Liou (1982) and Yamamoto *et al.* (1985, 1992). They found a good agreement between inactivation experiments and drying model simulations. Zimmerman (1987) modelled the inactivation of intra-cellular enzymes during fluidized bed drying of yeast and verified the model experimentally. However, the appropriateness of the drying kinetics model as applied by Zimmerman (1987), namely a shrinking core model, is disputable.

The objectives of the drying experiments with the suspended droplets are:
- to measure and model the inactivation kinetics of the enzyme α-amylase.
- to model the enzyme inactivation in a drying droplet and to validate the model with drying experiments. The integration of experimentally determined inactivation kinetics and drying parameters should result in an overall model.

The objective of the drying experiments with the free falling droplets is:
- to test the developed enzyme inactivation model under spray-drying conditions.

1.4 SEGREGATION OF SOLUTE MATERIAL DURING DRYING

Liquid foods consist of many solutes, which have widely different diffusivities. The values of the binary diffusion coefficients in dilute aqueous solutions can vary at least two orders of magnitude for low and high molecular weight components, respectively. During drying the concentration gradients originating from the water transport will induce mass transport of the (non-volatile) solutes in opposite direction. The transport velocities of the different solutes depend on the values of their diffusion coefficients. Given the large difference in these coefficients, it can be expected that segregation of components can occur during drying. At the surface the concentration of components with a low diffusivity will be relatively high as compared with the concentration of components with a high diffusivity. In the centre the reversed situation will exist. This phenomenon is neglected in the binary approach of drying kinetics.

The extent of this segregation will depend on the difference in the component diffusivities, the initial water concentration and the drying process conditions. The product quality will be influenced dependent on the extent of this segregation, in particular the surface properties. Considering the fact that liquid foods are mostly dried in spray-dryers, segregation can influence powder characteristics in this way.

In literature on drying, very little attention is paid to segregation of non-aqueous components and relevant information is almost non-existing. An important exception is the retention of volatile aroma components during drying of foods (Chandrasekaran and King (1972a, b), Kerkhof (1975), Riede and Schlünder (1988)). A few fundamental studies are reported on dilute non-electrolyte ternary mixtures in water (Dunlop and Gosting (1957), Dunlop and Gosting (1964), Ellerton and Dunlop (1967)). In these studies multicomponent diffusion coefficients were measured at high water concentrations, using solutes with a low molecular weight.

The objectives of the drying experiments are:
- to measure if segregation occurs during drying of liquid foods.
- to develop a drying model which describes the measured segregation.

The objective of the model simulations is:
- to evaluate the extent of segregation during spray-drying.

1.5 OUTLINE OF THE THESIS

In figure 1.1 the coherence and outline of this thesis is shown.

Chapter 2 describes the droplet drying kinetics model and the drying kinetics experiments with the suspended and free falling droplets. The experimental drying kinetics are compared with model simulations.

Chapter 3 deals with the modelling and measurement of the thermal enzyme inactivation kinetics and the coupling of these kinetics to the drying model as described in chapter 2. The experimental enzyme inactivation during drying is compared with model simulations.

Chapter 4 describes the developed ternary drying model and the measurement of segregation during drying. The experimental concentration profiles are compared with model simulations.

Chapter 5 discusses the influence of the spray-air mixing pattern on enzyme inactivation, the significance of measured inactivation constants for spray-drying calculations and the extent of segregation during spray-drying.
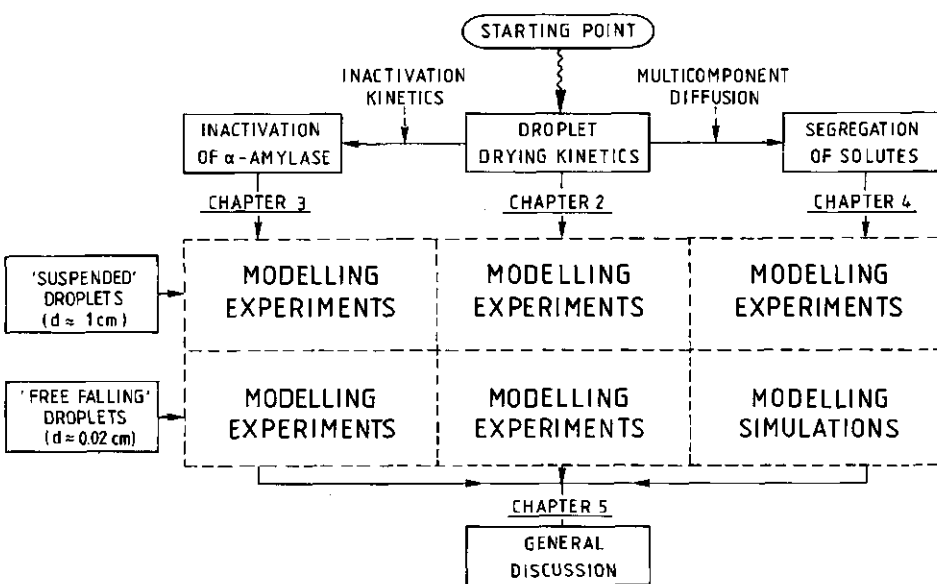

Figure 1.1 Outline of this thesis

Chapter 2

DROPLET DRYING KINETICS

2.1 INTRODUCTION

In this chapter the applied droplet drying kinetics model and the results of the droplet drying experiments are described. The experimental data are compared with model predictions. The experiments with the suspended droplets ($d_d \approx 1 \text{cm}$) and the experiments with the free falling droplets ($d_d \approx 0.02 \text{cm}$) are discussed separately.

In the suspended droplet experiments a wider range of initial moisture contents is used, than is applied in the studies described in literature (Liou (1982), Sano and Keey (1982), Yamamoto *et al.* (1985), Furuta *et al.* (1985)).

The experiments with the free falling droplets are performed in a specially designed drying apparatus. This equipment consists of two main parts: the resonance nozzle and the drying tower. The resonance nozzle is capable of producing equally sized (uniform) droplets. The drying tower is designed in a such way that the drying conditions are uniform and comparable with spray-drying conditions.

In the drying experiments maltodextrin solutions and skim-milk are used.

2.2 THEORETICAL MODEL

The drying model is based on the 'effective' water diffusivity concept (see chapter 1.2). The model consists of three main equations. Water concentration profiles inside a droplet are calculated by solving the unsteady state diffusion equation for binary systems. A heat balance gives the droplet temperature during the drying process. The droplet trajectory is calculated by using a momentum balance. Major assumptions regarding the drying behaviour of a droplet are: the droplet is and remains perfectly spherical, the change in volume of the droplet corresponds to the volume of water evaporated ('ideal shrinkage') and no vacuole formation occurs during drying.

- Diffusion equation

The internal transport of water in a shrinking, drying droplet can be described by means of the following diffusion equation:

$$\frac{\partial C_w}{\partial t} = \frac{1}{r^2} \frac{\partial}{\partial r}\left[r^2 D_w(C_w, T) \frac{\partial C_w}{\partial r} \right]$$
(2.1)

where C_w is the water concentration, t is the drying time, r is the space co-ordinate, D_w is the water diffusion coefficient, and T is the temperature.

The initial and boundary conditions are:

$$t = 0 \qquad 0 \le r \le R_{d,0} \qquad C_w = C_{w,0}$$
(2.2)

$$t > 0 \qquad r = 0 \qquad \frac{dC_w}{dr} = 0$$
(2.3)

$$t > 0 \qquad r = R_{d,t} \qquad \frac{-D_w \dfrac{dC_w}{dr}}{1 - C_w V_w} = k_{g,eff} \left(\rho_{w,i} - \rho_{w,b} \right)$$
(2.4)

where R_d is the droplet radius, V_w is the partial volume of water, $k_{g,eff}$ is the effective external mass transfer coefficient, ρ_w is the gas phase water concentration, and the subscripts 0, t, i and b denote initial, drying time, interface and bulk phase, respectively. The boundary condition 2.4 gives the water flux with respect to the receding external surface. The equilibrium relation between the internal and external water concentration at the surface is given by the water sorption isotherm. The effective external mass transfer coefficient $k_{g,eff}$ is the external mass transfer coefficient k_g corrected for Stefan-diffusion, because a net mass flow exists in the gas phase. Through the interface there is an outward directed moisture flux, but no opposite air flux. The external mass transfer coefficient k_g is calculated from the correlation of Ranz and Marshall (1952):

$$Sh = 2 + 0.6 Re^{0.5} Sc^{0.33}$$
(2.5)

where Sh, Re and Sc are the Sherwood, Reynolds and Schmidt number, respectively.

- Heat balance

The heat balance is based on the assumption that there is no temperature gradient within the droplet, because the characteristic time for internal heat transfer is much smaller than for internal mass transfer. In addition, the Biot number Bi for heat transfer is small (suspended droplets: $Bi \approx 0.5$, free falling droplets: $Bi \approx 0.1$). Moreover a part of the heat transferred to the surface is used immediately for the evaporation of water. Accordingly, the heat balance equation becomes:

$$\frac{1}{3} R_{d,t} c_{p,d} \rho_d \frac{dT_d}{dt} = \alpha_{g,eff} \left(T_{g,b} - T_d \right) - k_{g,eff} \left(\rho_{w,i} - \rho_{w,b} \right) \Delta H_v \tag{2.6}$$

where $c_{p,d}$ is the specific heat, ρ_d is the droplet mass density, $\alpha_{g,eff}$ is the effective external heat transfer coefficient, ΔH_v is the heat of evaporation at the temperature of the droplet, and the subscripts d and g denote droplet and gas phase, respectively. The heat balance equation correlates the droplet temperature change with the difference between the heat transferred by convection and that needed for evaporation. The effective external heat transfer coefficient $\alpha_{g,eff}$ is the external heat transfer coefficient α_g corrected for the uni-directional mass transport in the gas phase. The external heat transfer coefficient α_g is calculated applying the heat transfer analogue of equation 2.5:

$$Nu = 2 + 0.6 \, Re^{0.5} \, Pr^{0.33} \tag{2.7}$$

where Nu and Pr are the Nusselt and Prandtl number, respectively.

- Momentum balance

Important assumptions regarding the falling behaviour are: the droplet moves in vertical direction only, the falling behaviour of the droplet is not influenced by the presence of other droplets and the droplet behaves as a rigid sphere. The momentum balance becomes then:

$$\frac{dv_d}{dt} = \left(\frac{\rho_d - \rho_g}{\rho_d}\right) g - \frac{3}{8} \frac{C_d \rho_g \left(v_d - v_g\right)^2}{\rho_d R_d} \tag{2.8}$$

where v is the velocity, g is the gravity constant and C_d the drag coefficient. The drag coefficient is calculated by the next expressions (Bird *et al.* (1960)):

$$Re \leq 2 \qquad\qquad C_d = \frac{24}{Re} \tag{2.9}$$

$$2 < Re < 500 \qquad\qquad C_d = \frac{18.5}{Re^{0.6}} \tag{2.10}$$

$$Re \geq 500 \qquad\qquad C_d = 0.44 \tag{2.11}$$

- Numerical solution

The set of differential equations 2.1, 2.6 and 2.8 is solved by an implicit difference technique taking unequal space and time intervals. Because of the moving outer boundary of the droplet, the diffusion equation 2.1 and the initial and boundary conditions 2.2, 2.3 and 2.4 are transformed applying a dissolved solids centred space co-ordinate. In this way the movement of the external interface through the space co-ordinate grid is avoided. The transformed space co-ordinate is defined as:

$$\sigma = \int_0^r C_{ds} r^2 \, dr \tag{2.12}$$

where σ is the transformed space co-ordinate and C_{ds} is the dissolved solids concentration. The water concentration in the transformed co-ordinate system is defined as:

$$u_w = \frac{C_w}{C_{ds}} \tag{2.13}$$

where u_w is the transformed water concentration. The transformed diffusion equation has a form similar to equation 2.1. The computer program used is an adapted and extended version of the programs developed by Van der Lijn (1976) and Wijlhuizen *et al.* (1979).

- *Physical data*

The physical data used in the simulations are given in the tables 2.1 (skim-milk) and 2.2 (maltodextrin). The water sorption isotherm of skim-milk and the temperature dependence of the isotherm are based on data given by Walstra and Jennes (1984). The concentration and temperature dependence of the water diffusion coefficient in skim-milk are based on data obtained by Ferrari *et al.* (1989). The concentration and temperature dependence of the diffusion coefficient was measured in a water concentration range from 0.25 - 0.8 kg H_2O(kg ds)$^{-1}$ and for temperatures from 30 - 70 °C.

The water sorption isotherm of maltodextrin and the water concentration and temperature dependence of the water diffusion coefficient in maltodextrin are based on the data obtained by Furuta *et al.* (1984). They present diffusion data for water concentrations from 0.1 - 9 kg H_2O(kg ds)$^{-1}$ and for a temperature range of 25 - 45 °C. The temperature dependence of the water sorption isotherm is neglected. The maltodextrin used by Furuta *et*

Table 2.1. Physical data skim-milk

Skim-milk solids density	1470 kg m^{-3}
Specific heat of skim-milk solids	$1790 \text{ J kg}^{-1} \text{ K}^{-1}$
Sorption isotherm of skim-milk at $T = 293\text{K}$	$\omega_w < 0.125 \qquad a_w = 5.6\,\omega_w$ $\omega_w > 0.125 \qquad a_w = \exp\!\left(-0.0028/\omega_w^{2.34}\right)$
Temperature dependence of the sorption isotherm	$a_{w,T} = a_{w,293} \exp\!\left[-\dfrac{E_{a,w}}{R}\left(\dfrac{1}{T}-\dfrac{1}{293}\right)\right]$ $E_{a,w} = 33860 \exp\!\left(-22.38\,\omega_w\right) \text{ J mol}^{-1}$
Diffusion coefficient of water in skim-milk at $T = 323\text{K}$	$D_{w,323} = \exp\!\left[-\dfrac{82.50 + 1700\,\omega_w}{1+79.61\omega_w}\right] \text{ m}^2 \text{ s}^{-1}$
Temperature dependence of the water diffusion coefficient	$D_{w,T} = D_{w,323} \exp\!\left[-\dfrac{E_{a,w}}{R}\left(\dfrac{1}{T}-\dfrac{1}{323}\right)\right] \text{ m}^2 \text{ s}^{-1}$ $E_{a,w} = 139000 \exp\!\left(-3.32\,\omega_w\right) \text{ J mol}^{-1}$

al. (1984) has the same Dextrose Equivalent value as the maltodextrin used in the experiments reported here.

Table 2.2. Physical data maltodextrin

Maltodextrin density	1600 kg m^{-3}
Specific heat of maltodextrin	$1500 \text{ J kg}^{-1} \text{ K}^{-1}$
Sorption isotherm of maltodextrin	$\omega_w > 0.35 \qquad a_w = 1$ $\omega_w < 0.35 \qquad a_w = \sum\limits_{n=1}^{5} e_n m_w$ $e_1 = 5.38828 \qquad e_2 = 20.6498 \qquad e_3 = -197.015$ $e_4 = 443.880 \qquad e_5 = -315.853$
Diffusion coefficient of water in skim-milk at $T = 308 \text{ K}$	$D_{w,308} = 10^{\sum\limits_{n=1}^{9} a_n (1-m_w)^{n-1}} \quad 10^{-4} \text{ m}^2 \text{ s}^{-1}$ $a_1 = -5.62029 \qquad a_2 = 3.75424 \qquad a_3 = -86.5335$ $a_4 = 704.872 \qquad a_5 = -2853.10 \qquad a_6 = 6354.49$ $a_7 = -7952.04 \qquad a_8 = 5245.81 \qquad a_9 = -1424.05$
Temperature dependence of the water diffusion coefficient	$D_{w,T} = D_{w,308} \exp\left[-\dfrac{E_{a,w}}{R}\left(\dfrac{1}{T} - \dfrac{1}{308}\right) \right] \text{ m}^2 \text{ s}^{-1}$
Moisture dependence of the activation energy (Furuta et *al.* (1984))	$E_{a,w} = 4200 \sum\limits_{n=1}^{6} c_n (1-m_w)^{n-1} \text{ J mol}^{-1}$ $c_1 = 3.32582 \qquad c_2 = -15.8667 \qquad c_3 = 151.217$ $c_4 = -443.608 \qquad c_5 = 481.664 \qquad c_6 = -146.387$
Adapted relation for the moisture dependence of the activation energy	$E_{a,w} = 75000 \exp(-6\,\omega_w) + 25000 \text{ J mol}^{-1}$

2.3 MATERIALS AND METHODS

2.3.1 Suspended droplets

- *Skim-milk*

The drying experiments were performed in a laboratory-scale fluid-bed dryer (PRL Engineering Ltd., UK). The droplets were placed in the dryer on a perforated tray ($\varnothing = 10$ cm). In a drying experiment about 20 droplets were dried simultaneously. The air temperature and velocity were controlled and kept constant during an experiment. Ambient air was used as drying medium. The air velocity used (0.7 ms^{-1}) was below the terminal falling velocity of the droplets (10 ms^{-1}), consequently the droplets were not fluidized. The droplets to be dried consisted of jellified spheres (agar (Merck), 0.5 % on total basis) of concentrated skim-milk with an initial moisture content of 4.5 kg H_2O(kg ds)$^{-1}$ and an initial diameter of 1 cm. The droplets were produced using a perspex mould. The water content of the droplets was determined by weighing the droplets before and after the drying experiment. At different time intervals a sphere was taken from the dryer and weighted. The drying experiments were performed at 55, 75 and 95 °C.

- *Maltodextrin*

The drying experiments were performed in a vertical tube ($\varnothing = 12$ cm), which was connected with a drying apparatus (Kiekens nv., The Netherlands). In the tube about 10 droplets were dried simultaneously. The droplets were distributed over the cross-sectional area of the tube. One of the droplets was attached to a thin thermocouple, the others to cotton strings. The air flow in the tube had a downward direction. The air temperature and velocity were controlled and kept constant during an experiment. Dried air was used as drying medium. The droplets to be dried consisted of jellified spheres (agar (Merck), 2 % on total basis) of maltodextrin solutions (MOR-SWEET 01921, DE 20-22, Cerestar) with different initial moisture contents. The droplets were produced by using a perspex mould with a diameter of 1 cm. For the drying experiment with an initial moisture content of 0.47 kg H_2O(kg ds)$^{-1}$ the droplets were pre-dried. The initial diameter was 0.86 cm in that experiment. The water content of the droplets was determined by weighing the droplets before and after the drying experiment. A droplet was removed at different times and the weight was determined. The change in the droplet temperature during the drying process was followed with the inserted thermocouple.

In the drying experiments, the initial water content varied between 3.0 and 0.47 kg H_2O(kg ds)$^{-1}$. The temperature of the drying air varied between 97 and 105 °C and the air

velocity was 2.5 ms^{-1}. Higher drying temperatures gave practical problems such as crust formation, loss of the spherical shape of the droplets, vacuole formation and boiling phenomena.

2.3.2. Free falling droplets

2.3.2.1. Drying equipment

- *Resonance nozzle*

In the resonance nozzle a laminar liquid jet is broken up in uniform droplets by applying a controlled external sinusoidal disturbance (Hulst *et al.* (1985), Hunik and Tramper (1992)). In figure 2.1 a schematic representation of the resonance nozzle is depicted. The membrane is connected by means of the pin with an electromagnetic vibration exciter (Bruel & Kjaer). The charged electrode is meant for charging of the droplets to avoid coalescence of the droplets. Moreover it causes the formation of a droplet spray inside the drying tower, instead of a very narrow 'droplet jet'. This spray enhances the uniformity of the droplet drying conditions.

The break-up of a laminar jet in equally sized droplets is described for non-viscous liquids by Rayleigh and for viscous newtonian liquids by Weber (Lefebvre (1988)). Weber (Lefebvre (1988)) has developed a relation to calculate the optimal frequency of the sinusoidal disturbance for newtonian liquids, which contains the density, viscosity and surface tension of the liquid as well as the jet velocity and the diameter of the nozzle orifice. The droplet diameter can be calculated by adding a mass balance equation, resulting in equation 2.14.

$$d_d = \left(\frac{6 \Phi_m}{\pi f \rho_d} \right)^{\frac{1}{3}} \tag{2.14}$$

where Φ_m is the mass flow and f is the frequency of the sinusoidal disturbance. In the experiments nozzle orifice diameters d_n of 80 µm, 88 µm and 103 µm were used. The mass flow Φ_m was always 8.3 10^{-5} kgs^{-1}, resulting in jet velocities v_j of respectively 14.1 ms^{-1} (d_n = 80 µm), 11.7 ms^{-1} (d_n = 88 µm) and 8.5 ms^{-1} (d_n = 103 µm) for a maltodextrin

solution with a moisture content of 1.5 kg $H_2O(kg\ ds)^{-1}$. The applied frequencies were 34400 Hz (d_n = 80 µm) and 16000 Hz (d_n = 88, 103 µm), respectively. The frequencies used with the nozzle orifices of 80 µm and 103 µm are equal to the optimal frequency. The frequency used with a nozzle orifice of 88 µm is smaller than the optimal frequency of 25600 Hz, but also at this frequency uniform droplets were produced. The calculated droplet diameters at these frequencies are 158 µm (34400 Hz) and 204 µm (16000 Hz). Droplet diameters were determined using a measuring microscope (Zeiss). The voltage on the charging electrode varied between 50 and 150 V depending on the nozzle orifice diameter, the applied frequency, the distance between resonance nozzle and charging electrode, the desired spray-angle (higher voltages resulted in larger spray-angles), and the moisture concentration of the solution.
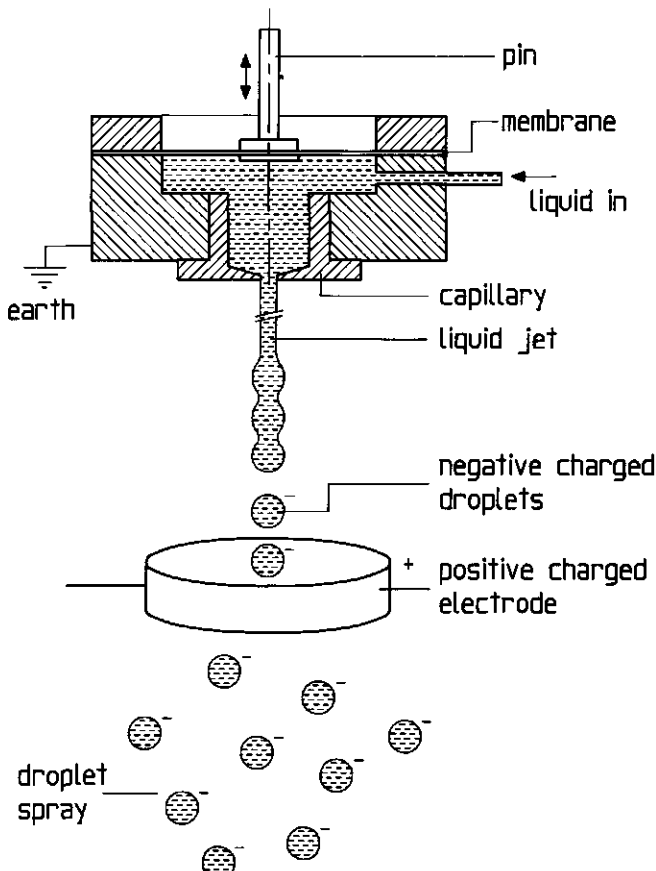

Figure 2.1   Schematic representation of the resonance nozzle.

- *Drying tower*

The drying tower is depicted in figure 2.2. The height of the tower is 6 m and the diameter 0.63 m. The tower is insulated and electrical heating cables are applied to prevent axial temperature gradients. The aim of the sieve plate is to reduce the development of radial velocity profiles. Ambient air was used as drying medium. The drying air was heated directly by means of a natural gas burner. At different heights in the drying tower, sample ports ($\varnothing$ = 10 cm) are present through which samples could be taken. The average air velocity in the tower was 0.2 ms^{-1} in the drying experiments. The value of the Reynolds number is, accordingly, about 6500, indicating the presence of a turbulent flow pattern. Air temperature and velocity were kept constant during a drying experiment.

Axial and radial air temperature and velocity profiles were measured in an 'empty' drying tower using thermocouples and a heat wire anemometer (Alnor), respectively. The air velocity measurements were performed at ambient temperatures.

In the experiments an excess of drying air was used to ensure the uniformity of the drying conditions. As a result there is only a small increase of the air humidity (about 1 g H$_2$O(kg da)$^{-1}$) and a small decrease of the drying air temperature (about 2 °C), assuming that the drying process is performed under adiabatic conditions. These changes are about 50 times smaller than in actual spray-drying processes. The outlet relative humidity was always less than 10%.

2.3.2.2 Drying experiments

- *Determination of the droplet drying kinetics*

The drying kinetics of the droplets was determined by collecting droplets at different sample ports. The samples were taken in the centre of the drying tower. The droplets were catched in a water cooled sample holder ($\varnothing$ = 7 cm, T $\approx$ 35 °C) filled with paraffin oil (Merck, art. 1760). Dependent on the height of the sample port, the sample time varied from 1 - 2 min at the top up to 30 - 45 min at the bottom as a result of the decreasing spray droplet density. The sample size ranged for the same reason from about 1 g at the top down to about 0.1 g at the bottom. The moisture content of the droplets was determined using a vacuum-dryer. The droplets did coalesce in the sample holder to one droplet at high moisture contents. This droplet could be removed with a injection needle. At lower moisture contents the droplets were too viscous to coalesce, the paraffin oil was then removed by decanting followed by rinsing with a small amount of petroleum ether.
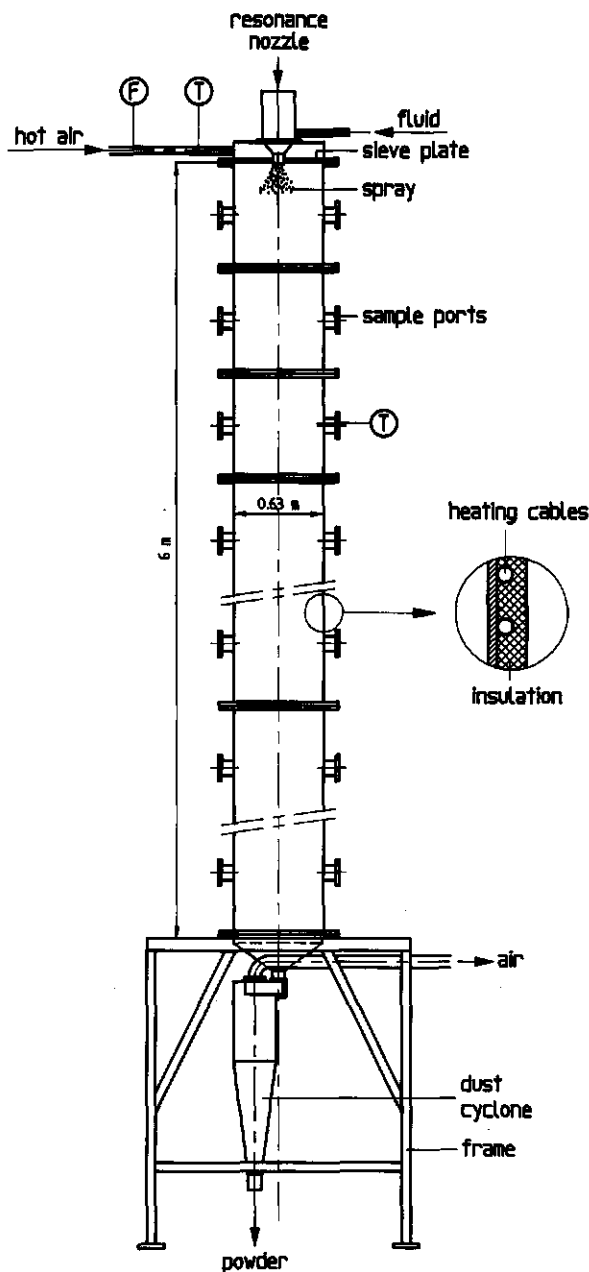
Figure 2.2 The drying tower

Droplet uniformity was controlled several times in each experiment by visual observation of a sample catched with a petri-dish filled with paraffin oil, using a stereo-microscope (40 times magnification). Photographs of (partially) dried droplets, and scanning and cryo scanning electron microscope pictures of dried droplets were made in several experiments. The aim was to determine if coalescence of droplets in the drying tower occurred and to identify changes in droplet shape and the presence of vacuoles. However, as pointed out by El-Sayed (1987) and El-Sayed *et al.* (1990), morphological changes are difficult to determine by the methods applied and therefore the results have to be interpreted with care.

- *Maltodextrin*
In the experiments the same maltodextrin was used as in the experiments with the suspended droplets (chapter 2.3.1). The initial moisture content varied from 1 - 4 kg $H_2O(kg\ ds)^{-1}$, and the drying air temperatures from 80 - 150 °C.

- *Skim-milk*
In the experiments the same skim-milk was used as in the experiments with the suspended droplets (chapter 2.3.1). The initial moisture content varied from 1.5 - 4 kg $H_2O(kg\ ds)^{-1}$, and the drying air temperature was 110 °C.

The drying experiments with skim-milk were, however, seriously disturbed by many experimental problems. In particular the resonance nozzle clogged up very often (each 1 à 10 min) during a drying experiment. In this way it was impossible to measure the drying kinetics of skim-milk droplets properly. Although it was possible to produce uniform droplets with initial moisture contents of 2.3 - 4 kg $H_2O(kg\ ds)^{-1}$, this was impossible at lower moisture contents.

2.4 RESULTS AND DISCUSSION

2.4.1. Suspended droplets

- *Model simulation*
Figure 2.3 gives a typical simulation of the drying of a maltodextrin droplet, using an 'average' set of experimental conditions. The characteristic drying time τ_d (defined as the time needed to reach $\omega_{w,0}/\omega_{w,t} = 0.37$) is 3500 s. The characteristic time of heat transfer τ_h (defined as the time needed to reach $\left(T_g - T_{d,t}\right)/\left(T_g - T_{d,0}\right) = 0.37$) is 300 s. As shown

in figure 2.3 the constant (water) activity period is very short ($t = 0.007\,\tau_d$). At the end of the constant activity period, the surface water activity decreases very fast (when $t = 0.3\,\tau_d$ then $a_{w,surface} = 0.01$ (the equilibrium water activity is zero)) and the droplet temperature starts to increase rapidly from the wet-bulb temperature to the drying air temperature ($\tau_h = 0.09\,\tau_d$). Consequently the drying process takes place almost completely in the falling (water) activity period, while furthermore in a large part of the drying process the droplet temperature is at most a few degrees centigrade below the drying air temperature and the surface water concentration is nearly in equilibrium with the moisture content of the air.

In figure 2.4 the water diffusion coefficient in maltodextrin is given as function of moisture content and temperature, together with the changes in the diffusion coefficients in the droplet centre and at the droplet surface as calculated in the model simulation. Furthermore the change of the 'average' diffusion coefficient is given. This 'average' diffusion coefficient is calculated using the average water concentration and droplet temperature as calculated in the model simulation and the relation for the diffusion coefficient.
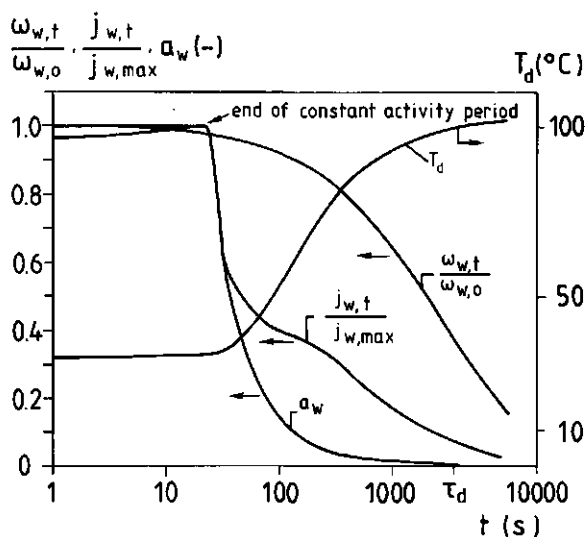

Figure 2.3 Model simulation. The changes in time are shown of the average water concentration, droplet temperature, drying flux and water activity at the surface. Initial conditions: $\omega_{w,0} = 1.25$ kg H_2O(kg ds)$^{-1}$, $d_{d,0} = 10^{-2}$ m, $T_g = 102.5$ °C, $v_g = 2.5$ ms^{-1} and $H = 0$ kg H_2O(kg da)$^{-1}$. Physical data table 2.2, applying the relation of Furuta *et al.* (1984) for the activation energy. The maximum drying flux $j_{w,max} = 1.52\ 10^{-3}$ kgm^{-2}s^{-1}.

As can seen from figure 2.4 the three 'diffusion coefficient' histories differ strongly as a result of the water concentration profiles. Dependent on the 'temperature - water concentration' histories, the diffusion coefficients start with an decrease or increase in time, to be followed by an increase and decrease respectively, and logically minimum or maximum values occur. A decreasing diffusion coefficient in the drying droplet as caused by the decreasing moisture content can partially or completly be compensated by the droplet temperature increase. Consequently the drying flux during the falling water activity period decreases less as expected given the strong concentration dependence of the water diffusion coefficient at constant temperature.

- *Sensitivity analysis*
The accuracy of drying model predictions are determined by the accuracy of the (measured or estimated) physical parameters used and by the sensitivity for variations in (initial) experimental drying conditions.

The important physical parameters are the water diffusion coefficient, the water sorption isotherm and the external mass and heat transfer coefficients. The values of the water
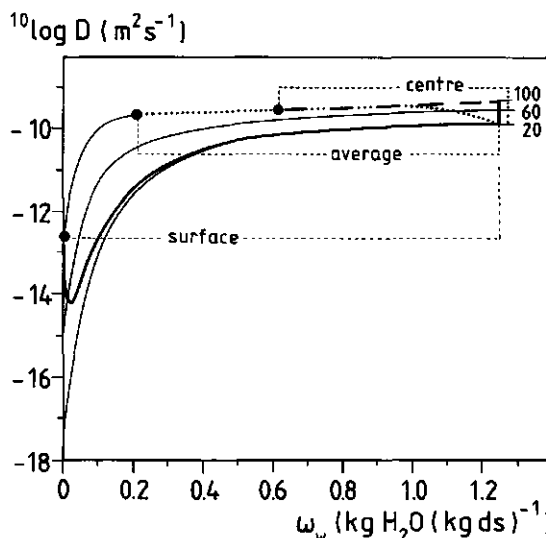

Figure 2.4   The water diffusion coefficient of maltodextrin as function of water concentration and temperature, and the calculated centre (— —), surface (———) and average (······) 'diffusion coefficients - water concentration' histories. Initial conditions model simulation and physical data: see figure 2.3. ●: final value.

diffusion coefficients and water sorption isotherms for maltodextrin as well as for skim-milk as for other (liquid) foods, however, are known only by approximation. In particular the values of the water diffusion coefficients have never been determined experimentally at low water concentrations (respectively, ω_w < 0.25 kg H_2O(kg ds)$^{-1}$ for skim-milk and ω_w < 0.10 kg H_2O(kg ds)$^{-1}$ for maltodextrin) and at higher temperatures (respectively, T > 70 °C for skim-milk and T > 45 °C for maltodextrin). Regarding the water sorption isotherm of maltodextrin, no experimental data are available at temperatures above 45 °C. The relation for the water sorption isotherm of skim-milk, as given in table 2.1, is derived from sorption data at ambient temperature and at water concentrations for which crystallisation does not occur of the lactose present in skim-milk. Therefore the values of the diffusion coefficient and the water activity at low water concentrations and high temperatures have to be determined by extrapolation. The external transport coefficients are calculated by the Ranz and Marshall correlation. The accuracy of these calculated values is limited and errors up to 50% can occur. Moreover during drying the surface of the droplets does not remain smooth but surface folds appear. Above that the air flow pattern is not well defined in the experiments, and the droplets can move a little up and down. All these effects will influence the external transfer coefficients. Knowledge about the importance of the variations is therefore needed.

In figure 2.5 the influence is given on the residual water concentration for a drying time of 7200 s of feasible variations of the different physical and experimental parameters, for the example given in figure 2.3. In each analysis only one parameter was varied, while the other parameters remained at their base-case values. As can seen from figure 2.5 the drying flux is in particular sensitive to small variations (+/- 20%) in the activation energy values of the temperature dependence of the diffusion coefficient. This reflects the fact that the mass transfer is primarily internal 'diffusion' controlled, as shown in the model simulation. The influence of variations in the water sorption isotherm (a_w) is negligible. This is caused by the fact that the average moisture content is much higher than the surface water concentration during a large part of the drying process (see figure 2.3). In the base-case the average and surface moisture content after 7200 s were respectively, 28 10^{-2} kg H_2O(kg ds)$^{-1}$ and 28 10^{-5} kg H_2O(kg ds)$^{-1}$. During the falling activity period the drying flux is, by approximation, proportional with the difference between the average and the surface water concentration. As a consequence changes in the water sorption isotherm will influence the drying kinetics only if they result in large changes in the difference between average and surface moisture content. Changing the sorption isotherm results in variations of the surface
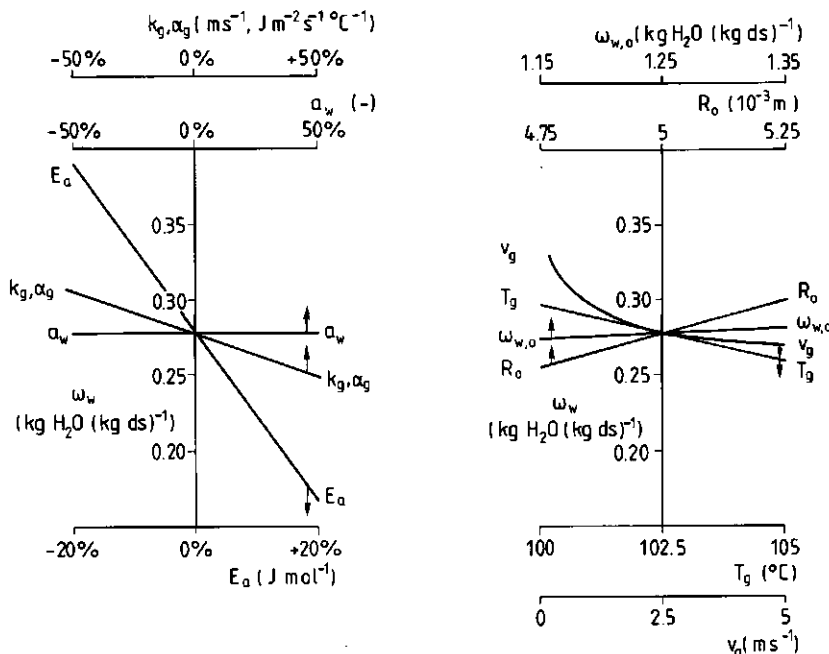
a Influence of variations in physical parameters.   **b** Influence of variations in experimental conditions.

Figure 2.5   Influence of variations in important variables on the residual water concentration. Base
                     case: see figure 2.3. Drying time is 7200 s.

water concentration $(14 \cdot 10^{-5} - 42 \cdot 10^{-5}$ kg H_2O(kg ds)$^{-1})$ that can be neglected with respect
to the average moisture content.

- Skim-milk

In the figures 2.6a-c the experimental drying results at three different drying air temperatures
(55, 75 and 95 °C) are shown. As can seen the experimental data are scattered (up to about
$\pm$ 20%), especially at lower water contents ($\omega_w < 0.3$ kg H_2O(kg ds)$^{-1}$). The differences
between duplicate experiments are of the same order of magnitude. This might be because
during drying the spheres did not remain perfectly spherical, but deformed gradually in 'dried
currant' like structures.

     The calculated drying kinetics is in good accordance with the experimental results. The
discrepancies between calculated and measured average moisture contents are of the same
magnitude as the differences between duplicate experiments, no systematic deviations occur.
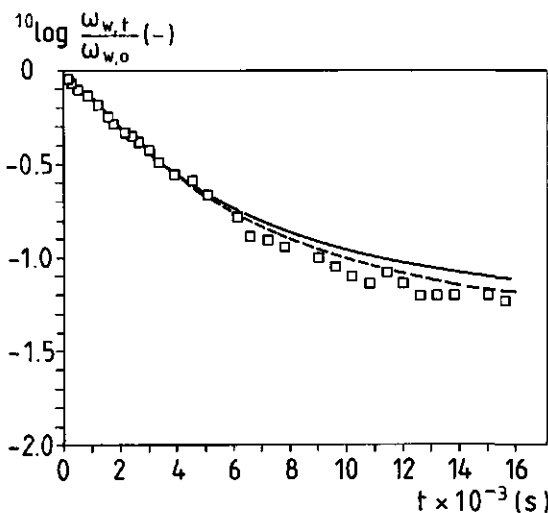
a   Experimental conditions: $\omega_{w,0} = 4.8$ kg H_2O(kg ds)$^{-1}$, $d_{d,0} = 10^{-2}$ m, $T_g = 55$ °C,

$v_g = 0.7$ ms^{-1} and $H = 0.01$ kg H_2O(kg da)$^{-1}$.
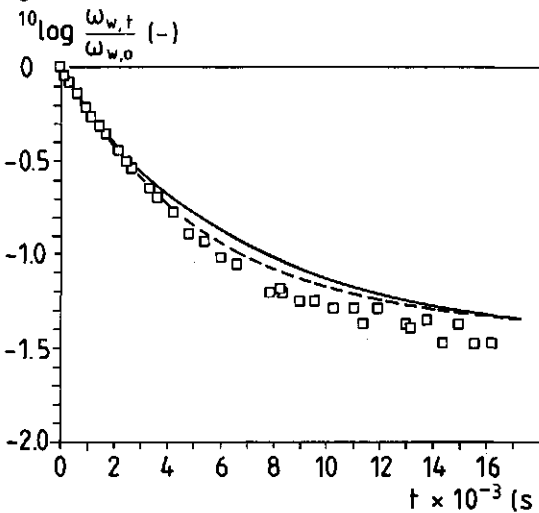
b   Experimental conditions: $\omega_{w,0} = 4.4$ kg H_2O(kg ds)$^{-1}$, $d_{d,0} = 10^{-2}$ m, $T_g = 75$ °C,

$v_g = 0.7$ ms^{-1} and $H = 0.01$ kg H_2O(kg da)$^{-1}$.

Figure 2.6   Drying kinetics of skim-milk droplets. ———: model simulation, physical data table 2.1;
— —: model simulation, using the relation for the water diffusion coefficient in skim-milk
as given by Wijlhuizen *et al.* (1979).
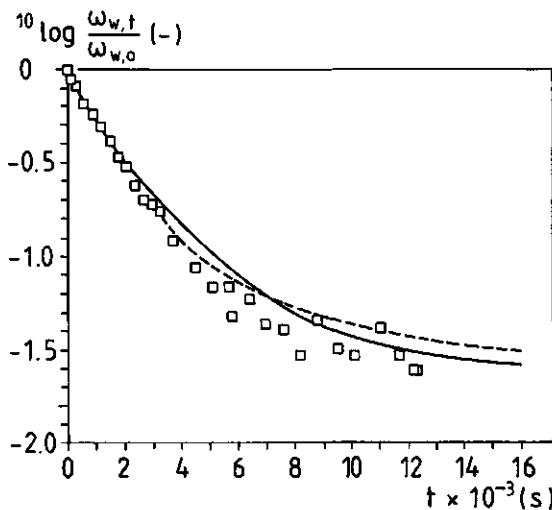
Figure 2.6c   Experimental conditions: $\omega_{w,0} = 4.8\ \text{kg}\ H_2O(\text{kg ds})^{-1}$, $d_{d,0} = 10^{-2}\ \text{m}$, $T_g = 95\ °\text{C}$, $v_g = 0.7\ \text{ms}^{-1}$ and $H = 0.01\ \text{kg}\ H_2O(\text{kg da})^{-1}$.

Applying the relation for the diffusion coefficient in skim-milk as given by Wijlhuizen *et al.* (1979) does not significantly change the predictions of the experimental drying results. The difference between the relations for the diffusion coefficient as given by Wijlhuizen *et al.* (1979) and Ferrari *et al.* (1989) lies primarily in the method of extrapolation to low moisture content and high temperature values.

Sano and Keey (1982) found similar experimental and modelling results with respect to the drying kinetics of skim-milk droplets, although their experimental circumstances were different: the initial and final moisture contents were 2.33 and 0.30 $\text{kg}\ H_2O(\text{kg ds})^{-1}$ respectively, the initial drop diameter was 2 mm and the drying air temperature was 100 °C. Moreover they performed experiments at drying air temperatures of 150 °C, investigating droplet expansion and inflation. Sano and Keey (1982) used the diffusion relation as given by Wijlhuizen *et al.* (1979). They found, however, discrepancies between measured and simulated droplet temperatures. Sano and Keey (1982) give no explanation for this phenomenon. Droplet temperature measurements as performed a few times during the experiments showed similar behaviour. Analysis of the simulations revealed that the observed discrepancies can be overcome by a 30-50 % increase of the external mass and heat transfer coefficients. This is true for the data published by Sano and Keey (1982) as

well as for our own data. The accuracy of the prediction of the experimental drying kinetics is not influenced by this increase, as expected (see figure 2.5a).

The irregular shrinkage of the droplets does not cause a systematic deviation from the calculated drying kinetics, as expected. This can be a consequence of the limited accuracy of the measurements, but also of the way in which the diffusion coefficients are determined. The equations as given by Wijlhuizen *et al.* (1979) and Ferrari *et al.* (1989) are both based on drying experiments in which a single droplet was dried. These droplets showed irregular shrinkage also, but this was not taken into account when the diffusion coefficients were calculated. As a consequence irregular shrinkage is taken into account in an indirect way in the determined diffusion coefficients.

- *Maltodextrin*

The experimental results of drying experiments at four different initial water contents (3.0, 1.86, 1.04 and 0.47 kg H_2O(kg ds)$^{-1}$) are shown in the figures 2.7a-d. Detailed results for the first stage of a drying experiment (the initial water content was 1.04 kg H_2O(kg ds)$^{-1}$) are plotted in figure 2.7e. During the drying process the droplets lost, in an irregular way, their perfect spherical shape and surface folds appeared.

Drying model simulations (not shown in figure 2.7) using the physical data given in table 2.2 and the relation for the moisture dependence of the activation energy as given by Furuta *et al.* (1984), showed a systematic underestimation of the drying flux at the highest initial moisture content (3.0 kg H_2O(kg ds)$^{-1}$) and an overestimation of the drying flux at the lowest initial moisture content (0.47 kg H_2O(kg ds)$^{-1}$), when compared with the experimental data. The average discrepancy between experimental and calculated moisture content was 18 %. As shown, the sensitivity analysis reveals that the drying flux is very sensitive to variations in the activation energy of the temperature dependence of the diffusion coefficient. In the model simulations that are shown in the figure 2.7, a modified relation for the moisture dependence of the activation energy is used. This relation is given in table 2.2. The relation was estimated by comparison of the calculated drying curves with the experimental data using different relations for the moisture dependence of the activation energy. The relation is modified in such a way that the activation energy is lower at low moisture contents (lower droplet drying rates) and higher at high moisture contents (higher droplet drying rates) compared with the relation as given by Furuta *et al.* (1984).
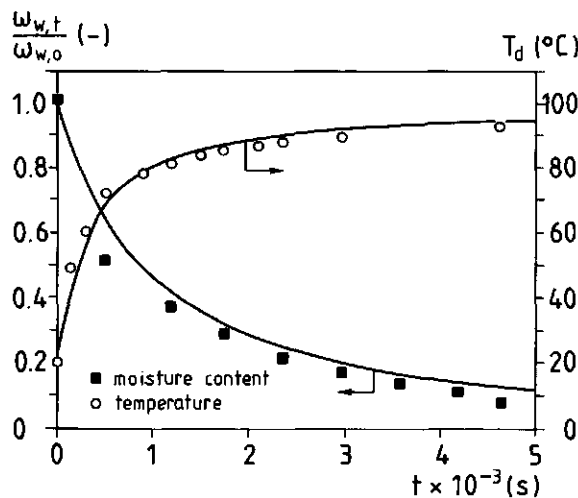
a   Experimental conditions: $\omega_{w,0} = 3.0\ \mathrm{kg\ H_2O(kg\ ds)}^{-1}$, $d_{d,0} = 10^{-2}\ \mathrm{m}$, $T_g = 97\ ^\circ\mathrm{C}$, $v_g = 3.8\ \mathrm{ms}^{-1}$ and $H = 0.0\ \mathrm{kg\ H_2O(kg\ da)}^{-1}$.
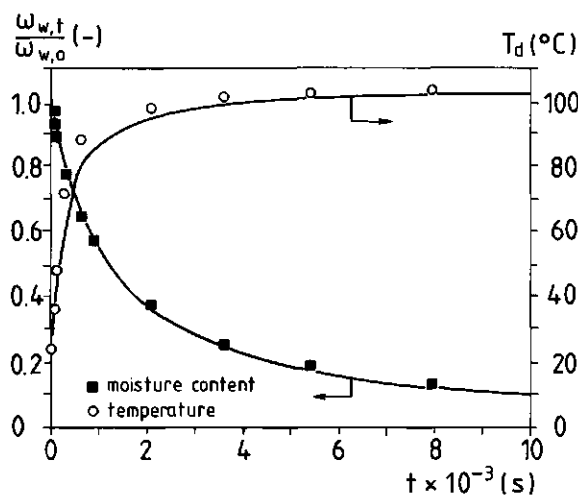
b   Experimental conditions: $\omega_{w,0} = 1.86\ \mathrm{kg\ H_2O(kg\ ds)}^{-1}$, $d_{d,0} = 10^{-2}\ \mathrm{m}$, $T_g = 103\ ^\circ\mathrm{C}$, $v_g = 2.5\ \mathrm{ms}^{-1}$ and $H = 0.0\ \mathrm{kg\ H_2O(kg\ da)}^{-1}$.

Figure 2.7   Drying kinetics of maltodextrin droplets. The change in time is given of the average moisture content and droplet temperature. ————: model simulation, physical data table 2.2, applying the 'adapted' relation for the activation energy.
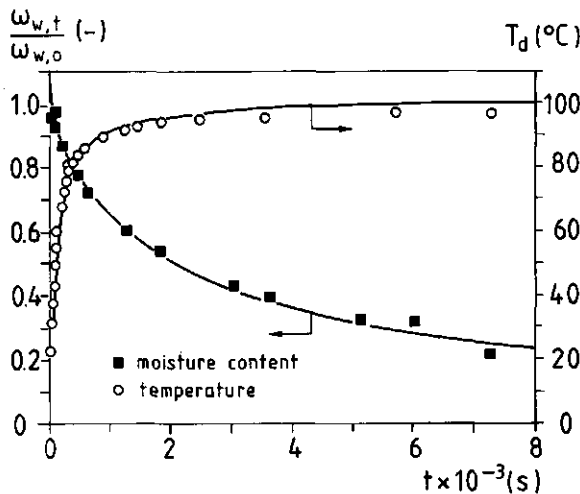
Figure 2.7c Experimental conditions: $\omega_{w,0} = 1.04$ kg H_2O(kg ds)$^{-1}$, $d_{d,0} = 10^{-2}$ m, $T_g = 101$ °C, $v_g = 2.5$ ms^{-1} and $H = 0.0$ kg H_2O(kg da)$^{-1}$.
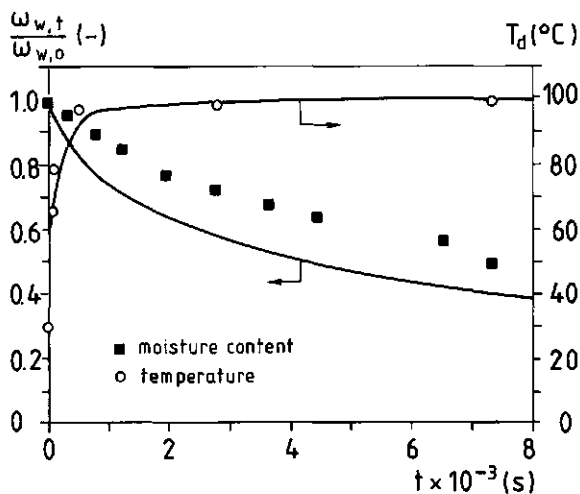
Figure 2.7d Experimental conditions: $\omega_{w,0} = 0.47$ kg H_2O(kg ds)$^{-1}$, $d_{d,0} = 0.86\ 10^{-2}$ m, $T_g = 101.5$ °C, $v_g = 2.5$ ms^{-1} and $H = 0.0$ kg H_2O(kg da)$^{-1}$.

A further analysis of the relations used is done: in figure 2.8 the diffusion coefficients as calculated by both activation energy relations are compared. Besides that the range of conditions (water concentrations and temperatures) as applied in the diffusion experiments (Furuta *et al.* (1984)), is plotted. The diffusion coefficients as calculated from the relations and as shown in figure 2.8, differ at most 6 fold. The largest difference is at a temperature of 100 °C and moisture content of 0 kg H_2O(kg ds)$^{-1}$ (as expected), that is far outside the range of the experimental conditions. Comparison of the diffusion coefficient 'histories' as given in figure 2.4 and the range of experimental conditions reveals that the diffusion coefficients as used in the drying calculations are mainly based on extrapolations. These extrapolations are strongly influenced by the accuracy of the estimation of the activation energy. Given the limited range of temperatures used (25 - 45 °C) in the diffusion experiments, the estimate cannot be very accurate and consequently the modified relation results in (calculated) diffusion coefficients which differ not significantly from those calculated with the relation given by Furuta *et al.* (1984). The drying kinetics is, however, influenced significantly. Applying the adjusted relation for the activation energy a good description of the experimental drying kinetics and droplet temperatures is obtained, as can seen from figure 2.7. The average discrepancy between experimental and calculated moisture content is 10 %, instead of 18%.
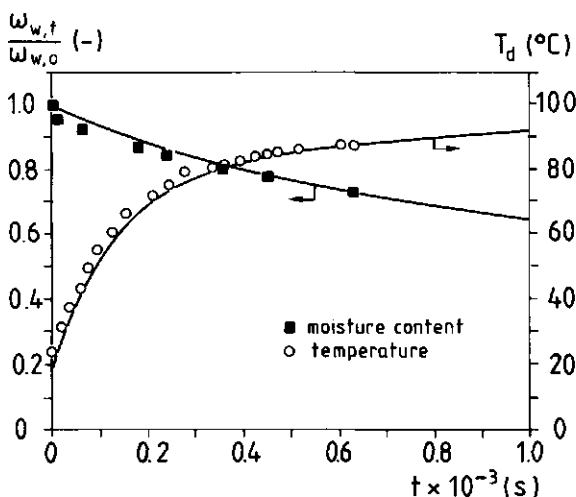
**Figure 2.7e**   Drying kinetics during the first stage of drying. Experimental conditions: $\omega_{w,0} = 1.04$ kg H_2O(kg ds)$^{-1}$, $d_{d,0} = 10^{-2}$ m, $T_g = 101$ °C, $v_g = 2.5$ ms^{-1} and $H = 0.0$ kg H_2O(kg da)$^{-1}$.

Analysis showed that also a combination of increasing the external heat and mass transfer coefficients with 30-50 % and decreasing the activation energy at low water contents can be used to improve the prediction of the drying kinetics. This, however, is not examined in more detail.

Another source of error might be the non-ideal shrinkage behaviour of the maltodextrin droplets, given the experimental conditions. As has been described in the previous paragraph this phenomenon is taken into account in the diffusion coefficient in an indirect way.
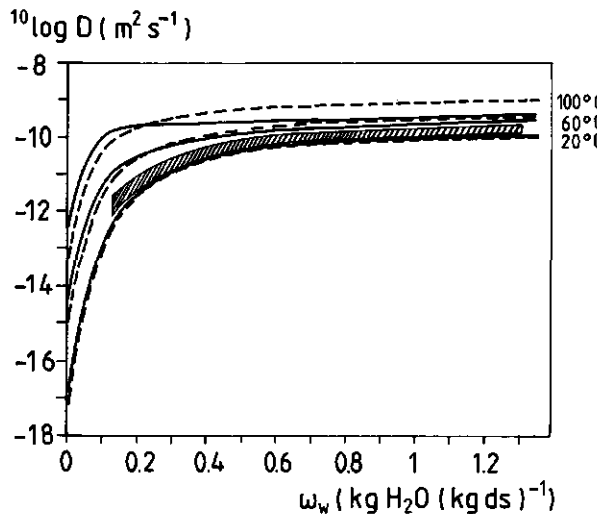

Figure 2.8   The concentration and temperature dependence of the water diffusion coefficient of maltodextrin as calculated by two different relations for the moisture dependence of the activation energy. Physical data table 2.2; ———: relation Furuta *et al.* (1984); — —: 'adapted' relation; ⁄⁄: experimental conditions diffusion experiments (Furuta *et al.* (1984)).

2.4.2 Free falling droplets

- Model simulation

In figure 2.9 the results of a simulation of the drying of a free falling maltodextrin droplet are depicted, using an 'average' set of experimental conditions. In the simulation it is assumed that the drying air temperature and humidity are constant. The characteristic time of the drying process τ_d is 1.5 s and the characteristic time of heat transfer τ_h is 2 s. Consequently the drying process takes place primarily at 'intermediate' temperatures. Moreover as can seen from figure 2.9 the main part of the drying process in the drying tower occurs in the falling water activity period $(a_{w,surface} < 1)$. The shift from the constant water activity period $(a_{w,surface} = 1)$ to the falling water activity period takes place already at a falling distance of 0.55 m (t = 0.25 τ_d). This transition is reflected also in the temperature curve, the droplet temperature increases from the wet-bulb temperature (during the constant water activity period) up till the drying air temperature. During the constant water activity period the droplet decelerates very fast from the initial jet velocity down to the terminal falling velocity. The decrease of the drying flux during the constant water activity period is a result of the decrease of the external mass transfer coefficient caused by the decrease in droplet velocity.

In figure 2.9a the point on the drying curve is indicated were the droplet temperature reaches 100 °C. The average and surface water concentration are then 0.4 kg H_2O(kg ds)$^{-1}$ and 0.009 kg H_2O(kg ds)$^{-1}$, respectively. The calculated water activities belonging to these concentrations are 1 and 0.05. Consequently internal boiling can take place, and internal vapour bubbles can develop, accompanied (eventually) by droplet expansion, surface ruptures, droplet collapse and vacuole formation (El-Sayed (1987), Wallack (1988), El-Sayed *et al.* (1990), Wallack *et al.* (1990)). Whether boiling occurs will depend also on the presence or formation of nuclei. For spontaneous nucleation the droplet temperature must be at least 10 up to 20 °C above the boiling temperature (Verhey (1973)). Also the desorption of dissolved gases, caused by the increase in droplet temperature and dissolved solids concentration can be a factor in bubble formation and droplet expansion (Greenwald (1980), El-Sayed (1987)). However, the experimental evidence for and knowledge of the mentioned processes is limited. An increase of the drying flux is expected if expansion etc. occurs, and the drying model will underestimate the drying rate (van der Lijn (1976), Wijlhuizen *et al.* (1979), Sano and Keey (1982)).
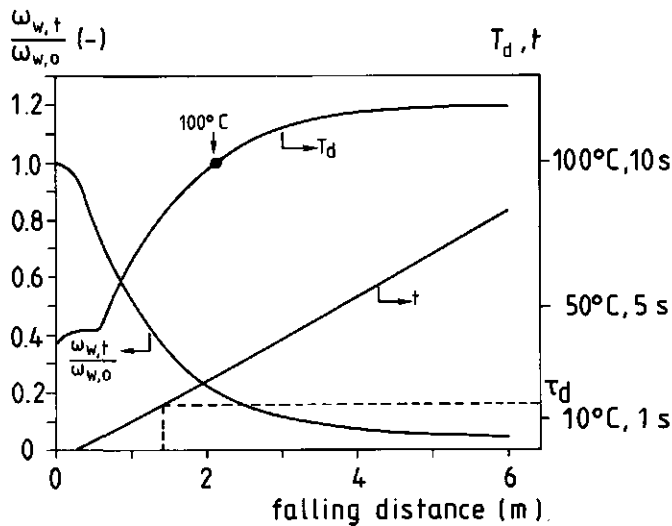
a The average water concentration, droplet temperature and drying time as function of the falling distance.
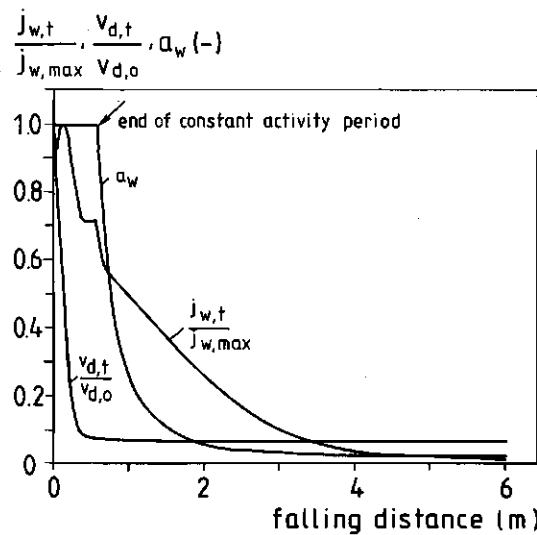
b The drying flux, droplet velocity and water activity at the surface as function of the falling distance.

Figure 2.9 Model simulation. Initial conditions: $\omega_{w,0} = 2.0$ kg H_2O(kg ds)$^{-1}$, $d_{d,0} = 200\,\mu$m, $T_g = 120\,^\circ$C, $v_{d,0} = 10$ ms^{-1}, $v_g = 0.2$ ms^{-1} and $H = 0.025$ kg H_2O(kg da)$^{-1}$. Physical data table 2.2, applying the 'adapted' relation for the activation energy. The maximum drying flux $j_{w,max} = 2.81\,10^{-2}$ kgm^{-2}s^{-1}.

- Sensitivity analysis

A sensitivity analysis similar as described for the suspended droplets (see chapter 2.4.1) was performed. In figure 2.10 the influence on the residual water concentration of parameter variations around their base-case values is shown at a falling distance of 2.6 m (= sample port 4), for the example given in figure 2.9. The results are similar as found for the suspended droplets, but there are two exceptions. Firstly, the influence of changes in the activation energy of the diffusion coefficient is for the free falling droplets smaller than for the suspended droplets. This is caused by the fact that the Biot-number for mass transfer of the suspended droplets is about one order of magnitude larger than that for the free falling droplets (at the same temperature) and consequently the drying process of the suspended droplets is more internal mass transfer controlled. However, also in the case of free falling droplets the Biot number for mass transfer is larger than 1. Furthermore the residual moisture content is very sensitive to the value of the drag coefficient C_d (or, in other words, to the estimation of the droplet velocity), as expected. A 50% change in C_d results in an about 25 % change in the terminal falling velocity and in an about 35 % change in the residence time of the droplets before arriving at sample port 4. The terminal falling velocity has an average value of about 0.5 ms^{-1} for the base-case and the residence time is 3.25 s. The influence of a variation of the drying air velocity is limited because the terminal droplet velocity is about 2.5 times the air velocity.

- Drying equipment

Resonance nozzle

In figure 2.11 the break-up of a jet in individual droplets and the spray-formation is shown. As can be seen a droplet jet is formed first and after that a spray is formed, caused by the electrostatic repulsion of the droplets (Crowley (1968)). The measured droplet diameters were in accordance with the diameters as calculated from equation 2.14. The average discrepancy between measured and calculated diameters is 3%.

Electrode voltages above 150 V were not useful because higher voltages resulted in a too wide droplet spray. The resultant low spray droplet densities led up to too long sampling times (> 0.5 h) at the bottom of the drying tower. Moreover a considerable part of the droplets then stuck to the tower wall.

a Influence of variations in physical parameters.   b Influence of variations in experimental conditions.
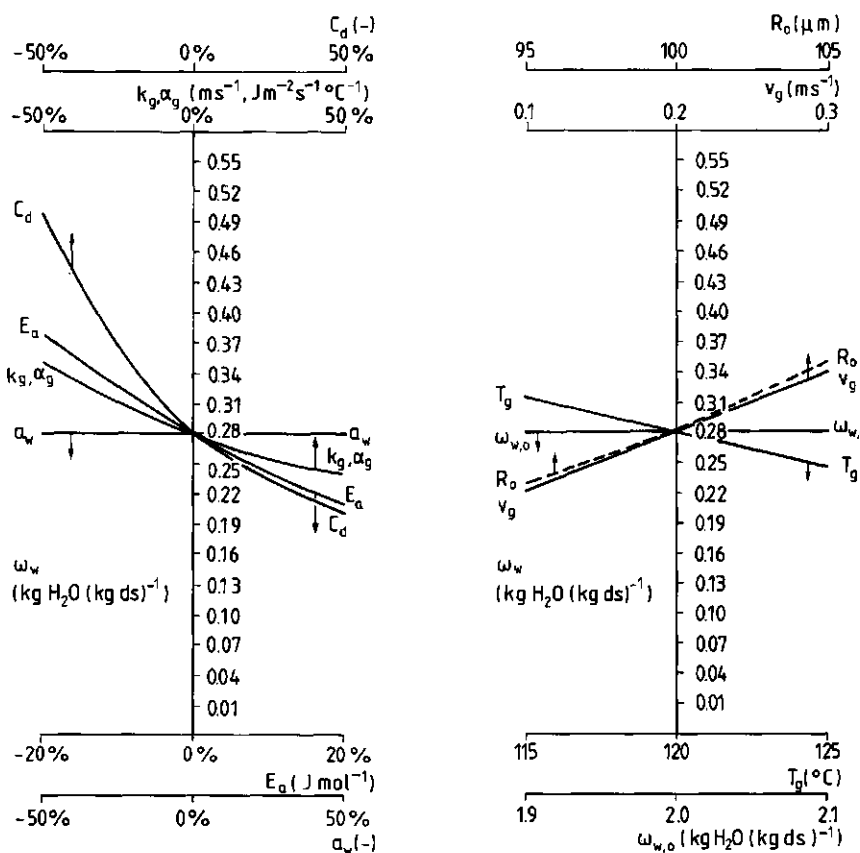
Figure 2.10   Influence of changes in important variables on the residual water concentration. Base-case values: see figure 2.9. Falling distance is 2.6 m. The variations in the external transfer coefficients relate to variations in the variable parts of the equations 2.5 and 2.7.
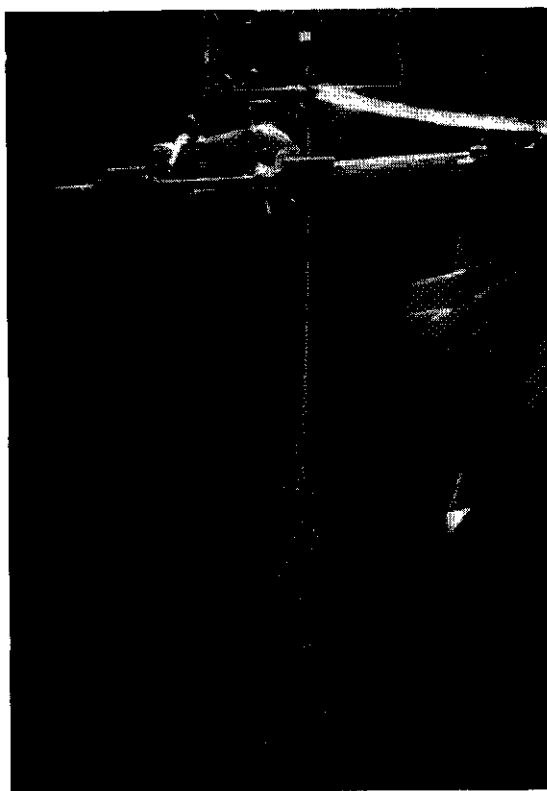
Figure 2.11   Break-up and charging of the laminar jet.

Drying tower

The axial temperature gradients in an 'empty' drying tower were 5 °C at most. Radial velocity differences of about 0.1 ms^{-1} were measured, with the highest values at the top of the tower. The influence of these variations on the residual moisture content is limited, see the preceeding paragraph and figure 2.10b.

Drying kinetics

It turned out that it was very difficult to obtain the same experimental conditions in different experiments. Furthermore water concentrations in duplicate measurements showed often a considerable scatter of up to 25 % (see also figure 2.13). Separate experiments
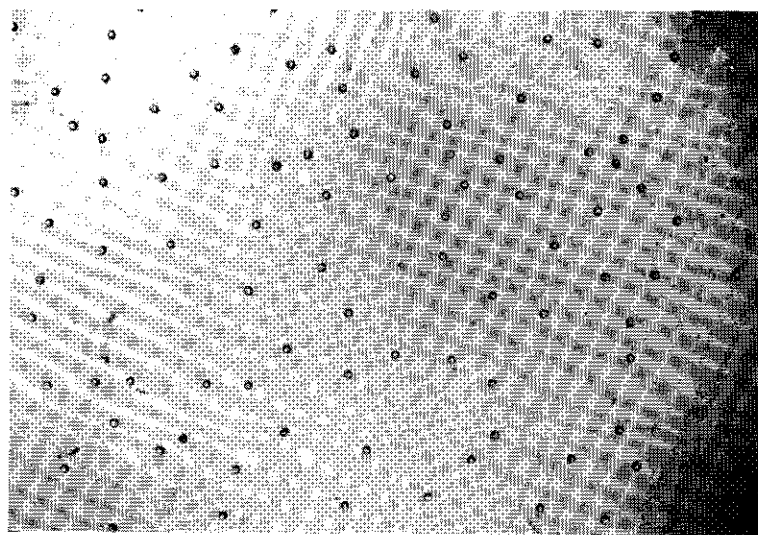
a Photograph of a sample of dried droplets.
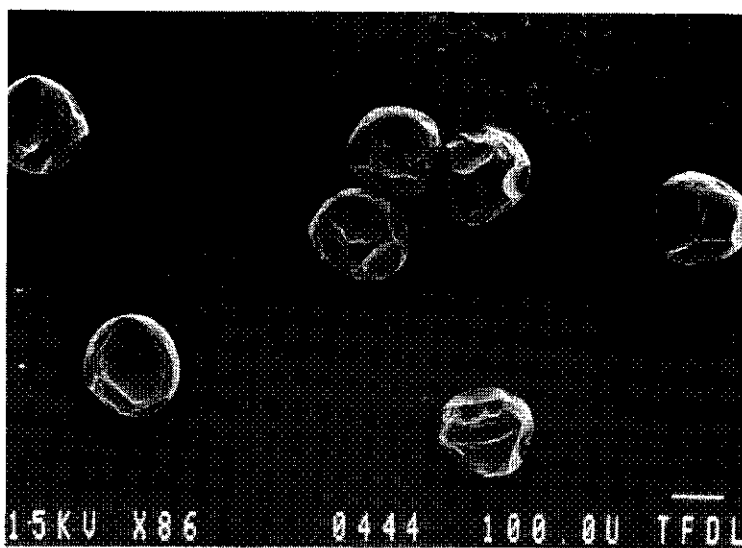
b Scanning electron microscope photograph of a few dried droplets.

Figure 2.12 Photographs of dried maltodextrin droplets. Experimental conditions: $\omega_{w,0} = 1.5 \text{ kg H}_2\text{O}(\text{kg ds})^{-1}$, $d_{d,0} = 204 \ \mu\text{m}$ and $T_g = 150 \ ^\circ\text{C}$.
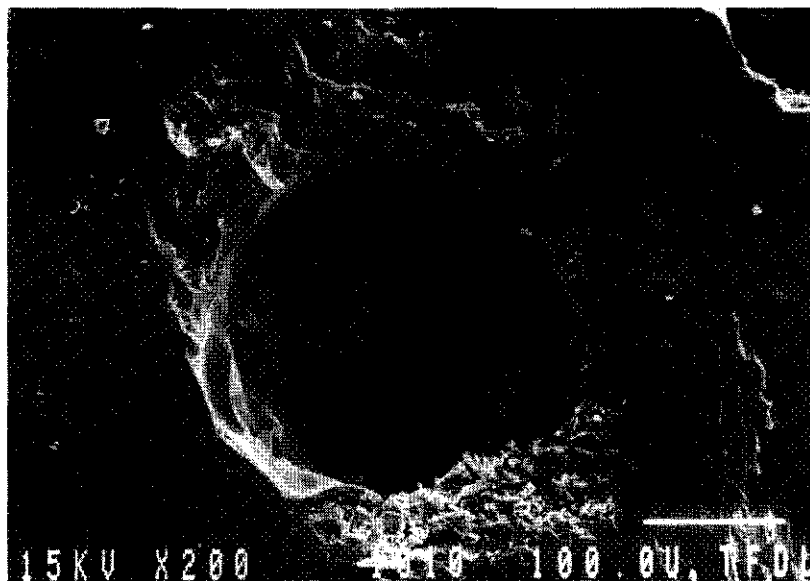
Figure 2.12c   Cryo scanning electron microscope photograph of the interior of a dried droplet.

showed that this scatter can not be explained by the inaccuracy of the applied moisture determination method only.

- Drying kinetics of maltodextrin droplets

In figure 2.12 three characteristic photographs are given of dried droplets catched at the bottom of the tower. The drying air temperature was 150 °C. As can seen from the figures 2.12a and b, the resonance nozzle is capable of producing uniform droplets and coalescence of the drops in the tower was absent. The photographs indicate that during the drying process the maltodextrin droplets remained more or less 'spherical', but with a 'crater' like surface. El-Sayed (1987), Wallack (1988), El-Sayed *et al.* (1990) and Wallack *et al.* (1990) also found that free falling maltodextrin droplets were 'spherical', however, their droplets contained one or more (water vapour) bubbles and expansion of the droplets took place. This is not found in the experiments reported here, see figure 2.12c. The drying air temperatures (180-240 °C) used in the experiments of El-Sayed (1987), Wallack (1988), El-Sayed *et al.* (1990) and Wallack *et al.* (1990) were much higher than used here (150 °C); conditions which favor the onset of nucleation and expansion in the experiments of El-Sayed

(1987), Wallack (1988), El-Sayed *et al.* (1990) and Wallack *et al.* (1990). The appearance of their (partly) dried droplets is, however, similar to that of the droplets shown in figure 2.12b. This appearance, they argue, is probable an artefact due to the collapse of the expanded droplets caused by the strong fall in temperature when the partly dried droplets were catched in liquid nitrogen. In our experiments the removal of the samples from the drying tower caused a similar strong temperature fall (although less than in their experiments), but in our experiments the water concentration of the droplets is lower (they are almost dry) and consequently a more rigid structure is present, perhaps preventing collapse. Verhey (1972) spray-dried different liquid foods, including maltodextrin solutions, using process conditions which prevent vacuole (vapour bubble) formation. Electron microscope pictures of the produced powder particles show that the appearance of these droplets is similar to that from this research work. Consequently, although vacuole formation and droplet expansion cannot be excluded to have happened in the experiments reported here at $T_g = 150\ ^\circ$C, the experimental evidence for these phenomena direct to its absence. In the experiments performed at drying air temperatures below 150 °C, it is even more likely that vacuole formation and bubble expansion was absent.
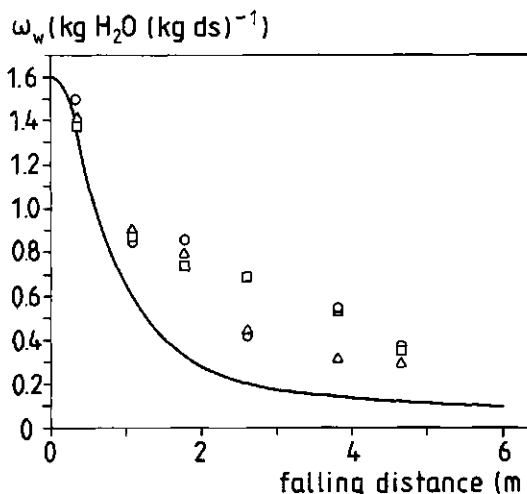
a   Experimental conditions: $\omega_{w,0} = 1.6$ kg H_2O(kg ds)$^{-1}$, $d_{d,0} = 158\ \mu$m, $T_g = 100\ ^\circ$C and charging voltage = 70–80 V. O, □, △ : results of 3 experimental runs.

Figure 2.13   Drying kinetics of maltodextrin droplets. ————: model simulation; physical data table 2.2, applying the adapted relation for the activation energy.
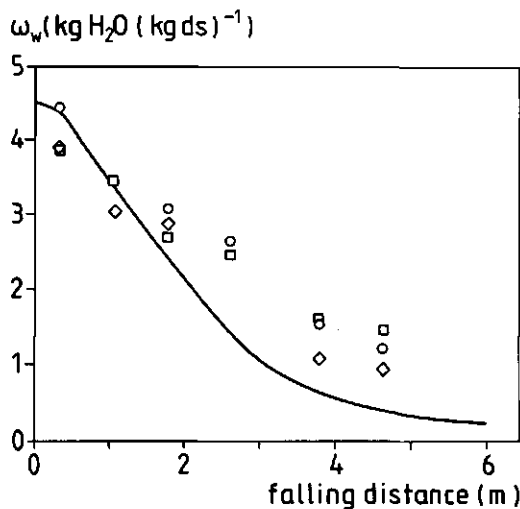
Figure 2.13b   Experimental conditions: $\omega_{w,0} = 4.5 \text{ kg H}_2\text{O(kg ds)}^{-1}$, $d_{d,0} = 210 \, \mu\text{m}$, $T_g = 80\ ^\circ\text{C}$ and charging voltage = 100–130 V. O, □, △ : results of 3 experimental runs.
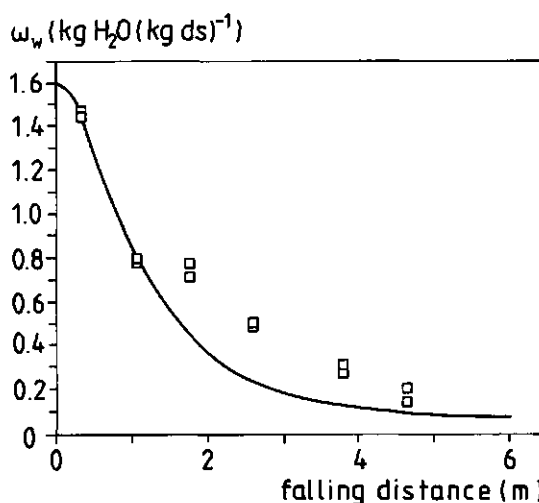

Figure 2.13c   Experimental conditions: $\omega_{w,0} = 1.6 \text{ kg H}_2\text{O(kg ds)}^{-1}$, $d_{d,0} = 204 \, \mu\text{m}$, $T_g = 130\ ^\circ\text{C}$ and charging voltage = 110–130 V. The duplicate results are shown of 1 experimental run.

In figure 2.13 typical drying results are shown at a broad range of experimental conditions. In the model simulations it was assumed that the drying air temperature and humidity are constant. As can be seen, the experimental results show sometimes a considerable scatter, as mentioned before. In all experiments there exists a large systematic discrepancy between experimental data and model predictions. The drying model overestimates the drying rate in all cases. The discrepancies can not be explained by experimental inaccuracies.

Feasible explanations for this large discrepancy are: the erroneous estimation of the residence time of the droplets and the assumption in the model simulations that the drying air temperature and humidity are constant in the air around the droplets. Variations in other physical and experimental parameters can not explain this difference, given the results of the sensitivity analysis (see figure 2.10).

The momentum balance (equation 2.8) used for the prediction of the droplet residence time is in principle only valid in the 'ideal' case of a 'free' falling rigid sphere. In the drying tower these conditions are not fulfilled completely:

- The droplets are charged and consequently electrical attraction and repulsion forces (of an unknown size) play a role (Crowley (1968), Alexander (1983)).

- After the break-up of the liquid jet issuing from the resonance nozzle, a stream of droplets exists over a short distance, merging in a dense spray. The falling velocity of the droplets in the droplet stream is larger than calculated by the impulse balance (Arrowsmith and Foster (1973)) and in the dense spray the reverse situation exists.

- At low water concentrations the droplets lose their perfect spherical shape (see figure 2.12) causing an increase of the friction coefficient, resulting in a lower terminal falling velocity.

- In the drying tower there exists a (limited) air velocity profile, leading to a residence time distribution of the droplets.

The exact consequences of these deviations from the 'ideal' case are unknown, and have to be evaluated by setting-up droplet residence time distribution experiments. This kind of experiments has not been performed.

The assumption of constant drying air temperature is examined in a few experiments by measuring the axial and radial temperature profiles in the drying tower, using different charging voltages. In this way the angle of the spray-cone was varied. The temperature profiles were measured with a thermocouple, in such a way that the attachment of drying droplets was avoided. It appeared to be very difficult to obtain reproducible results at the first sample port (falling distance = 0.33 m), because minor changes in the position of the thermocouple resulted in significant temperature changes.

falling distance (m) tower | centre
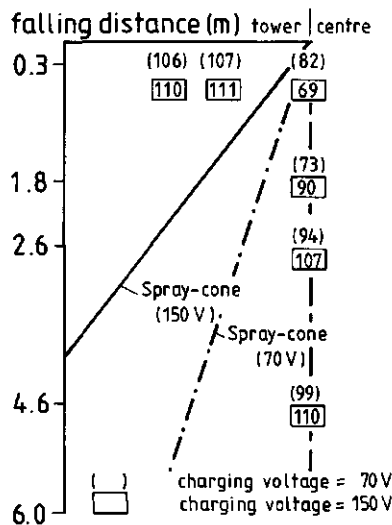
Figure 2.14   Axial and radial air temperature profiles in the drying tower. Experimental conditions: $\omega_{w,0} = 2.3 \text{ kg H}_2\text{O(kg ds)}^{-1}$, $d_{d,0} = 204 \text{ } \mu\text{m}$ and $T_g = 110 \text{ °C}$.

The results for two 'extreme' voltages (70 V and 150 V) are depicted in figure 2.14. The 'average' drying air temperature was 110 °C. As can be seen from figure 2.14 strong axial and radial drying air temperature profiles especially exist at the top of the tower. The profiles depend on the applied charging voltage. In both cases there is a small spray-cone at the top in which the air temperature (about 70 °C) is considerable lower than the 'average' temperature. At a charging voltage of 70 V the air temperature in the tower centre (about 100 °C) at a falling distance of 4.6 m (sample port 6) is still lower than the 'average' temperature. The indicated spray-cones are based on the measurement of spray diameters at different sample ports. Air humidity profiles are not measured, but these will exist also in connection with the air temperature profiles. Droplet drying experiments indicate that applying an 'extreme' charging voltage such as 150 V, results in lower average residual moisture contents than at lower voltages, as expected. However, also in that case the discrepancy between model simulations, assuming constant air temperature and humidity, and experiments remained. Furthermore the differences between duplicate experiments are in the same order of magnitude as between very different charging voltages.
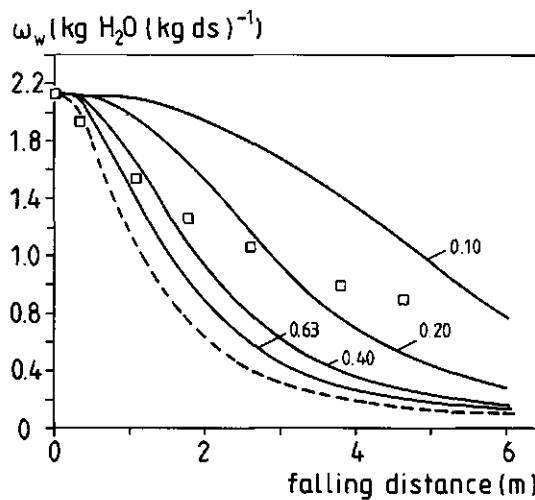
$\omega_w (\text{kg } H_2O \, (\text{kg ds})^{-1})$

a The average water concentration as function of the falling distance. Experimental conditions: $\omega_{w,0} = 2.3 \text{ kg } H_2O (\text{kg ds})^{-1}$, $d_{d,0} = 204 \, \mu m$, $T_g = 110 \, °C$ and charging voltage $= 110$ V

$T_g (°C)$
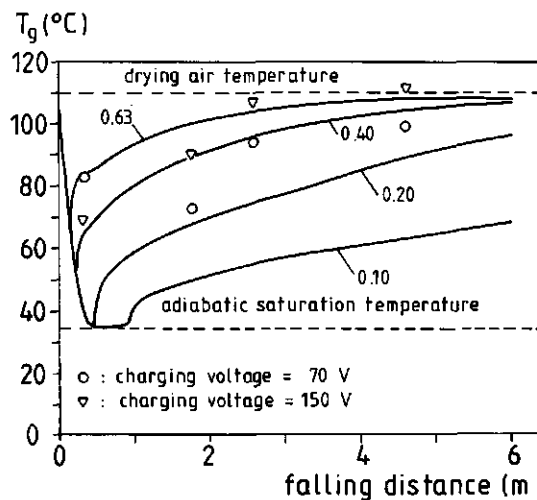
b Air temperatures at the centre of the drying tower. Experimental conditions: see figure 2.14

Figure 2.15 Drying kinetics and air temperatures. ———: 'spray' model simulation; — —: 'ideal' model simulation; physical data table 2.2, applying the adapted relation for the activation energy. The values at the drawn lines indicate the spray diameters (m) at a falling distance of 4.6 m (sample port 6).

To examine the consequences of the existence of temperature and humidity profiles for the predicted droplet drying kinetics, the 'ideal' drying model was adapted. In the adapted 'spray' drying model two important assumptions were made: the drying process is adiabatic and the fraction of the drying air entrained in the spray after a certain falling distance is equal to the square of the ratio of the diameter of the spray at that distance and the diameter of the drying tower. New 'fresh' drying air entrained in the spray at a given falling distance is ideally mixed up with the air already present in the spray. The change of air temperature and humidity inside the spray is determined by the heat and mass transferred to and from the droplets, respectively. The heat transfer from the drying tower wall is neglected, moreover it is assumed that no droplets stick to the tower wall and that the droplets are evenly distributed in space. This latter assumption is certainly not valid. During the spray diameter measurements it was seen that the droplet density gradually decreases from the tower centre to the edge of the spray, indicating that in all cases a kind of spray 'core' exists within the spray itself with a diameter of about 20-30 cm at a falling distance of 4.6 m. In figure 2.15 the results of simulations using the 'spray' drying model are compared with experimental moisture contents and temperatures, and with a 'ideal' drying model simulation. As can seen the droplet drying kinetics and air temperature are influenced strongly by the spray diameter. A 'reasonable' agreement is found when in the simulation a spray-diameter of 20 cm at a falling distance of 4.6 m is used, corresponding with the diameter of the 'inner' spray core. Although still (considerable) discrepancies exist between measured and calculated drying kinetics and air temperatures, the results show that an appropriate description of the spray-air mixing pattern is a prerequisite for a successful prediction of the droplet drying kinetics.

2.5 CONCLUSIONS

The change in time of the average moisture content and temperature of suspended droplets can be predicted by the droplet drying kinetics model. The approach adopted in this part of the study of using independent measured physical constants, and adjusting them, if necessary, within the existing uncertainty limits to satisfy the results of drying experiments, leads to models which can used for design or optimisation of the drying process.

The drying kinetics of equally sized free falling droplets could not be predicted. In all cases the drying rate was overestimated. An important reason is that the drying air conditions within the droplet spray did differ strongly from the surrounding drying air. This was not expected given the low 'average' droplet densities, as compared with practical spray-dryers, used in the experiments. Consequently, drying experiments aimed at verifying the

droplet kinetics model under spray-drying conditions, have to designed in such way that spray formation is avoided. Moreover drying kinetics calculations for spray-dryers which do not take into account the existence of sprays, are of very limited value.

ACKNOWLEDGEMENTS
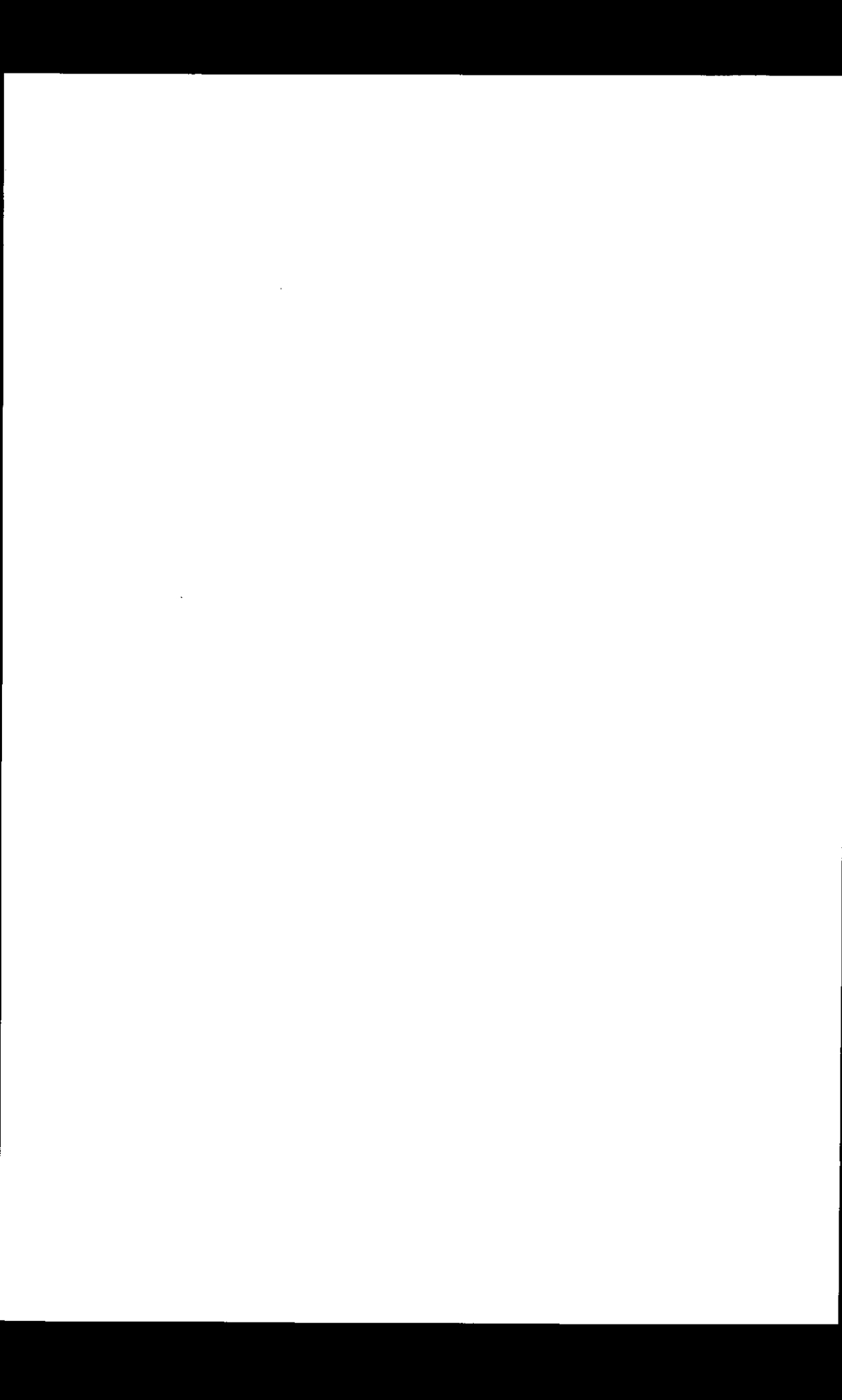
Chapter 3

INACTIVATION OF α - AMYLASE DURING DRYING

3.1 INTRODUCTION

This chapter describes the applied inactivation kinetics model and the set-up and results of
the inactivation and drying experiments. The drying kinetics model has been described in
chapter 2. The experimental inactivation data are compared with simultaneous drying and
inactivation model simulations. The experiments with the suspended droplets $(d_d \approx 1\,\text{cm})$
and those with the free falling droplets $(d_d \approx 0.02\,\text{cm})$ are discussed separately. Two
different α-amylases are used, because of the different characteristic times of the two drying
processes, 3500 s and 1.5 s, respectively. A thermostable α-amylase is used in the suspended
droplets experiments and a thermo-unstable α-amylase in the free falling droplets
experiments. Maltodextrin is used as support material in all experiments. The temperatures
used in the suspended droplets experiments are higher and the range of initial water
concentrations is wider than applied in the enzyme inactivation experiments reported before
in literature. Inactivation experiments using free falling droplets are not described in
literature.

3.2 THEORETICAL MODEL

The inactivation of enzymes can often be described as a first order reaction. The integrated
equation is:

$$\ln\left[\frac{C_e(t)}{C_e(0)}\right] = -k_e\,t \tag{3.1}$$

where C_e is the concentration active enzyme, t is the reaction time and k_e is the inactivation
constant.

The inactivation constant k_e depends on temperature and water concentration. In
literature (Kerkhof and Schoeber (1974), Wijlhuizen *et al.* (1979), Luyben *et al.* (1982),

Liou (1982) and Zimmerman (1987)) several models are used to describe this dependence. These models are all based on an Arrhenius-type equation.

$$k_e = k_\infty \exp\left(-\frac{E_a}{RT}\right) \tag{3.2}$$

where k_∞ is the pre-exponential factor, E_a is the activation energy, R is the general gas law constant, and T is the absolute temperature. The values of E_a and k_∞ can be obtained by linear regression of $\ln k_e$ vs $1/T$. None of the relations in literature are based on fundamental insights into the enzyme inactivation mechanism at different water contents. In this study also a mathematical description is used without theoretical justification.

The moisture dependence of E_a and $\ln k_\infty$ is described by the next two equations:

$$E_a = E_{a,0} + a(\omega_w)^b \tag{3.3}$$

$$\ln k_\infty = \ln k_{\infty,0} + c(\omega_w)^d \tag{3.4}$$

where ω_w is the moisture content, a, b, c and d are fitting parameters, and subscript 0 denote the value of a parameter at zero moisture content.

The parameters $a, b, c, d, E_{a,0}$ and $\ln k_{\infty,0}$ are determined by a non-linear optimisation program based on the Downhill simplex method (Press *et al.* (1989)). The sum of squares of the relative error between measured and calculated inactivation constants is used as optimisation criterion.

The residual enzyme activity during drying is calculated by combining the inactivation kinetics model and the droplet drying kinetics model. The calculation method is shown in figure 3.1. The drying kinetics model calculates the moisture concentration profiles in the droplet and the droplet temperature at each time step. The inactivation model calculates then the different inactivation constants as function of the droplet radius, and the resulting change in enzyme activity. The overall residual enzyme activity is determined by integration over the droplet radius.

START

$t_{old} = 0$

$t_{new} = t_{old} + \triangle t$

DRYING KINETICS MODEL

T_d = droplet temperature (no profile)

$C_w (r)$ = water concentration profile

INACTIVATION KINETICS MODEL

$k_e (r)$ = inactivation constant profile

1ST ORDER REACTION × Δt

$R_a (r)$ = residual enzyme activity profile

INTEGRATION OVER THE RADIUS

AVERAGE RESIDUAL ENZYME ACTIVITY

yes $t_{new} <$ t_{final}

no

STOP
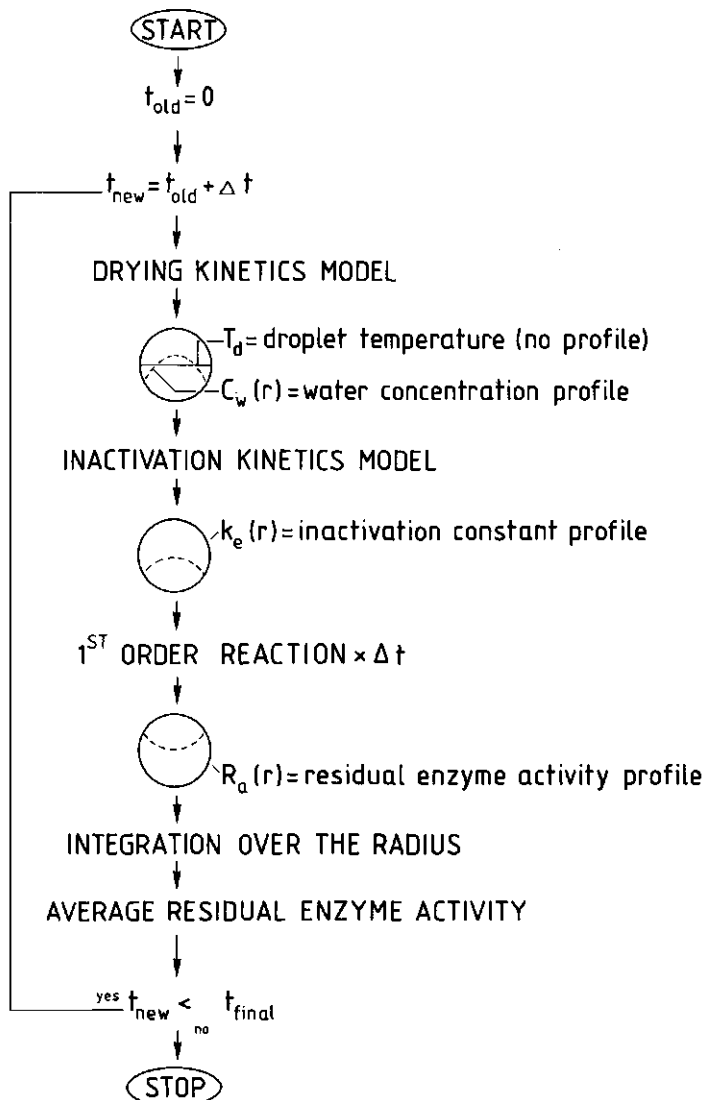
**Figure 3.1**   Calculation of the residual enzyme activity during drying.

3.3 MATERIALS AND METHODS

3.3.1 Inactivation kinetics experiments

3.3.1.1 Thermostable α-amylase

The enzyme used was a commercial thermostable α-amylase (Maxamyl, Gist-brocades nv.) from *Bacillus licheniformis*. The experiments were performed with a model system, consisting of a concentrated solution of Maxamyl, maltodextrin (MOR-SWEET 01921, D.E. 20-22, CPC), water (demineralised), $CaCl_2.2H_2O$ (Merck) and NaOH (Merck). $CaCl_2$ was added to increase the heat stability of the α-amylase (Fogarty (1983), Violet and Meunier (1989)). The pH of the model system was 5.5. During the preparation of the samples for the inactivation experiments, the pH of the model system decreased as a result of non-enzymatic breakdown reactions of the sugars present in the maltodextrin (Feather and Harris (1973)). Just that amount of NaOH was added to obtain a pH of the samples of 5.5 before the inactivation experiments were performed. In the preparation procedure the enzyme activity did not change.

The standard enzyme solution was: maltodextrin (m_m = 0.35 mass fraction), water (demineralised, m_w = 0.65 mass fraction), $CaCl_2$ (1 mM $CaCl_2$(kg maltodextrin)$^{-1}$) and Maxamyl (5 10^{-4} ml Maxamyl(kg maltodextrin)$^{-1}$). The pH of the solution was adjusted with 0.01 N NaOH. In the experiments inactivation cells were used (Liou (1982)). The inactivation cells (see figure 3.2) consisted of two sections, with the enzyme solution in between. Low initial water concentrations were obtained by adjusting the water content of the standard solution by pre-drying to the desired moisture content. For pre-drying the bottom section was placed in a drying stove at 70 °C and reduced pressure. After pre-drying the cells were stored for 24 h in a refrigerator to equilibrate the moisture concentration.


layer with enzyme   1 cm
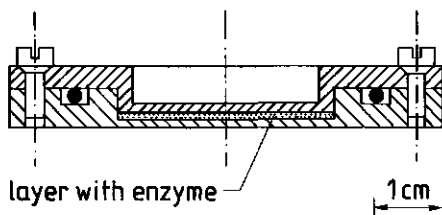
Figure 3.2   Inactivation cell (Liou (1982)).

Usually 8 inactivation cells were used, with two of them serving as reference samples. The 6 others were immersed in a thermostated (+/- 0.2 °C) glycerol bath for different time periods. The time for 99% temperature equilibration within the inactivation cells can be estimated to be 150 seconds. After the heat treatment the cells were cooled in melting ice. The treated samples were then rehydrated to obtain the standard enzyme solution ($m_w = 0.65$ mass fraction). Next the α-amylase activity of the treated samples was measured and compared with the α-amylase activity of the reference cells. In this way the change in the enzymatic activity with time could be followed at a given temperature and water content.

The α-amylase activity was determined with a slightly modified Phadebas amylase test (Pharmacia Diagnostics AB, Uppsala, Sweden). Instead of distilled water a 10 mM Na-maleate buffer with 50 ppm Ca^{2+} was used. The pH of the assay was 6.5. Samples of 100 μl of the standard solution were used in the analysis. A linear relation was found between the enzyme concentrations as used in the experiments and the measured α-amylase activity in the presence of maltodextrin. The accuracy of the analysis as determined from duplicated experiments was 5 %.

In the experiments performed, the water content varied between 1.86 (= 0.65 on total basis) and 0.09 kg H_2O(kg ds)$^{-1}$, and the temperature between 100 °C and 130 °C.

3.3.1.2 Thermo-unstable α-amylase

A commercial thermo-unstable α-amylase (Fungamyl, Novo Nordisk) from *Aspergillus Oryzae* was used. In general the same materials and methods were used as in the inactivation experiments with the thermostable α-amylase. The differences were: the mass fraction water in the standard enzyme solution was 0.70, the initial pH of the standard solution was 6.5, the amount of added Fungamyl solution was 2 10^{-4} ml(kg maltodextrin)$^{-1}$, the pre-drying of the enzyme solutions was performed at 50 °C and a water bath was used. The time for 99% temperature equilibration within the inactivation cells is 5 s in the water bath. The water content varied between 0.11 and 2.33 kg H_2O(kg ds)$^{-1}$, and the temperature between 75 and 100 °C.

3.3.2 Drying experiments

3.3.2.1 Suspended droplets

Themostable α-amylase (Maxamyl) was used in the suspended droplet experiments. The enzyme inactivation rate and the drying kinetics were determined simultaneously. The drying apparatus and the determination of the drying kinetics is described in more detail in chapter 2.3.1. The composition of the dry solids of the droplets equaled the standard solution used in the inactivation experiments, except that the amount of added Maxamyl was increased 10 fold in order to have a measurable amount of enzyme activity after rehydration of the dried droplets. The droplets were adjusted to pH 5.5 with 0.01N NaOH before the drying experiments were performed. The droplets were jellified with agar (Merck, 2.0 % on total basis). The droplets were produced by using a perspex mould with a diameter of 1 cm. For drying experiments with low initial water contents the droplets were pre-dried at 70 °C. In a drying experiment about 10 droplets were dried simultaneously. At different times a droplet was removed and the water concentration and residual enzyme activity were determined. In each experiment two droplets were not dried but used as reference samples. The water content of the dried droplets was determined by weighing the droplets before and after the drying experiment. For the determination of the residual α-amylase activity the dried droplets were rehydrated again by boiling (10 minutes) in a concentrated maltodextrin solution ($m_w = 0.49$, $CaCl_2 = 90$ ppm). After that the water content was adjusted to 65 % on total basis. The enzyme activity in this solution was measured in the same way as in the inactivation kinetics experiments. The resolving procedure and the boiling step did not give a significant reduction in enzyme activity. The accuracy of the measuring procedure of the enzyme activity as determined from duplicated experiments was 10 %.

The initial water content varied between 3.0 and 0.47 kg H_2O(kg ds)$^{-1}$ in the drying experiments. The temperature of the drying air varied between 97 and 105 $\pm$ 0.5 °C and the air velocity was 2.5 $\pm$ 0.5 m/s.

3.3.2.2 Free falling droplets

The thermo-unstable α-amylase (Fungamyl) was used in the free falling droplet experiments. The experiments were performed in a drying tower as described in chapter 2.3.2.1. In the tower equally sized (uniform) droplets can be dried at constant external drying conditions. The dry solids composition of the droplets was the same as used in the inactivation kinetics

experiments. The drying kinetics was determined using the methods as described in chapter 2.3.2.2. The residual enzyme activity of the droplets was measured after rehydration to a water content of 0.70 kg H_2O(kg total)$^{-1}$. The amount of water to be added was based on the determination of the water content of the droplets before rehydration, using the same sample. The enzyme activity was measured in the same way as in the inactivation kinetics experiments.

In the drying experiments the initial moisture content and droplet diameter were 1.7 kg H_2O(kg ds)$^{-1}$ and 204 μm, respectively. The temperature of the drying air varied between 110 and 150 °C.

3.4. RESULTS AND DISCUSSION

### 3.4.1 Inactivation kinetics experiments

The results of the inactivation kinetics experiments are given in the figures 3.3 and 3.4. The measured and calculated inactivation constants k_e for the thermostable and thermo-unstable α-amylase are given in the tables 3.1 and 3.2, respectively. The moisture dependencies of the estimated E_a and $\ln k_\infty$ values are given in the figures 3.5 and 3.6. The inactivation constant data are fitted to the inactivation kinetics model as given by the equations 3.2, 3.3 and 3.4. The obtained parameter values are given in table 3.3. The drawn curves in the figures 3.4, 3.5, 3.6 and the calculated k_e values in the tables 3.1 and 3.2 are calculated with the estimated parameter values and the equations 3.2, 3.3 and 3.4.

The characteristic times of the inactivation experiments τ_r (defined as: $\tau_r = k_e^{-1}$) are at least 5 times the time needed for 99% temperature equilibration within the inactivation cells. Consequently it can be assumed that on the time scale of the inactivation kinetics experiments, the temperature within the inactivation cells equals the temperature of the water or glycerol bath.

From figure 3.3 it can be concluded that the thermal inactivation of both α-amylases can be described by a first order reaction. The experimental results, as shown in the figure 3.4, are fully in agreement with the general assumption that the heat stability of an enzyme increases at lower moisture contents.

$$\ln (C_e(t)/C_e(o)) \ (-)$$
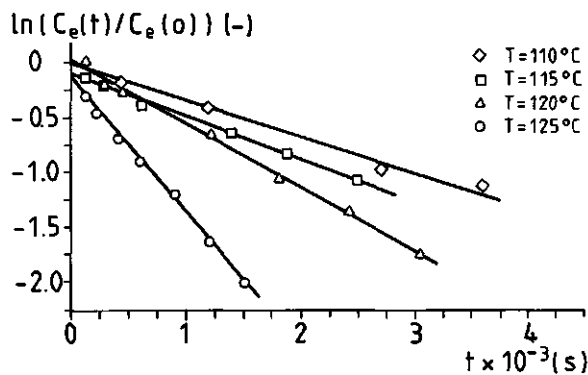
a   Thermostable α-amylase, $\omega_w = 0.45 \, \mathrm{kg\,H_2O(kg\,ds)^{-1}}$.

$$\ln (C_e(t)/C_e(o)) \ (-)$$
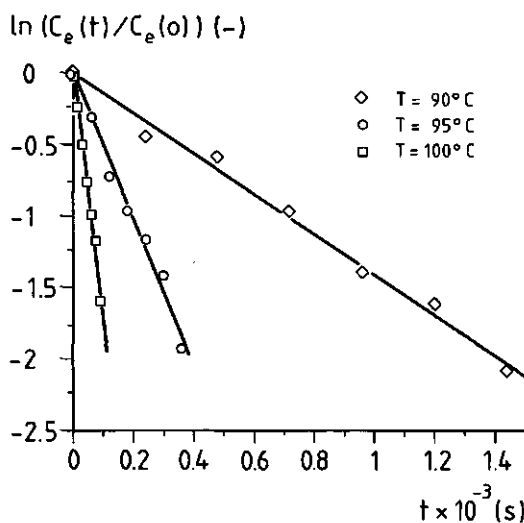
b   Thermo-unstable α-amylase, $\omega_w = 0.18 \, \mathrm{kg\,H_2O(kg\,ds)^{-1}}$.

Figure 3.3   The residual α-amylase activity as function of time at different temperatures and one water content. ———: best fit.
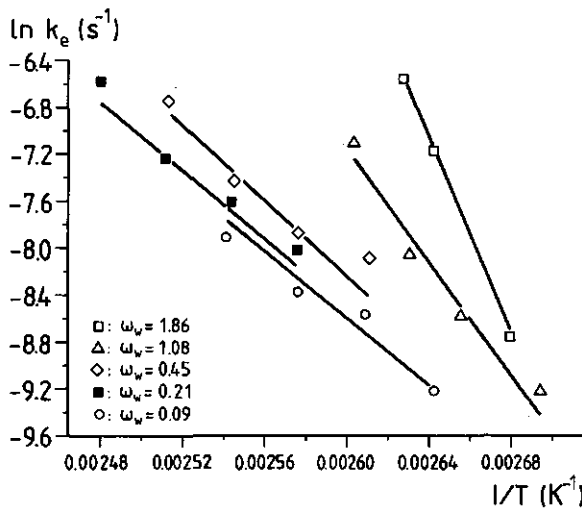
a   Thermostable α-amylase.
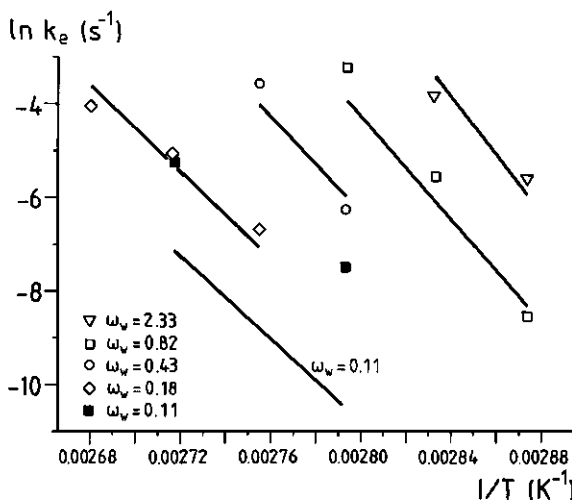
b   Thermo-unstable α-amylase

Figure 3.4   Arrhenius plots of the inactivation constant k_e at different temperatures and water
concentrations. ————: calculated by the inactivation kinetics model using the parameter
values from table 3.3.

Table 3.1 Inactivation constants k_e of the thermostable α-amylase.

ω_w kg H$_2$O(kg ds)$^{-1}$	T °C	k_e [1] (measured) 10^{-4} s	k_e (calculated) 10^{-4} s
1.86	100.3	1.6	1.7
	105.5	7.7	7.9
	107.7	14	15
1.08	98.2	1.0	0.81
	103.6	1.9	2.1
	107.1	3.2	3.7
	111.1	8.4	7.1
0.45	110.0	3.1	2.2
	115.3	3.8	3.9
	120.0	5.9	6.4
	124.9	12	10
0.21	115.3	3.3	2.9
	120.2	5.0	4.6
	125.3	7.2	7.4
	130.3	14	11
0.09	105.4	1.0	1.0
	110.3	1.9	1.6
	115.2	2.3	2.6
	120.5	3.7	4.2

1) the average of the in experiment 95% confidence interval is 23%.

The experimental results found by Liou (1982) indicate that the heat stability shows an optimum for the enzyme lipoxygenase at a water content of around 0.35 kg H$_2$O(kg ds)$^{-1}$, while it decreases again at lower water concentrations. This certainly is not the case for the enzymes used in this study, given the range of water concentrations and temperatures studied.

The E_a and $\ln k_\infty$ value decrease at lower water contents for both enzymes, similar results are found in literature (Daemen (1981), Liou (1982), Yamamoto *et al.* (1985, 1992), Zimmermann (1987)). The estimated E_a values are in the same range as found in literature. As a result of the decrease of E_a the temperature sensitivity of the enzyme inactivation decreases with decreasing moisture content. The accuracy of the E_a and $\ln k_\infty$ values of the thermo-unstable α-amylase, however, is very limited. The inactivation constants at a certain

Table 3.2 Inactivation constants k_e of the thermo-unstable α-amylase.

ω_w kg H$_2$O(kg ds)$^{-1}$	T °C	k_e [1,2] (measured) 10^{-4} s	k_e (calculated) 10^{-4} s
2.33	75	3.7	2.6
	85	20	33
0.82	75	0.19	0.25
	80	3.9	2.3
	85	40	20
0.43	85	1.9	2.5
	90	28	18
0.18	90	1.4	0.84
	95	5.8	4.8
	100	19	26
0.11	85	0.55	0.027
	95	6.1	0.80

1) the values given are the average of at least two experiments.

2) the average of the between experiment 95% confidence interval is 70%.

moisture content were measured at two or three different temperatures only and in a small temperature range (10 °C at maximum). Furthermore the estimated E_a and $\ln k_\infty$ values are strongly correlated, in such a way that low and high values for E_a correspond with low and high values for $\ln k_\infty$, respectively.

The estimated parameter values given in table 3.3 must be interpreted with caution, because of the correlation between the different parameters. The moisture and temperature dependence of the inactivation constants of the enzymes can be described by different sets of fitting parameters with almost the same value for the applied optimisation criterion. This is caused by the fact that the number of experimental data is small (19 and 12, respectively) compared with the number of fitting parameters (6). Extrapolation of the results to higher or lower temperatures therefore must be done with great care.

The inactivation kinetics model gives a good description of the experimental data of the thermostable α-amylase. The average discrepancy between measured values and model predictions of k_e is 13 %. Also the water concentration dependencies of E_a and $\ln k_\infty$ are described well.

a E_a dependency.
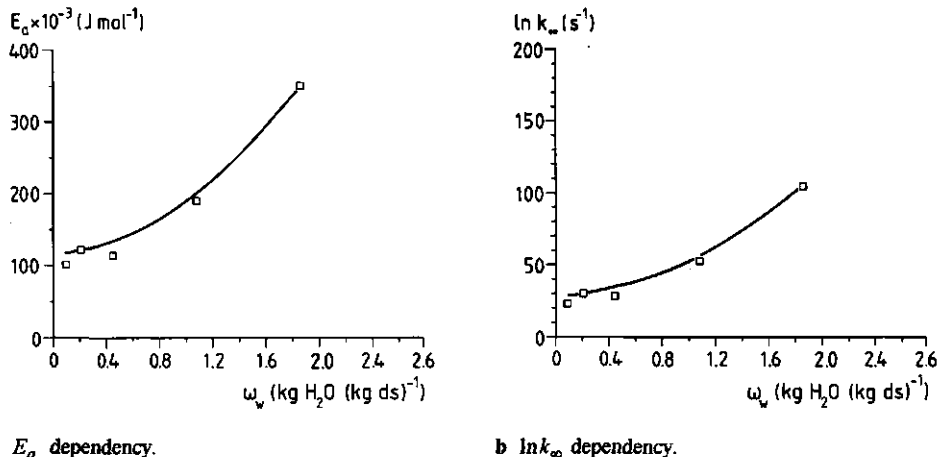
b $\ln k_\infty$ dependency.

Figure 3.5   The water concentration dependencies of E_a and $\ln k_\infty$ of the thermostable α-amylase.
□: calculated from measured inactivation data; ———; calculated by the inactivation
kinetics model using the parameter values from table 3.3.

a E_a dependency.
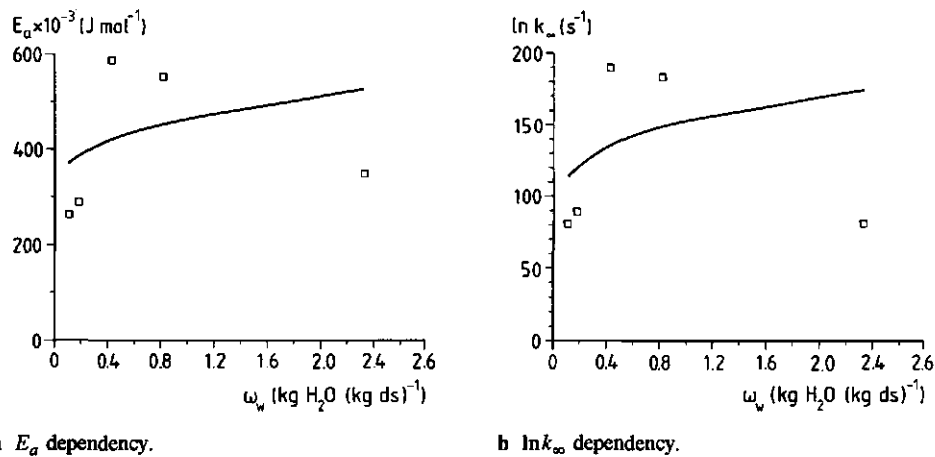
b $\ln k_\infty$ dependency.

Figure 3.6   The water concentration dependencies of E_a and $\ln k_\infty$ of the thermo-unstable α-amylase.
□: calculated from measured inactivation data; ———; calculated by the inactivation
kinetics model using the parameter values from table 3.3.

Table 3.3 Parameter values in the inactivation kinetics model.

Parameter	Value thermostable α-amylase	Value thermo-unstable α-amylase
$E_{a,0}$	117.3	245.1
a	71.5	221.6
b	1.88	0.26
$\ln k_{\infty,0}$	28.1	44.8
c	23.7	108.7
d	1.86	0.21

The description of the experimental data of the thermo-unstable α-amylase by the inactivation kinetics model is not very satisfactory. The average discrepancy between experimental inactivation constants and model predictions is 50 %. It is not expected, however, that other empirical relations, with the same number of parameters, improve the description of the experimental data significantly. As can be seen from figure 3.4b there is a tendency to underestimate the inactivation rate of the thermo-unstable α-amylase at higher temperatures. Consequently it is expected that the inactivation rate will be underestimated at the temperatures used in the drying experiments. Moreover, as will be shown in paragraph 3.4.2.2, the inactivation takes place at 'intermediate' moisture contents (about 0.4 kg H_2O(kg ds)$^{-1}$). In order to improve the description of the inactivation constants in particular at intermediate moisture contents, the parameters of the inactivation model are estimated again by omitting the inactivation constants obtained at a moisture content of 2.33 kg H_2O(kg ds)$^{-1}$. Furthermore it was assumed that the relation between E_a and $\ln k_{\infty}$, and the water concentration is linear and consequently the fitting parameters b and d are equal to 1. The estimated parameter values are given in table 3.4. As shown in figure 3.7 the description of the inactivation constants at intermediate moisture contents has been improved, as anticipated. The average discrepancy between model predictions and experimental inactivation constants, used in the parameter estimation, is 34 % instead of 47 % by the non-linear model.

Table 3.4   Parameter values of the linear inactivation kinetics model.

| Parameter	Value thermo-unstable α-amylase
$E_{a,0}$	247.3
a	341.0
b	1
$\ln k_{\infty,0}$	73.9
c	121.8
d	1
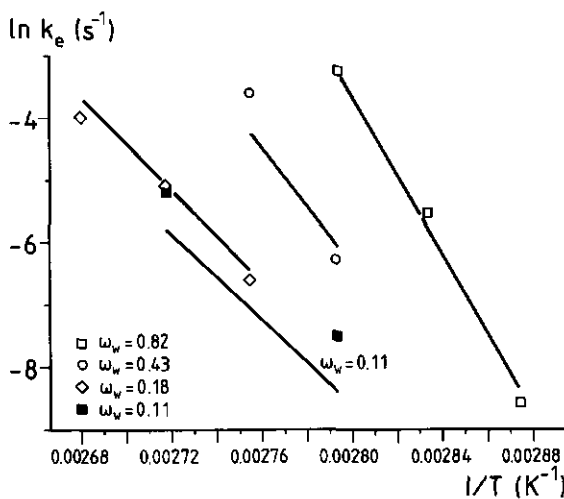
Figure 3.7   Arrhenius plots of the inactivation constant k_e of the thermo-unstable α-amylase at different temperatures and water concentrations. ————: calculated by the inactivation kinetics model using the parameters values from table 3.4.

The expected difference in thermostability of both enzymes is clearly reflected by the obtained results. The (estimated) inactivation constants of the thermo-unstable α-amylase at 100 °C are four orders of magnitude larger than those of the thermostable α-amylase. The calculated characteristic times of the inactivation process τ_r at 100 °C and 0.4 kg H_2O(kg ds)$^{-1}$ are for the thermo-unstable and thermo-stable α-amylase 1.7 s and 14100 s, respectively.

Violet and Meunier (1989) found a two stage inactivation kinetics for *Bacillus licheniformis* α-amylase at temperatures lower than 85 °C. Tomazic and Klibanov (1988a, b) have studied the mechanism of the irreversible thermal inactivation of different *Bacillus α*-amylases in dilute aqueous solutions. They found that two different mechanisms can be responsible for the thermal inactivation of the *Bacillus licheniformis* α-amylase: the monomolecular conformational change of the enzyme and the deamidation of the asparagine and glutamine residues. The determined activation energies E_a of both inactivation mechanism differ and are about 300 and 100 kJ mol^{-1}, respectively. Given their results and the values found in this study for the activation energy E_a of the inactivation process at different water concentrations (see figure 3.5a) it might be that these two mechanisms are also responsible for the thermal inactivation of the thermostable α-amylase used in this study. The possible existence of two inactivation mechanisms with different activation energies should result in curved Arrhenius-plots. This is, however, not found in this study. Moreover to determine the existence of such curved plots, the inactivation kinetics experiments have to be performed using a much wider temperature range as has been done in this study.

3.4.2. Drying experiments

3.4.2.1. Suspended droplets

- Model simulation
Figure 3.8 shows the inactivation of the thermostable α-amylase in a suspended droplet. The drying process as such is discussed in chapter 2.4.1. It can been seen that the enzyme activity starts to decrease when the droplet temperature approaches the temperature of the drying air. This can be explained by the differences between the characteristic times of the drying process, the temperature increase and the inactivation reaction. During a large part of
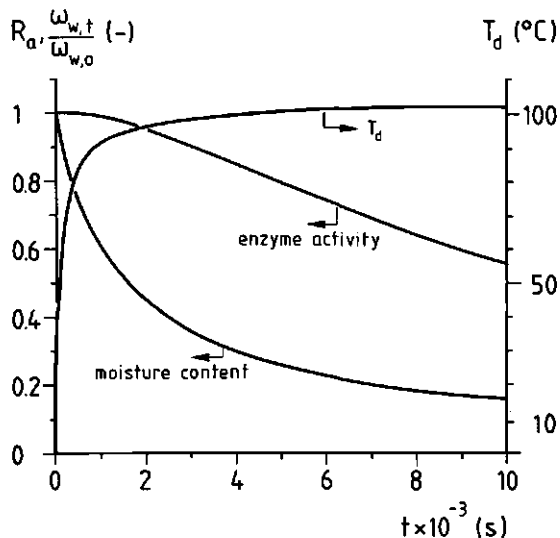
Figure 3.8   Model simulation. The changes in time are given of the water concentration, droplet
temperature and residual enzyme activity. Initial conditions (see also figure 2.3):
$\omega_{w,0} = 1.25\,\mathrm{kgH_2O(kgds)}^{-1}$, $d_{d,0} = 0.01\mathrm{m}$, $T_g = 102.5\,°\mathrm{C}$, $v_g = 2.5\,\mathrm{ms}^{-1}$ and
$H = 0\,\mathrm{kgH_2O(kgda)}^{-1}$. Physical data table 2.2, applying the adapted relation for the
activation energy; kinetic data table 3.3 (thermostable α-amylase).

the drying process the droplet temperature is almost equal to the drying air temperature,
since the characteristic time for drying τ_d is much larger than that for heat transfer τ_h
($\tau_d\,(=3500\,s) >> \tau_h\,(=300\,s)$) (see chapter 2.4.1 and figure 2.3). The (calculated)
characteristic times of the inactivation reaction τ_r at the drying air temperature (102.5 °C)
varies from 5000 s, at the initial moisture content, to 13000 s when the moisture content is
zero. Both values are larger than the characteristic time of drying. Consequently the enzyme
inactivation takes mainly place when the droplet temperature approaches the drying air
temperature.

Figure 3.9 shows the steep water concentration profiles which occur during drying. As a
result an inactivation constant profile is present, caused by the water concentration
dependence of the inactivation constant at constant temperature (see also figure 3.1). The
inactivation constant at the droplet centre (high moisture content) is higher than at the
surface (low moisture content). Consequently a residual enzyme activity profiles develops in
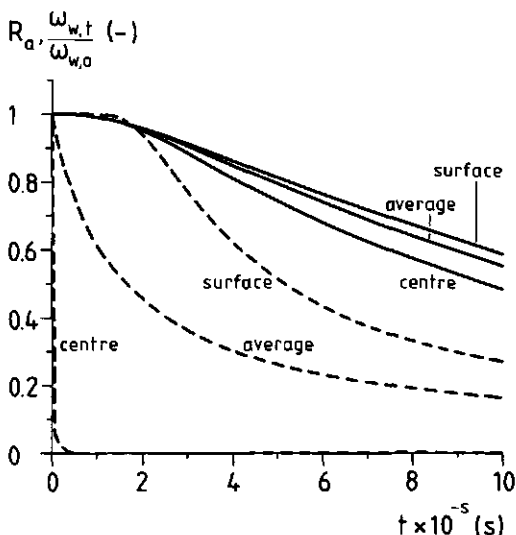
Figure 3.9 The change in time of the surface, centre and average water concentrations and residual enzyme activities. Initial conditions: see figure 3.8. — —: water concentration; ————: residual enzyme activity

such a way that the residual enzyme activity in the centre is lower than at the surface of the droplet.

- Sensitivity analysis

A sensitivity analysis, similar as discussed in chapter 2.3.1, was performed to investigate the influence of small parameter variations around their base-case values on the residual enzyme activity after a drying time of 7200 s, for the example given in figure 3.8. The results are depicted in figure 3.10. The most important parameters influencing the predicted residual enzyme activity are the drying air temperature (as expected), the external transfer coefficients and the air velocity. The effect of the latter two is a result of the fact that the heat transfer is externally limited (see chapter 2.2). The maximum change in the residual activity in figure 3.10 corresponds to an error of 50% in the estimated value for the inactivation constant k_e. An error of such a size can easily occur given the fact that in the

model simulation an extrapolation of the measured k_e values takes place to lower temperatures as well as to lower moisture contents.
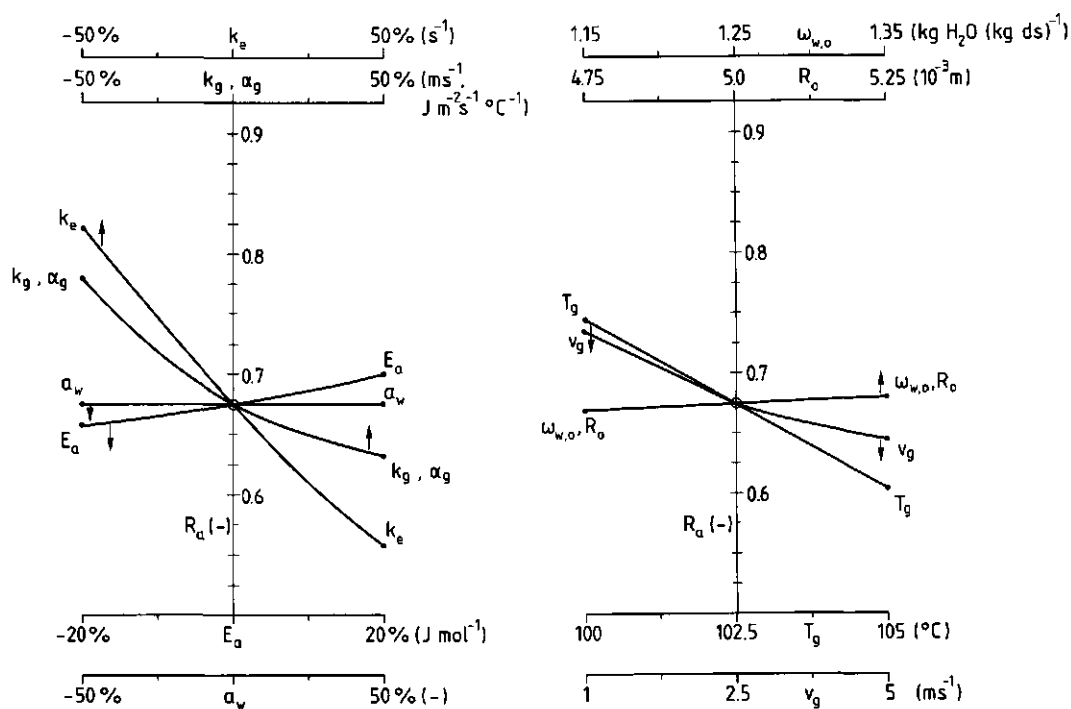
a Influence of variations in physical parameters.   b Influence of variations in experimental conditions.

Figure 3.10   Influence of changes in important variables on the residual enzyme activity. Base-case values: see figure 3.8. Drying time 7200 s.

- Experimental results and model simulations

The experimental results of the drying experiments at the four different initial water contents (3.0, 1.86, 1.04 and 0.47 kg H_2O(kg ds)$^{-1}$) are shown in the figure 3.11. The results for the first stage of a drying experiment (initial water content was 1.04 kg H_2O(kg ds)$^{-1}$) are plotted in figure 3.11e. The modelling of the drying kinetics has been discussed in chapter 2.4.1.

The drying model gives an adequate description of the experimental residual enzyme activities. The estimated residual enzymes activities are within, or nearly within, the 50% 'uncertainty limits' represented by the dotted lines, except for the experiment with an initial moisture content of 3 kg H_2O(kg ds)$^{-1}$. However, it seems that there is a tendency that higher intitial moisture contents results in higher experimental inactivation rates as calculated by the drying model. In the experiment with an initial water concentration of 3 kg H_2O(kg ds)$^{-1}$ a considerable inactivation occurs at relatively low temperatures (approx. 85 °C) and high average water contents (approx. 2.5 kg H_2O(kg ds)$^{-1}$). This discrepancy can not be explained by small variations in experimental and physical parameters (see figure 3.10). To predict the experimental inactivation data, the inactivation constant in the model must be increased by a factor 25. The reason for this high inactivation is not understood.

### 3.4.2.2. Free falling droplets

- Model simulation

Figure 3.12 shows the inactivation of the thermo-unstable α-amylase in a free falling droplet. An important assumption is that the external drying air temperature and humidity are constant. The residual enzyme activities are calculated using the non-linear as well as the linear kinetics model. The drying process as such is discussed in chapter 2.4.2.

The enzyme inactivation, as calculated by using the non-linear model, 'starts' (residual enzyme activity is 99%) at an average moisture content and droplet temperature of 0.56 kg H_2O(kg ds)$^{-1}$ and 91 °C, respectively. A residual α-amylase activity of 50% is reached when these values are 0.25 kg H_2O(kg ds)$^{-1}$ and 110 °C. The (calculated) inactivation constants k_e belonging to these values are 0.05 s^{-1} and 0.5 s^{-1}, corresponding to characteristic inactivation times τ_r of 20 s and 2 s, respectively. These values are in the same order of magnitude as the characteristic times of the drying process ($\tau_d = 1.5$ s) and heat transfer ($\tau_h = 2$ s). Accordingly the enzyme inactivation takes place at an 'intermediate' stage of the drying process.
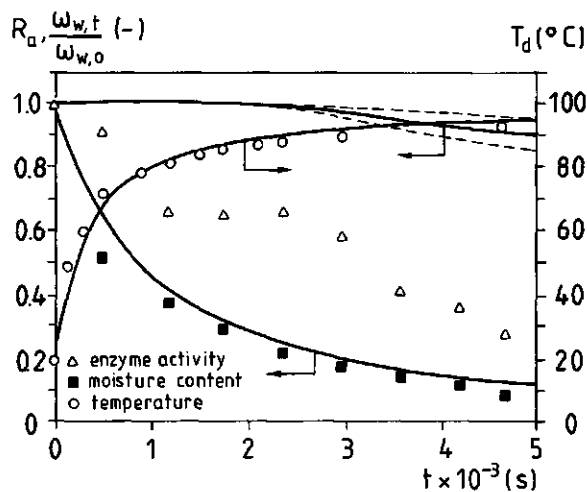
a Experimental conditions: $\omega_{w,0} = 3\,\mathrm{kg\,H_2O(kg\,ds)}^{-1}$, $d_{d,0} = 0.01\,\mathrm{m}$, $T_g = 97\,^{\circ}\mathrm{C}$ and $v_g = 3.8\,\mathrm{ms}^{-1}$.
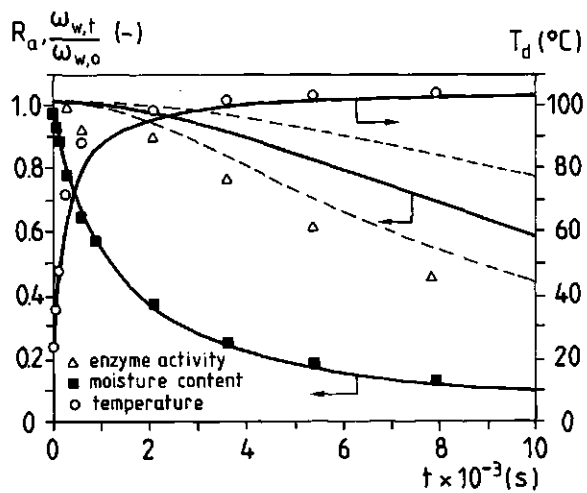
b Experimental conditions: $\omega_{w,0} = 1.86\,\mathrm{kg\,H_2O(kg\,ds)}^{-1}$, $d_{d,0} = 0.01\,\mathrm{m}$, $T_g = 103\,^{\circ}\mathrm{C}$ and $v_g = 2.4\,\mathrm{ms}^{-1}$.

Figure 3.11   Enzyme inactivation during drying; the changes in time are given of the water concentration, droplet temperature and residual enzyme activity. ———: model simulation, physical data table 2.2, applying the adapted relation for the activation energy, kinetic data table 3.3 (thermostable α-amylase); — —: uncertainity limits, calculated by applying inactivation constants which differ +/- 50 % from the calculated constants using the inactivation kinetics model. H is in all experiments $0\,\mathrm{kg\,H_2O(kg\,da)}^{-1}$.
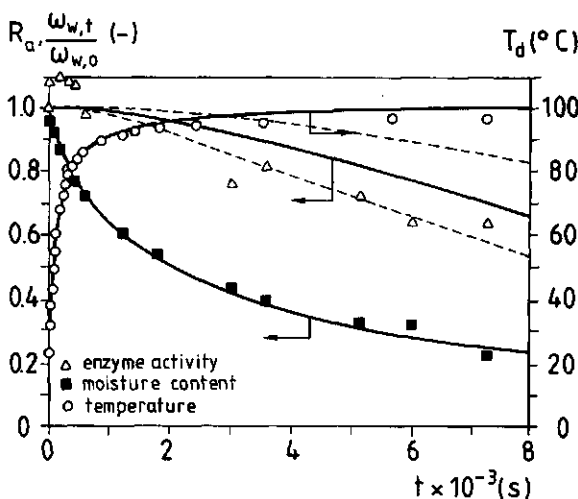
Figure 3.13c   Experimental conditions: $\omega_{w,0} = 1.04\ \mathrm{kg\,H_2O(kg\,ds)}^{-1}$, $d_{d,0} = 0.01\mathrm{m}$, $T_g = 101\ °\mathrm{C}$ and
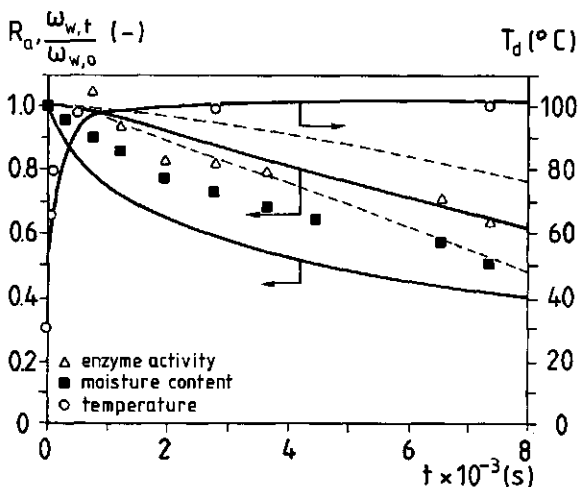
$v_g = 2.5\,\mathrm{ms}^{-1}$.

Figure 3.13d   Experimental conditions: $\omega_{w,0} = 0.47\ \mathrm{kg\,H_2O(kg\,ds)}^{-1}$, $d_{d,0} = 0.0086\mathrm{m}$, $T_g = 101.5\ °\mathrm{C}$

and $v_g = 2.5\,\mathrm{ms}^{-1}$.
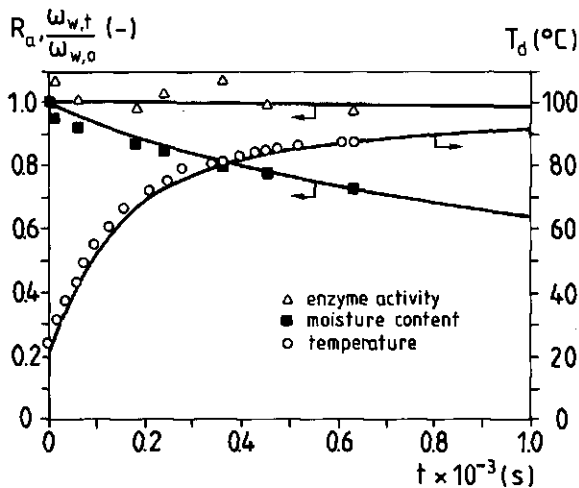
Figure 3.11e   Enzyme inactivation during the first stage of drying. Experimental conditions: $\omega_{w,0} = 1.04 \text{ kg H}_2\text{O}(\text{kgds})^{-1}$, $d_{d,0} = 0.01\text{m}$, $T_g = 101\,°\text{C}$ and $v_g = 2.5\text{ms}^{-1}$.
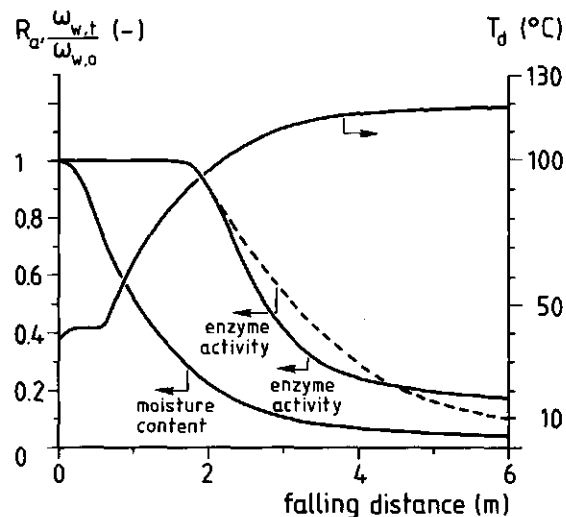

Figure 3.12   Model simulation. The water concentration, droplet temperature and residual enzyme activity are given as function of the falling distance. Initital conditions: $\omega_{w,0} = 2 \text{ kg H}_2\text{O}(\text{kgds})^{-1}$, $d_{d,0} = 200\,\mu\text{m}$, $T_g = 120\,°\text{C}$, $v_{d,0} = 10\text{ ms}^{-1}$, $v_g = 0.2\text{ ms}^{-1}$ and $H = 0.025\text{kg H}_2\text{O}(\text{kgda})^{-1}$ (see also figure 2.9). Physical data table 2.2, applying the adapted relation for the activation energy. ————: kinetic data table 3.3 (thermo-unstable α-amylase); — —: kinetic data table 3.4.

From figure 3.12 it can be seen the that final residual enzyme activity as calculated with the linear inactivation kinetics model is lower than obtained by applying the non-linear model. Also in case of the linear model the inactivation takes place at intermediate moisture concentrations and droplet temperatures. A residual enzyme activity of 50 % is reached when the average moisture content is 0.20 kg $H_2O(kg\ ds)^{-1}$ and at a droplet temperature of 113 °C. In the simulation it is assumed that if the moisture content is higher than 0.82 kg $H_2O(kg\ ds)^{-1}$, then the E_a and $\ln k_{\infty}$ values become constant and equal to the values at 0.82 kg $H_2O(kg\ ds)^{-1}$. In this way it is avoided that extrapolation of the linear model to higher moisture contents results in activation energy values which are much higher than feasible for enzyme inactivation.

- Sensitivity analysis

A sensitivity analysis similar as described in chapter 3.4.1 is performed. The variations of the residual enzyme activity around the base-case value, as caused by the parameter variations, are shown in figure 3.13. The falling distance is 2.6 m (sample port 4). The residual enzyme activity is calculated by applying the linear inactivation kinetics model.

In the base-case the average moisture content, temperature and residence time of the droplet are 0.28 kg $H_2O(kg\ ds)^{-1}$, 107 °C and 3.25 s, respectively. The variations in the residual enzyme activity are a result of the combined effect of changes in droplet temperature, moisture content and residence time. In most cases the changes offset each other, for example: a lower droplet temperature goes with a higher moisture content, assuming the same residence time. An increase of 0.01 kg $H_2O(kg\ ds)^{-1}$ in moisture content, 1 °C in temperature and 0.1 s in residence time of the droplet with respect to the base-case values, corresponds to relative changes in the inactivation constant of +12 %, +33% and +16%, respectively. The parameters which strongly influence the residual enzyme activity are the drag coefficient, the external transfer coefficients and the drying air temperature. The drag coefficient mainly influences the residence time of droplets, while the other two parameters determine the temperature history of the droplets. The maximum change in the residual activity in figure 3.13 is caused by the C_d change. The second maximum change corresponds to a change in the estimated value for k_e with a factor 3.
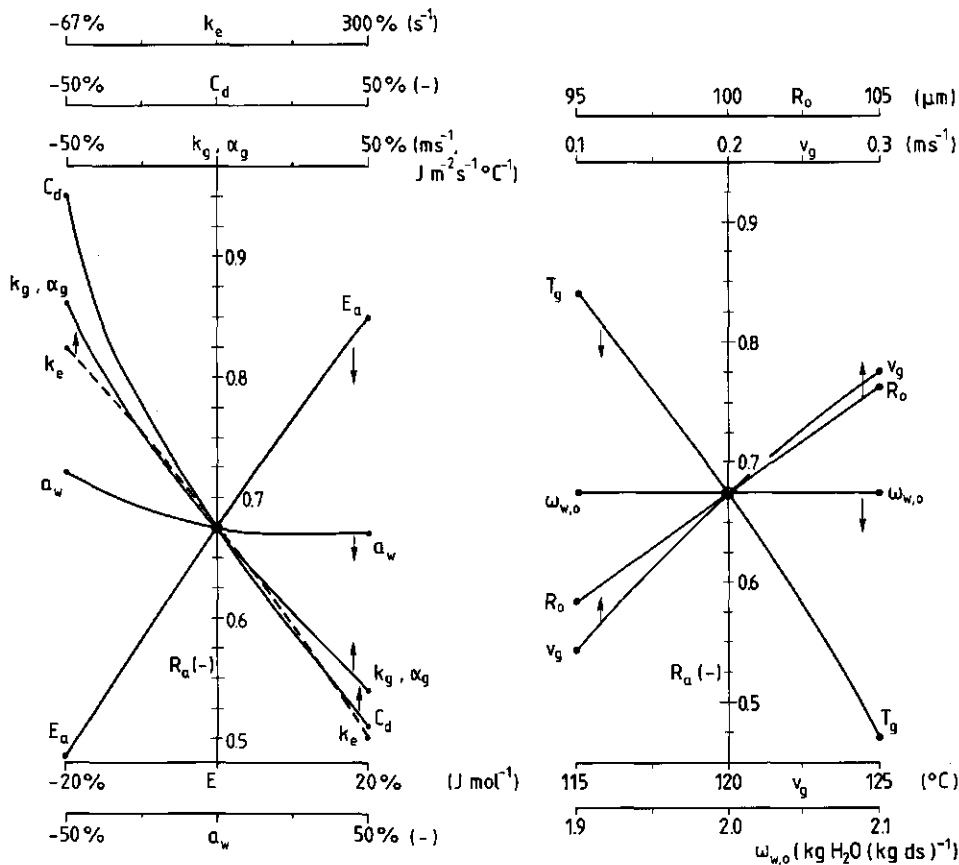
a Influence of variations in physical parameters.   b Influence of variations in experimental conditions.

Figure 3.13   Influence of changes in important variables on the residual enzyme activity. Base-case
               values: see figure 3.12. Falling distance 2.6 m. Kinetic data table 3.4.

- Experimental results and model simulations

In figure 3.14a the results of a drying experiment at 130 °C are shown. The experimental conditions used are almost the same as in figure 2.13c. The values given are the average of a duplicate experiment. The lines in figure 3.14a are calculated using the 'ideal' drying model, assuming constant air temperature and humidity, as well as the 'spray' drying model as discussed in chapter 2.4.2. The modelling of the drying kinetics as such is discussed in chapter 2.4.2.

The experimental drying kinetics agree with the experimental drying kinetics as shown in figure 2.13c. The enzyme inactivation takes place at an 'intermediate' stage of the drying process, as discussed before. As can seen from figure 3.14a the 'ideal' drying model overestimates the drying and inactivation rate. The overestimation of the drying rate has been discussed in chapter 2.4.2. In that chapter it is shown that the assumption is not valid that during drying the air temperature and humidity are constant. A 'spray' drying model resulted in an improved description of the experimental drying kinetics. When applying the 'ideal' drying model, the experimental enzyme inactivation can be described only by decreasing the inactivation constant with a factor 15. Parameter variations as discussed in the sensitivity analysis can therefore not explain this overestimation, with exception of the drag coefficient C_d. Furthermore the non-linear inactivation kinetics model using the parameter values of table 3.3, resulted in a similar overestimation. Consequently the overestimation of the enzyme inactivation might also primarily be a result of the 'spray' character of the drying process.

Application of the 'spray' drying model, represented by the drawn lines in figure 3.14a, results in a good description of the drying kinetics as well as a better description of the residual enzyme activity. The applied spray diameter of 0.35 m at a falling distance of 4.6 m, is a reasonable estimate of the 'inner' spray-core as discussed in chapter 2.4.2. In figure 3.15 the calculated droplet temperatures, and calculated and experimental residual enzyme activities are depicted using both drying models. The results show that the main reason for the shift of the residual enzyme activity values lies in the consequently lower droplet temperatures in the 'spray' model, caused by the lower air temperatures in the spray (see figure 2.15b).

The experimental results obtained at a drying air temperature of 150 °C show the same trends as those at 130 °C, see figure 3.14b. The drying kinetics can also be described reasonable by the 'spray' drying model, applying the same spray diameter of 0.35 m. In the drying experiments at 130 °C and evenmore at 150 °C, the inactivation rate at short falling distances is underestimated. At large falling distances it is overestimated to some extent.

$\dfrac{\omega_{w,t}}{\omega_{w,o}}, R_a \ (-)$

□ moisture content
○ enzyme activity

falling distance (m)

a $T_g = 130\,°C$

$\dfrac{\omega_{w,t}}{\omega_{w,o}}, R_a \ (-)$

□ moisture content
○ enzyme activity

falling distance (m)

b $T_g = 150\,°C$
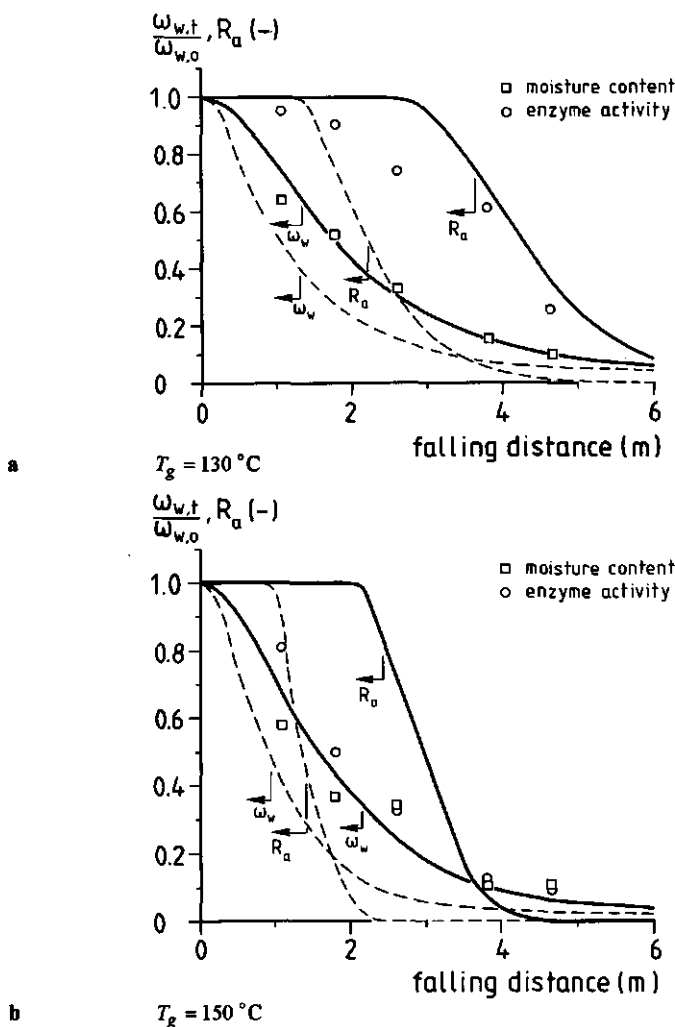
Figure 3.14   Enzyme inactivation during drying. The water concentration and residual enzyme activity are given as function of the falling distance. Experimental conditions: $\omega_{w,0} = 1.7\ \mathrm{kg\,H_2O(kgds)^{-1}}$, $d_{d,0} = 204\,\mu m$ and $H = 0.025\,\mathrm{kg\,H_2O(kgda)^{-1}}$. The temperature of the drying air is given at each figure. Physical data table 2.2, applying the adapted relation for the activation energy; kinetic data table 3.4. — —: 'ideal' drying model; ————: 'spray' drying model, a spray-diameter of 0.35 m at a falling distance of 4.6 m (sample port 6) is applied. The average relatieve error in a duplicate residual enzyme activity measurement is 20%.
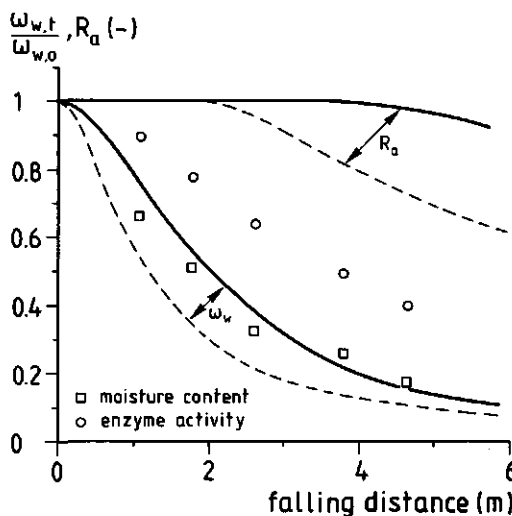
Figure 3.14c $T_g = 110\,^{\circ}C$

The experimental results obtained at a drying air temperature at 110 °C, as given in figure 3.14c, are with respect to the drying kinetics in accordance with the results at 130 and 150 °C. The experimental inactivation rate, however, differs strongly from the 'ideal' as well as the 'spray' drying model simulation. The experimental inactivation rate, as measured in a duplicate experiment, is even much larger than calculated by the 'ideal' drying model. The experimental inactivation rate at 110 °C can be described only if the inactivation constant is increased 500 fold in the 'ideal' model simulation. Comparison of the experimental data with those of figures 3.13a and b shows that for short falling distances the measured inactivation rate is even higher than measured at 130 and 150 °C. This will of course never be predicted by an Arrhenius-type of model. Given this difference, there must be another yet unknown reason.
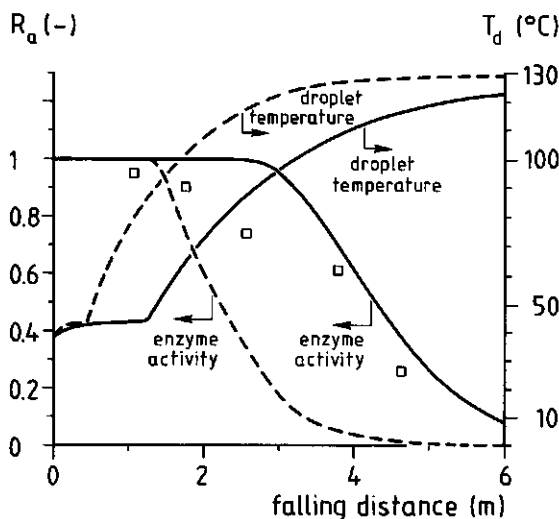
Figure 3.15   Enzyme inactivation and droplet temperature. The residual enzyme activity and droplet temperature are given as function of the falling distance Experimental conditions, and physical and kinetic data: see figure 3.14. $T_g = 130\,^{\circ}C$. — —: 'ideal' drying model; ————: 'spray' drying model.

3.5 CONCLUSIONS

The inactivation rate decreases at low water concentrations for both α-amylases. The thermal inactivation kinetics could be described by a first order Arrhenius-type mathematical model.

The residual activity of a thermo-stable α-amylase during drying of a suspended droplet was successfully predicted by the drying model. The thermal inactivation rate of the thermo-unstable α-amylase during drying of equally sized free falling droplets could be predicted reasonably by taking into account the 'spray' drying character of the drying process. In these simulations the diameter of the droplet spray had to be adjusted to describe the experimental results. Low temperature and high initial moisture studies indicate a yet unknown effect.

The approach in this part of the study of the independent measurement of inactivation kinetics, leads to models which can be used for design or optimisation of the drying process, including product quality.

ACKNOWLEDGEMENTS
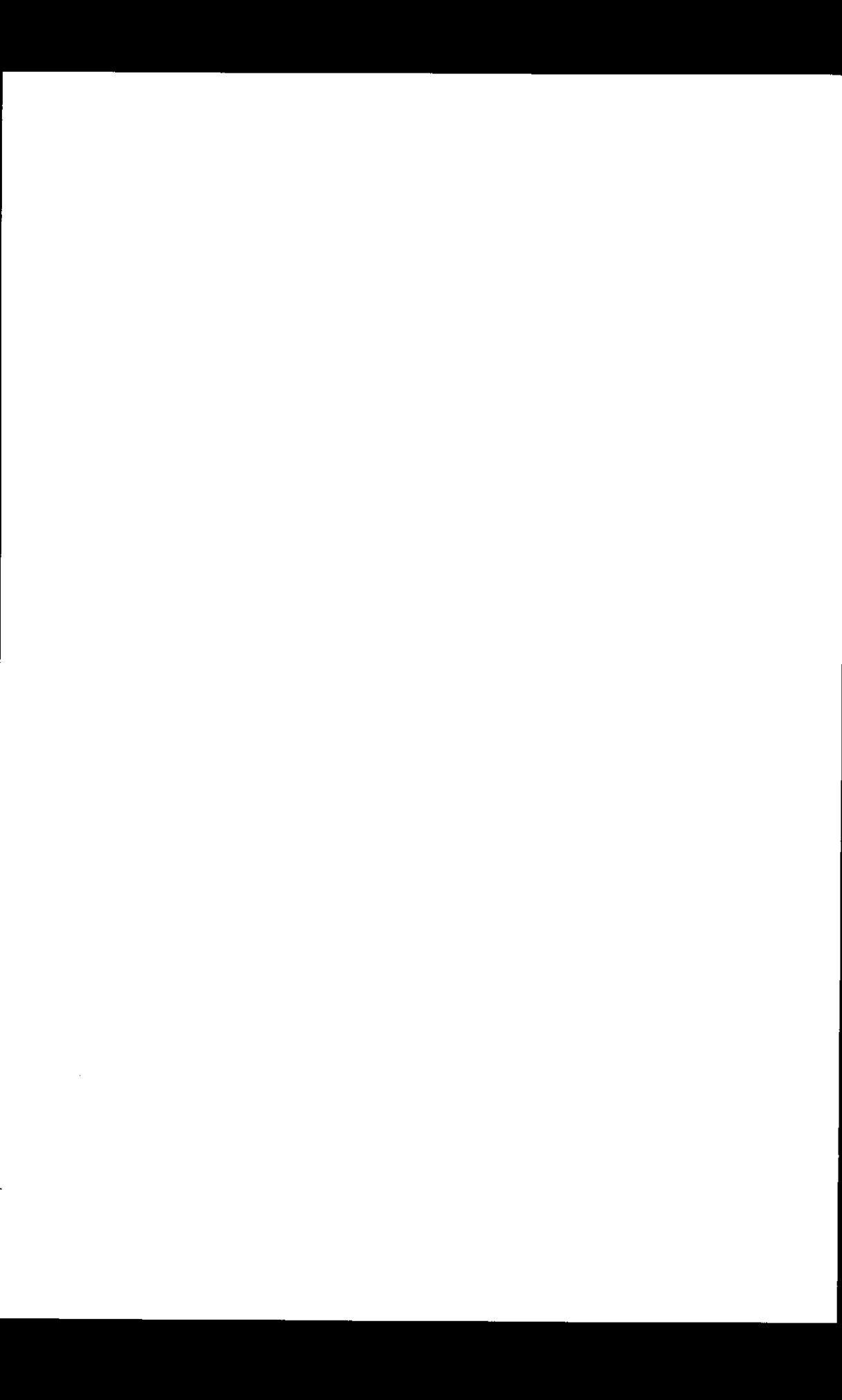
Chapter 4

SEGREGATION OF SOLUTE MATERIAL DURING DRYING

4.1 INTRODUCTION

This chapter describes the developed ternary drying model and the set-up and results of the segregation experiments. In the experiments slabs of a ternary food model system are dried and concentration profiles are measured. The food model system consists of water, sucrose, and sodium caseinate. The drying model is developed for the slab geometry and isothermal drying conditions. The model takes into account the shrinkage during drying and the concentration dependence of the diffusion coefficients. Because experimental data and estimation procedures are lacking for multicomponent diffusion coefficients in aqueous solutions, the multicomponent diffusion coefficients have been estimated using the results of the drying experiments.

4.2 THE TERNARY DRYING MODEL

4.2.1 The model formulation

The description of the diffusional mass transfer in multicomponent mixtures can be based on either the generalised Maxwell-Stefan (GMS) equations or on equations derived from the thermodynamics of irreversible processes (TIP) (Cussler (1976), Krishna and Taylor (1986), Wesselingh and Krishna (1990)). It can be shown, however, that these descriptions are equivalent. The ternary drying model used in this thesis is based on the GMS equations. An advantage of the GMS equations is that the Maxwell-Stefan (MS) multicomponent diffusion coefficients in the GMS equations have physical meaning in contradiction to the transport coefficients in the TIP equations. The MS diffusion coefficients are inversely proportional to the frictional drag that one set of molecules experiences when moving through another set molecules.

For a ternary mixture there are two independent GMS equations and three independent MS diffusion coefficients. The water diffusion and the diffusion of one of the dissolved components (in the model sucrose) can be described by the next equations:

$$\frac{1}{RT} x_w \frac{d\mu_w}{dr} = \frac{\left(x_w n_s - x_s n_w\right)}{C_t D_{ws}^{MS}} + \frac{\left(x_w n_p - x_p n_w\right)}{C_t D_{wp}^{MS}} \tag{4.1}$$

$$\frac{1}{RT} x_s \frac{d\mu_s}{dr} = \frac{\left(x_s n_w - x_w n_s\right)}{C_t D_{ws}^{MS}} + \frac{\left(x_s n_p - x_p n_s\right)}{C_t D_{sp}^{MS}} \tag{4.2}$$

where R is the general gas law constant, T is the absolute temperature, μ is the chemical potential, r is the space co-ordinate, x is the mole fraction, n is the molar flux with respect to a stationary co-ordinate system, D^{MS} is the MS (multicomponent) diffusion coefficient, C_t is the molar density of the mixture, and the subscripts w, s and p denote water, sucrose and sodium caseinate, respectively.

An important model assumption is that the volume decrease of the drying system equals the volume of the evaporated water during drying. Consequently there is no net volume flux, and the volume average velocity is zero, that is:

$$n_w V_w + n_s V_s + n_p V_p = 0 \tag{4.3}$$

where V is the partial molar volume.

Combining the GMS equations 4.1 and 4.2 with the continuity equations for water and sucrose in a slab, and using equation 4.3, two coupled partial differential equations are obtained describing the unsteady state transport of water and sucrose.

$$\frac{\partial C_w}{\partial t} = \frac{\partial}{\partial r} E_{ww} \frac{\partial C_w}{\partial r} + \frac{\partial}{\partial r} E_{ws} \frac{\partial C_s}{\partial r} \tag{4.4}$$

$$\frac{\partial C_s}{\partial t} = \frac{\partial}{\partial r} E_{sw} \frac{\partial C_w}{\partial r} + \frac{\partial}{\partial r} E_{ss} \frac{\partial C_s}{\partial r} \tag{4.5}$$

In which:

$$[E] = [P][B]^{-1}[\Gamma][P]^{-1} \tag{4.6}$$

with:

$$[E] = \begin{bmatrix} E_{ww} & E_{ws} \\ E_{sw} & E_{ss} \end{bmatrix} \tag{4.7}$$

$$[P] = \begin{bmatrix} 1 - C_w\left(V_w - V_p\right) & -C_w\left(V_w - V_p\right) \\ -C_s\left(V_s - V_p\right) & 1 - C_s\left(V_s - V_p\right) \end{bmatrix} \tag{4.8}$$

$$[B] = \begin{bmatrix} \dfrac{x_w}{D_{wp}^{MS}} + \dfrac{x_s}{D_{ws}^{MS}} + \dfrac{x_p}{D_{wp}^{MS}} & -x_w\left(\dfrac{1}{D_{ws}^{MS}} - \dfrac{1}{D_{wp}^{MS}}\right) \\ -x_s\left(\dfrac{1}{D_{ws}^{MS}} - \dfrac{1}{D_{sp}^{MS}}\right) & \dfrac{x_w}{D_{ws}^{MS}} + \dfrac{x_s}{D_{sp}^{MS}} + \dfrac{x_p}{D_{sp}^{MS}} \end{bmatrix} \tag{4.9}$$

$$[\Gamma] = \begin{bmatrix} 1 + x_w\dfrac{\partial \ln \gamma_w}{\partial x_w} & x_w\dfrac{\partial \ln \gamma_w}{\partial x_s} \\ x_s\dfrac{\partial \ln \gamma_s}{\partial x_w} & 1 + x_s\dfrac{\partial \ln \gamma_s}{\partial x_s} \end{bmatrix} \tag{4.10}$$

where C is the molar concentration, t is the drying time, $[E]$ is the matrix of transformed MS diffusion coefficients, $[P]$ is the concentration transformation matrix, $[B]$ is the matrix of the MS diffusion coefficients, $[\Gamma]$ is the matrix of the thermodynamic factors, and γ is the thermodynamic activity coefficient. The elements of the matrix $[E]$ are denoted as Fickian multicomponent diffusion coefficients, in literature. These Fickian multicomponent diffusion coefficients are not independent of each other. The cross diffusion coefficients can become negative.

The initial and boundary equations for these partial differential equations are:

$$t = 0 \qquad 0 \leq r \leq R_{e,0} \qquad C_w = C_{w,0} \qquad C_s = C_{s,0} \tag{4.11}$$

$$t > 0 \qquad r = 0 \qquad \frac{dC_w}{dr} = 0 \qquad \frac{dC_s}{dr} = 0 \tag{4.12}$$

$t > 0 \qquad r = R_{e,t}$

$$\left(E_{ww}\,E_{ss} - E_{ws}\,E_{sw}\right)\frac{dC_w}{dr} = -k_g\left(\rho_{w,i} - \rho_{w,b}\right)\left(E_{ws}\,C_s V_w + E_{ss}\left(1 - C_w V_w\right)\right) \quad (4.13)$$

$$\left(E_{ww}\,E_{ss} - E_{ws}\,E_{sw}\right)\frac{dC_s}{dr} = k_g\left(\rho_{w,i} - \rho_{w,b}\right)\left(E_{ww}\,C_s V_w + E_{sw}\left(1 - C_w V_w\right)\right) \quad (4.14)$$

where R_e is the external radius, k_g is the external mass transfer coefficient, ρ_w is the gas phase water concentration, and the subscripts 0, t, i and b denote initial, drying time, interface and bulk phase, respectively. The derivation of the boundary conditions 4.13 and 4.14 is given in appendix 4.1. The equilibrium relation between the internal and external water concentration at the surface is given by a linearized water sorption isotherm. The external mass transfer coefficient k_g is not corrected for the existence of a nett mass flow in the gas phase. This correction is negligible, given the experimental conditions used.

In the drying model no heat balance equation is included. It is assumed that the slab temperature during drying remains constant and equals the drying air temperature. In the drying experiments performed, convective as well as conductive heat transfer took place, leading to a rapid increase of the slab temperature to the drying air temperature.

The two partial differential equations can be solved analytically in some cases by defining two linear combinations of the concentrations of water and sucrose as new variables (Toor (1964a, b)). For non-shrinking systems with constant diffusivities and boundary conditions of the first or second kind this procedure leads to two uncoupled partial differential equations. For these equations standard solutions are available (Luikov (1968)). For the system described in this chapter no analytical solution is available. The two partial differential equations are therefore numerically solved by using a modified variable weighted Crank Nicolson's method (Lapidus and Pinder (1982), Kerkhof (1985)) by taking unequal space and time steps.

Because of the receding surface the two partial differential equations were transformed using a sodium caseinate centred space co-ordinate. This transformation avoids the movement of the external surface through the space co-ordinate grid. The transformed space co-ordinate is defined as:

$$\sigma = \int_0^r C_p V_p \, dr \qquad\qquad\qquad (4.15)$$

where σ is the transformed space co-ordinate.

The water and sucrose concentrations in the transformed co-ordinate system are defined as:

$$u_w = \frac{C_w}{C_p V_p} \qquad u_s = \frac{C_s}{C_p V_p} \qquad\qquad (4.16a, b)$$

where u is the transformed concentration. The final transformed partial differential equations have a form similar to the equations 4.4 and 4.5, see appendix 4.2.

4.2.2. The concentration dependence of the diffusion coefficients

Experimental data concerning MS multicomponent diffusion coefficients in concentrated aqueous solutions are lacking, and no reliable estimation methods have been developed (Wesselingh and Krishna (1990)). Moreover no methods are available to measure these coefficients in a wide range of water concentrations. Therefore the MS diffusion coefficients are estimated using the results of the drying experiments, including the concentration dependence.

In describing the concentration dependence of the MS diffusivities it was assumed that the water concentration is the main factor given its strong decrease during drying, and not the ratio of the other two components. It is expected that the MS diffusion coefficients strongly decrease at low water concentrations, as found for MS diffusion coefficients in concentrated binary aqueous solutions. The water concentration dependence of each MS diffusion coefficient is described by the next power law type of equation:

$$D_{nm}^{MS} = D_{nm,\infty}^{MS} \left(C_w V_w \right)^{a_{nm}} \qquad\qquad (4.17)$$

where a is the exponent in the power law relation, $D_{nm,\infty}^{MS}$ is the value of the MS diffusion coefficient at infinite dilute aqueous solution, and the subscripts n and m denote components i and j, respectively. The parameters a_{nm} and $D_{nm,\infty}^{MS}$ have to be estimated. Power law type of equations like 4.17 have been used in literature to describe the concentration dependence of the water diffusion coefficient in drying materials (Liou (1982), Coumans (1987)).

The thermodynamic activity coefficients γ are considered to be constant in the estimation procedure. Assumed values are: $\gamma_w = 1$, $\gamma_s = \gamma_s^\infty$ and $\gamma_p = \gamma_p^\infty$ (= values at infinite dilute aqueous solution). This means that the matrix of the thermodynamic factors $[\Gamma]$ (see equation 4.10) equals the unity matrix. This assumption is certainly not valid at low water concentrations $(\omega_w < 0.3\,\mathrm{kg\,H_2O(kg\,ds)}^{-1})$. At these water concentrations the thermodynamic activity coefficients become dependent on the water concentration, as indicated by water sorption isotherms given in literature for similar food systems (Iglesias and Chirife (1982)). However, thermodynamic models and data are lacking describing the change of the thermodynamic activity coefficients as function of water and solute concentrations. As a consequence the estimated concentration dependencies of the MS diffusion coefficients do not only reflect the effect of the decreasing water concentration on the mobility of water and solutes, but also the influence of the thermodynamic non-idealities on the driving force for diffusion, in particular at low water concentrations. In binary aqueous sugar and protein solutions the thermodynamic activity coefficients are less than one, and it is expected that this is also valid in the food model system used in the experiments. Consequently the driving forces are underestimated in the ternary drying model, leading probably to an overestimation of D_{ws}^{MS} and D_{wp}^{MS} at low water concentrations. The effect on the estimated value of D_{sp}^{MS} is difficult to assess. In binary drying calculations, as performed in literature and as discussed in chapter 2, usually the same assumption is made. Therefore, also those diffusion coefficients as used in the calculations, contain a thermodynamic factor.

The parameters $D_{nm,\infty}^{MS}$ and a_{nm} are estimated using the Downhill simplex method (Press *et al.* (1989)), a non-linear optimisation method. The sum of the absolute values of the relative error between measured and calculated ratio and water concentration profiles is taken as optimisation criterion. In total there are 6 parameters which have to be estimated. Attempts failed, however, to estimate all 6 parameters simultaneously. This is caused by a strong correlation between the parameters, in particular between a_{ws}, a_{wp}, $D_{ws,\infty}^{MS}$ and $D_{wp,\infty}^{MS}$, leading even to negative values of the parameter a_{ws} or a_{wp}. In the estimation procedure it is assumed therefore that the water concentration dependencies of D_{ws}^{MS} and D_{wp}^{MS} are identical, that is: $a_{ws} = a_{wp}$. The number of parameters to be estimated is reduced by one in this way down till 5. Moreover it is assumed that at a water concentration below 10 kgm^{-3}, the MS diffusion coefficients are constant. The results of drying experiments with

initial solids contents of 5, 10, 15 and 20% on total basis are used in the estimation procedure. At each moisture content the results of one experiment are taken. In total 204 data points are included in the optimisation.

4.3 MATERIALS AND METHODS

The drying experiments were performed with a food model system, consisting of water (demineralised), sucrose (Merck) and sodium-caseinate (DMV Campina). To avoid internal bulk flow and to simplify the experimental procedure, the model system was jellified by adding a small amount (0.4 % on total basis) of agar (Merck). The ratio between the sodium caseinate and sucrose concentration was 0.50 in all experiments. The diffusivity of sucrose is expected to be at least one order of magnitude larger than that of sodium caseinate.

The jellified food model system (thickness 1 cm) was dried in sample holders (figure 4.1), placed in a drying cell (figure 4.2). A sample holder consisted of a stack of 7 flat teflon rings and the sample holder was disassembled ring by ring after removal from the cell. Each time after one ring removal a slice protruded, that was cut off. Analysis of the slices gave the concentration profiles of water, sucrose and sodium caseinate in the slab. Eight slabs were dried simultaneously in each experiment. The temperature in the drying cell was controlled and the external mass transfer could be influenced by changing the stirrer speed. A constant flow of dry air was used as drying medium. The sample holders were removed from the drying cell at different times during the drying experiment.
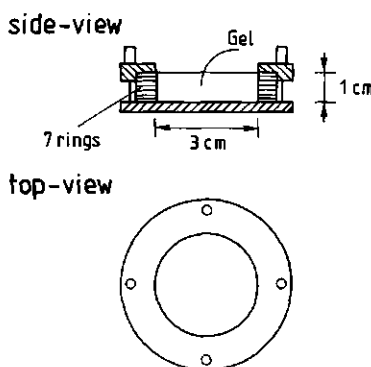
Figure 4.1   Sample holder
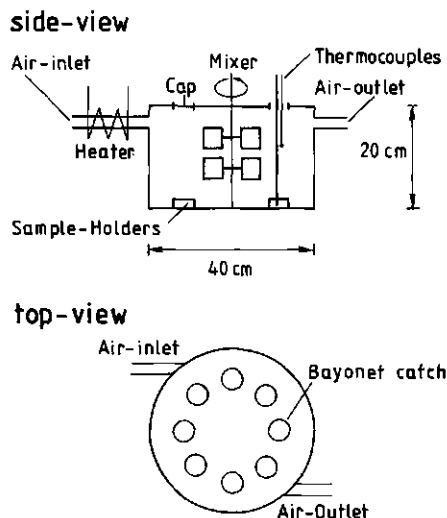
Figure 4.2   Drying cell

The analysis of the slices consisted of two steps. First the dry weight content was determined by means of a vacuum dryer, in which the slices were dried at 70 °C for two days. After that the sucrose and sodium caseinate concentrations were determined by an automatic infrared analyser, type Milkoscan 104 A/B (Foss Electric, Denmark) (Goulden, 1964)), after dissolution and dilution of the dried slices. The accuracy of the analysis depended on the initial solids content of the model system. The difference between the dry solids content in the slices as determined in the vacuum dryer, or as calculated on basis of the solute concentrations determined by the infrared analyser, was less than 3 % at an initial dry solids content of 15.9% on total basis. The error in the ratio between sodium caseinate and sucrose was less than 5% at the same initial dry solids content. In general the accuracy decreased at lower initial dry solids contents. It was impossible to cut slices with exactly the same thickness in different drying experiments. Consequently it was not possible to repeat a drying experiment in exactly the same way.

In the drying experiments performed, the dry solids content of the food model system varied between 5% and 20 % on total basis. The temperature of the drying air was 50 °C.

4.4 RESULTS AND DISCUSSION

4.4.1 Drying experiments

The results of a drying experiment with an initial dry solids content of 15.9% (on total basis) are given in the figures 4.3, 4.4, 4.5 and 4.6. The dimensionless distance X is defined as:

$$X = \frac{\int_0^r c_p \, dr}{\int_0^{R_s} c_p \, dr} \tag{4.18}$$

The profiles in the figures are given in the form of bar graphs, representing the average concentration as measured in each slice. The calculation of the deviations as given in the figures 4.5 and 4.6, is based on the assumption that no segregation occurs during drying.

In the earliest part of the drying process, the originally flat water concentration profile has changed only near the surface (figure 4.3a) and no segregation is measured (figure 4.4a). There is no significant deviation from the initial ratio of the two solutes. In the second part of the drying process (or penetration period) the water concentration profile is very steep, but the bottom concentration ($X = 0$) still has not changed (figure 4.3b), and a considerable degree of segregation occurs (figure 4.4b). Near the surface the ratio between the sodium caseinate and sucrose concentration increases from the initial ratio up to a value of 0.55. In the centre of the slab the situation is reversed, whereas at the bottom no segregation is found. In the last part of the drying process (or regular regime period) the water concentration profile starts to flatten and the bottom concentration decreases (figure 4.3c). The ratio between the dry solids components at the bottom now decreases down from the initial ratio and the ratio profile moves inward (figure 4.4c). The ratio near the surface is 0.60. The profiles in the figures 4.5 and 4.6 give a similar image as figure 4.4. The maximum deviation in the concentration near the surface is + 11% for sodium caseinate and - 6 % for sucrose. The experiments give an average value of the ratio in the surface layer of the slab only. It can be expected, however, that the ratio at the surface is higher than 0.60.
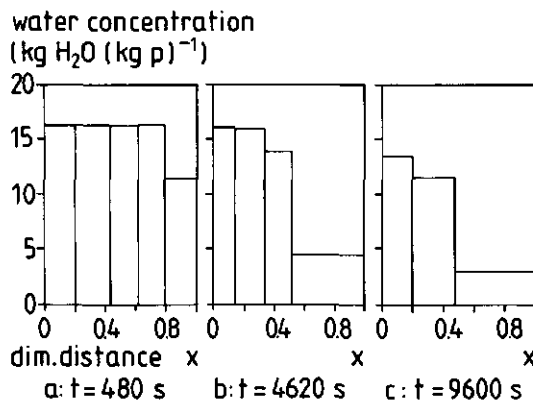
Figure 4.3   Water concentration profiles after drying at three different time values. The water concentration is defined as kg water per kg sodium caseinate. The initial water content is 16 kg H_2O(kg p)$^{-1}$. The initial ratio is 0.5 kg p(kg s)$^{-1}$.
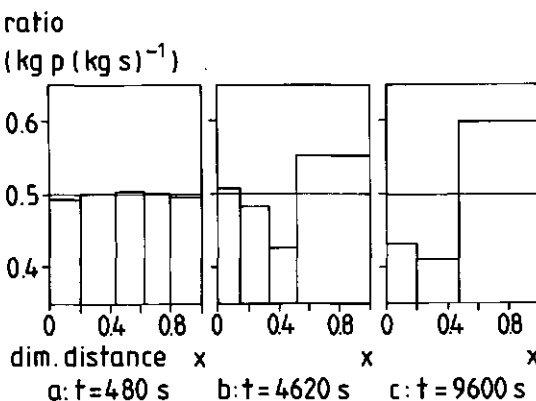
Figure 4.4   Ratio profiles after drying at three different time values. Experimental conditions see figure 4.3.

deviation caseinate concentration (%)
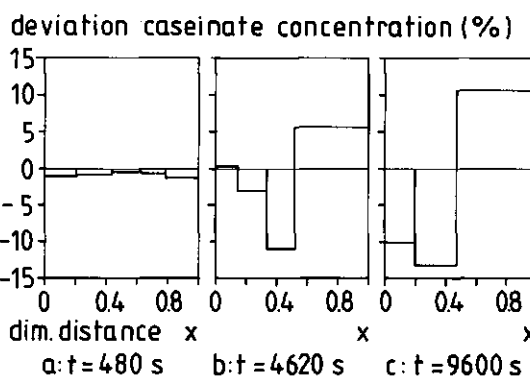
Figure 4.5 Deviations from the overall average sodium caseinate concentrations after drying at three different time values. Experimental conditions see figure 4.3.

deviation sucrose concentration (%)
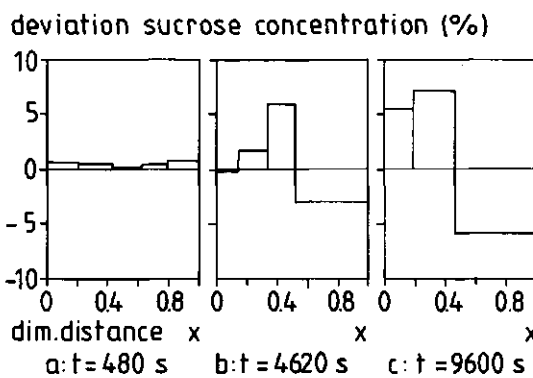
Figure 4.6 Deviations from the overall average sucrose concentrations after drying at three different time values. Experimental conditions see figure 4.3.

The experimental results agree qualitatively with our theoretical considerations: a water concentration gradient causes a considerable segregation when there is a large difference in diffusivities. The concentration at the surface of the component with the smallest diffusivity (sodium caseinate) is relatively high as compared with the other component (sucrose).

In figure 4.7 the 'final' ratio profiles are given as measured in drying experiments with other initial dry solids concentrations. The results indicate that the extent of segregation decreases when the dry solids content increases, as expected because of the decreased mutual mobility of sucrose and sodium caseinate.

4.3.2 Drying model simulations

- Simulation of the experimental drying data
Figure 4.8 shows drying model simulations compared with experimental drying data. The experimental data are the same as shown in the figures 4.3 and 4.4.

The drying model describes the experimental water concentration profiles as well as the ratio profiles reasonable good. The average relative discrepancy between simulation results and experimental water concentration and ratio profiles used in the optimisation is 16 %. Particularly the trend in the shape of the calculated profiles agrees well with the experimental profiles. However, the minimum values in the calculated ratio profiles are found at higher values of X compared with the experimental data. The calculated surface ratio's show a (strong) increase in the first and second part of the drying process, whereas in the third part of the drying process the value remains more or less constant. This phenomenon is caused by the already very low surface water concentrations at the end of the second drying period. At these water concentrations the mutual mobility of sucrose with respect to sodium caseinate has become very low. The degree of segregation attains then a 'fixed' value. The final value of the calculated surface ratio (1.51) is much higher than the initial ratio (0.50), indicating that segregation is in particular important at the surface. This means that the physical-chemical surface properties can be very different from the properties as determined from the average composition.
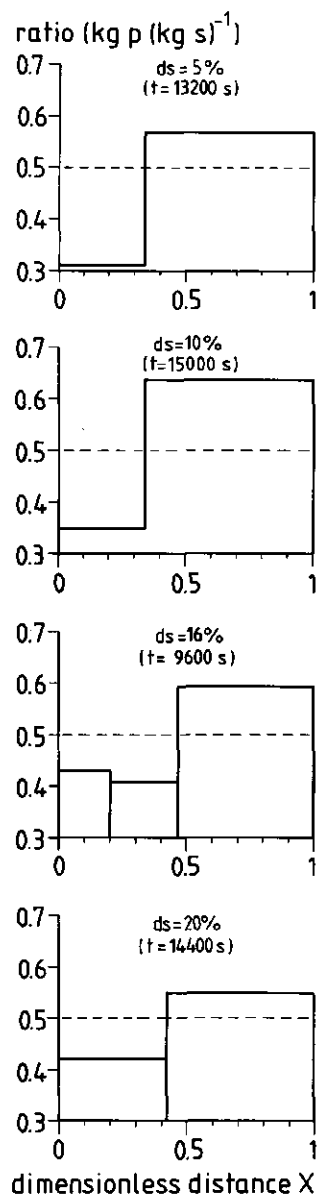
Figure 4.7 'Final' values of the ratio profiles at different initial dry solids contents. —— ——: initial ratio; ds = dry solids content on total basis.

water concentration
$(kg\ H_2O\ (kg\ p)^{-1})$
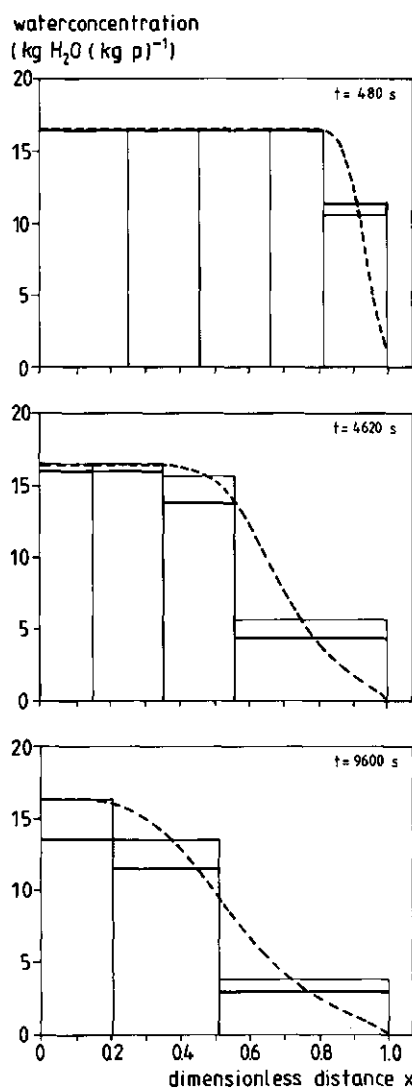
a　　　　　　　Water concentration profiles.

Figure 4.8　　Experimental and simulated profiles at three different drying times. The initial water content is 16 kg $H_2O(kg\ p)^{-1}$. The initial ratio is 0.5 kg p(kg s)$^{-1}$. ————: experimental data, see figures 4.3 and 4.4; — —: model simulation, physical data table 4.1; ————: averaged simulation results.
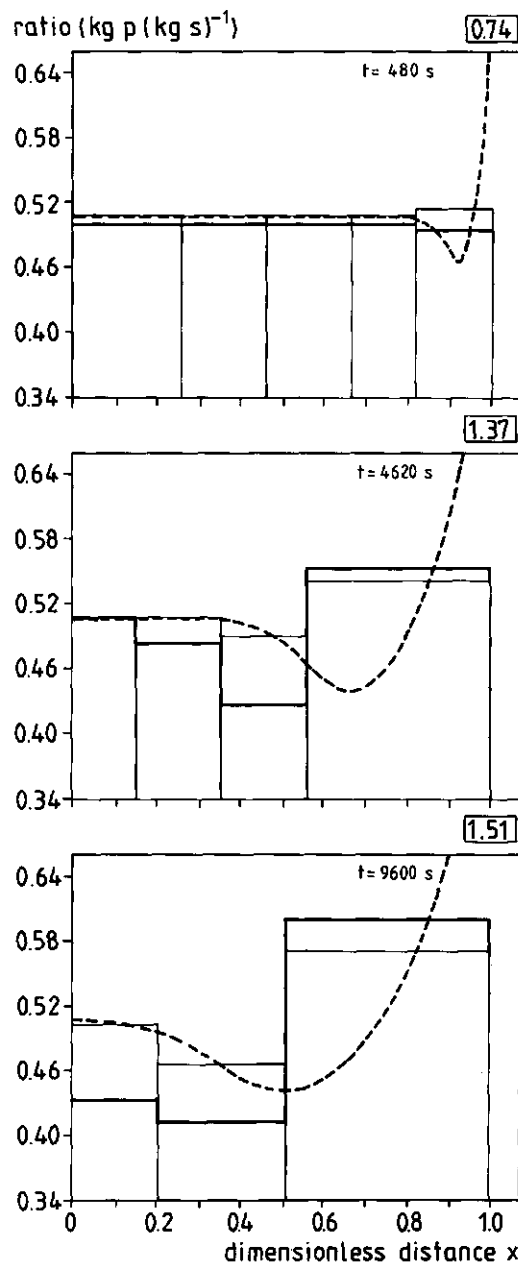
Figure 4.8b   Ratio profiles. □: calculated ratio at the surface.

Table 4.1   Physical data food model system.

Mass density:	
- water	1000 kg m^{-3}
- sucrose	1580 kg m^{-3}
- sodium caseinate[1]	1380 kg m^{-3}
Mol weight:	
- water	0.018 kg mol^{-1}
- sucrose	0.342 kg mol^{-1}
- sodium caseinate[1]	100 kg mol^{-1}
MS diffusion coefficients	$D_{ws}^{MS} = 4.7\,10^{-10}\left(C_w V_w\right)^{1.6}$ m^2 s^{-1} $D_{wp}^{MS} = 3.2\,10^{-10}\left(C_w V_w\right)^{1.6}$ m^2 s^{-1} $D_{sp}^{MS} = 6.7\,10^{-12}\left(C_w V_w\right)^{3.2}$ m^2 s^{-1}
Linearized water sorption isotherm	$C_{w,i} > 13889\,\text{mol m}^{-3} : \rho_{w,i} = 4.6\,\text{mol m}^{-3}$ $C_{w,i} < 13889\,\text{mol m}^{-3} : \rho_{w,i} = \dfrac{C_{w,i}}{3000}\,\text{mol m}^{-3}$
External mass transfer coefficient	$k_g = 1.5\,10^{-2}$ ms^{-1}

1) estimated value

- Estimated MS diffusion coefficients

The estimated equations for the MS diffusion coefficients are given in table 4.1 and depicted in figure 4.9. The estimated behaviour of D_{ws}^{MS} and D_{wp}^{MS} is in agreement with the general finding that the water diffusivity in foods decreases strongly at low moisture contents. The values of the estimated diffusion coefficients are in the same order of magnitude as found in literature for binary water diffusion coefficients in liquid foods (Menting (1970), Luyben *et al.* (1980), Furuta *et al.* (1984), Coumans (1987), Ferrari *et al.* (1989)). The estimated water concentration dependence of D_{sp}^{MS} is more pronounced than for D_{ws}^{MS} or D_{wp}^{MS}, as expected given the difference in molecular size of water and sucrose. As a result the mutual mobility of sucrose and sodium caseinate is very restricted at low water concentrations. Similar results are found for the water concentration dependence of aroma components in carbohydrate solutions (Menting (1970), Chandrasekaran and King (1972a), Furuta *et al.* (1984), Riede and Schlünder (1988)) and of proteins in sugar solutions (Loncin (1980)).
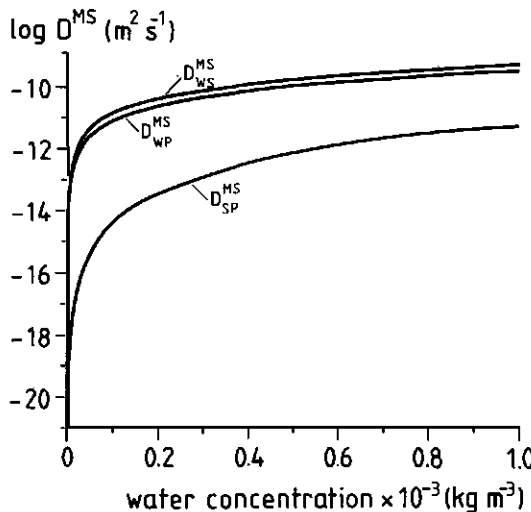
Figure 4.9 Estimated Maxwell-Stefan multicomponent diffusion coefficients. Equations table 4.1.

The estimated results as shown in figure 4.9 and in table 4.1 must be interpreted with care. Different set of values for the 'fitting' parameters can give appropriate descriptions of the experimental drying data, with almost the same value for the optimisation criterion, as mentioned before.

The very low values of D_{sp}^{MS} at low moisture contents compared with D_{ws}^{MS} and D_{wp}^{MS} indicate that the segregation can not proceed on the time scale of the drying process at low moisture concentrations. Consequently, at these moisture concentrations the ratio between the dry solids components attains a fixed value. In particular the ratio at the surface will attain a fixed value already soon after the beginning of the drying process given the existing low water concentrations, as shown in figure 4.8.

4.5 CONCLUSIONS

Segregation occurred during drying in the food model system studied. In slab drying experiments, the concentration of sodium caseinate was relatively high at the surface compared with the sucrose concentration, in the centre the reversed situation existed. In experiments with an initial dry solids content of 15.9 % on total basis, the measured ratio of sodium caseinate and sucrose in the surface layer increased from the initial ratio of 0.5 up to 0.6 kg sodium caseinate(kg sucrose)$^{-1}$. Simulations with a ternary drying model, based on the generalised Maxwell-Stefan equations, resulted in a good agreement with the drying experiments. The estimated Maxwell-Stefan diffusivities were comparable with values reported in literature. The calculated ratio at the surface increased from 0.5 to 1.51 kg sodium caseinate(kg sucrose)$^{-1}$ as the initial moisture is 15.9 % on total basis.

Appendix 4.1

In this appendix the boundary conditions at $R_{e,t}$ as given by the equations 4.13 and 4.14, are derived. The boundary condition for the water transport is based on the fact that at the surface the internal water flux equals the external water flux, both with respect to the receding surface. The boundary condition for the water flux n_w^i is:

$$n_w^i = C_w \left(v_w - v_i \right) = n_w - C_w v_i = k_g \left(\rho_{w,i} - \rho_{w,b} \right) \tag{4.19}$$

where v is the velocity and superscript i denotes interface.

Because there is no transport of sucrose through the external surface, the flux of sucrose with respect to the receding surface is zero. The boundary condition for the sucrose flux n_s^i is:

$$n_s^i = C_s \left(v_s - v_i \right) = n_s - C_s v_i = 0 \tag{4.20}$$

The receding velocity of the external surface v_i is:

$$v_i = \frac{dR_{e,t}}{dt} = -V_w k_g \left(\rho_{w,i} - \rho_{w,b} \right) \tag{4.21}$$

The right-hand part of equation 4.21 follows from a mass balance over the drying system.

The boundary conditions as given by the equations 4.13 and 4.14 can be derived by combining the equations 4.1, 4.2, 4.3, 4.19, 4.20 and 4.21, using the transformation as given by equation 4.6.

Appendix 4.2

In this appendix the transformed diffusion equations (equations: 4.4 and 4.5), and initial and boundary conditions (equations: 4.11, 4.12, 4.13 and 4.14) are given.

The transformed diffusion equations are:

$$\frac{\partial u_w}{\partial t} = -\frac{\partial}{\partial \sigma} A \frac{\partial u_w}{\partial \sigma} - \frac{\partial}{\partial \sigma} B \frac{\partial u_s}{\partial \sigma} \tag{4.22}$$

$$\frac{\partial u_s}{\partial t} = -\frac{\partial}{\partial \sigma} C \frac{\partial u_w}{\partial \sigma} - \frac{\partial}{\partial \sigma} D \frac{\partial u_s}{\partial \sigma} \tag{4.23}$$

The transformed initial and boundary conditions are:

$$t = 0 \qquad 0 \le \sigma \le C_{p,0} V_p R_{e,0} \qquad u_w = u_{w,0} \qquad u_s = u_{s,0} \tag{4.24}$$

$$t > 0 \qquad \sigma = 0 \qquad\qquad \frac{d u_w}{d \sigma} = 0 \qquad \frac{d u_s}{d \sigma} = 0 \tag{4.25}$$

$$t > 0 \qquad \sigma = C_{p,0} V_p R_{e,0}$$

$$(AD - BC)\frac{d u_w}{d \sigma} = D k_g \left(\rho_{w,i} - \rho_{w,b}\right) \tag{4.26}$$

$$(AD - BC)\frac{d u_s}{d \sigma} = -C k_g \left(\rho_{w,i} - \rho_{w,b}\right) \tag{4.27}$$

In which:

$$A = C_p V_p \left\{ -(1 - C_s V_s)\left((1 - C_w V_w) E_{ss} + C_s V_w E_{ws}\right) + C_w V_s \left((1 - C_w V_w) E_{sw} + C_s V_w E_{ww}\right) \right\}$$

$$B = C_p V_p \left\{ C_s V_w \left((1 - C_w V_w) E_{ss} + C_s V_w E_{ws}\right) - (1 - C_w V_w)\left((1 - C_w V_w) E_{sw} + C_s V_w E_{ww}\right) \right\}$$

$$C = C_p V_p \left\{ -(1 - C_w V_w)\left((1 - C_s V_s) E_{ww} + C_w V_s E_{sw}\right) + C_s V_w \left((1 - C_s V_s) E_{ws} + C_w V_s E_{ss}\right) \right\}$$

$$D = C_p V_p \left\{ C_w V_s \left((1 - C_s V_s) E_{ww} + C_w V_s E_{sw}\right) - (1 - C_s V_s)\left((1 - C_s V_s) E_{ws} + C_w V_s E_{ss}\right) \right\}$$

Chapter 5

GENERAL DISCUSSION

5.1 INTRODUCTION

The drying models, as described in this thesis, are finally intended to examine the effect of important process conditions and variables on drying kinetics, product quality (enzyme inactivation) and segregation; in particular during spray-drying of liquid foods. Three topics relevant for spray-drying will be discussed briefly in this chapter, the effect of the spray-air mixing pattern on enzyme inactivation, the significance of the measured inactivation constants for spray-drying calculations and the extent of segregation during spray-drying.

Important factors which impede the actual use of drying models for spray-drying calculations are:
- the size distribution of the droplets.
- the complicated spray-air mixing patterns, resulting in non-uniform drying conditions and droplet trajectories. Droplets of different sizes can have quite different drying histories.
- the changes in the physical structure of the droplets, like: vacuole formation, droplet inflation, shrivelling and shrinkage.

The effect of droplet size distribution on (overall) drying kinetics and product quality is discussed by Kerkhof and Coumans (1990) for an idealised spray-air mixing pattern. In that study it was assumed that the air was perfectly mixed while the particles moved in plug flow mode through the dryer. Van der Lijn (1976) analysed the relation between three different idealised spray-air mixing patterns and drying kinetics. The influence of vacuole formation and droplet inflation on drying kinetics is treated by Van der Lijn (1976) and on product quality by Wijlhuizen et al. (1979). The inactivation of the enzyme phosphatase (Daemen (1981)) was taken as quality parameter in the product quality studies mentioned. The relation between spray-air mixing pattern and product quality is, however, not examined yet. The importance of this mixing pattern is clearly demonstrated by the obtained experimental results shown in chapter 3.

To assess the consequences of process conditions during spray-drying on the (bio-) chemical product quality, reaction kinetics models like discussed in chapter 3, have to be used. The

parameters in these models are estimated using separately determined reaction constants. To obtain a reliable estimate these reaction constants have to be determined in a temperature and water concentration range relevant for the spray-drying process. A point of concern is therefore, whether the inactivation constants as calculated in spray-drying models are covered by experimental data or are based on extrapolation. In the latter case the reliability of the calculated quality changes is limited. Furthermore one can question if the methodology as applied in chapter 3 is always appropriate for determining the relevant inactivation constants, given the short particle residence times in a spray-dryer.

The drying kinetics of liquid foods and the quality of spray-dried powders can in principle be affected by segregation of the dissolved solids. Model simulations can show if and to which extent segregation can occur during spray-drying. This can be studied more extensively with the model developed in chapter 4.

5.2 SPRAY-AIR MIXING PATTERN AND ENZYME INACTIVATION

Van der Lijn (1976) distinguished three 'idealised' (extreme) mixing patterns:
1. Perfectly mixed air; the air temperature and humidity are constant during the drying process. The air temperature and humidity are at outlet conditions. The droplets move in plug flow mode through the dryer.
2. Perfectly cocurrent dryer operation; both air and droplets move in plug flow mode through the dryer. The wet droplets are brought in contact with the drying air at inlet conditions immediately after atomisation. During drying the air temperature decreases and the air humidity increases.
3. Gradual spray-dispersion; in practical spray-drying a droplet spray is formed and drying air is gradually admixed. An extreme situation arises in that case where the entrainment of drying air in the droplet spray is so slow that the drying droplets are in equilibrium with the air conditions inside the spray. As result water concentration profiles are absent inside the droplet. The droplet drying time is then completely controlled by the rate of admixing of drying air. However, combinations of droplet temperature and (average) water concentrations occurring during drying can be derived using the water sorption isotherm of the product (van der Lijn (1976)). The calculation of the drying time is only possible if the rate of admixing is known.

In actual spray-dryers the spray-air mixing patterns will be combinations of these three patterns, moreover the droplets will not move in plug flow. Attempts are reported in

literature (Lively *et al.* (1992)) in which the spray-air mixing pattern is modelled in detail by using computational fluid dynamics, but no experimentally validated models do yet exist. However, using 'idealised' patterns can give insight in the importance of the mixing pattern for drying kinetics and product quality, and in the limitations of model calculations based on simplified mixing assumptions.

In the model simulations performed, three 'idealised' mixing patters are used, namely: perfectly mixed air, perfectly cocurrent dryer operation and an 'idealised' droplet spray-drying air admixing pattern. The first two are similar to that of Van der Lijn (1976). The perfectly mixed air calculations are based on the 'ideal' drying model (chapter 2). In the perfectly cocurrent dryer operation the 'ideal' drying model is combined with heat and mass balances over the drying air 'attached' to the drying droplet. The 'spray' drying model as discussed in chapter 2.4.2.2 is used in the 'idealised' spray-air admixing pattern calculations. The consequences of the different patterns are evaluated for one droplet diameter only. It is

Table 5.1. Conditions and data used in the spray-drying simulations.

Process conditions		
- inlet:	air	$T = 250\,^{\circ}\mathrm{C}$ $H = 0.01\,\mathrm{kg\,H_2O(kg\,da)}^{-1}$
	product	$T = 50\,^{\circ}\mathrm{C}$ $\omega_w = 1.5\,\mathrm{kg\,H_2O(kg\,ds)}^{-1}$ $d_{d,0} = 200\,\mu\mathrm{m}$ $v_{d,0} = 100\,\mathrm{ms}^{-1}$
- outlet:	air	$T = 110\,^{\circ}\mathrm{C}$ $H = 0.0655\,\mathrm{kg\,H_2O(kg\,da)}^{-1}$
	product	$T = 110\,^{\circ}\mathrm{C}$ $\omega_w = 0.05\,\mathrm{kg\,H_2O(kg\,ds)}^{-1}$
- feed-air ratio		$0.0383\,\mathrm{kg\,ds(kg\,da)}^{-1}$
Data		
- physical data		table 2.2
- kinetic data		table 3.4

expected that the obtained results are similar for other diameters. In the simulations the inactivation kinetics of the thermo-unstable α-amylase is used. The inactivation is described by the 'linear' inactivation kinetics model (chapter 3.4.1).

In the simulation 'typical' spray-drying conditions are applied. These conditions are summarised in table 5.1. It is assumed that the drying process is adiabatic and that the final air and droplet temperatures are equal. The initial droplet diameter and velocity are 200 μm and 100 ms^{-1}, respectively. In the 'spray' drying model it is assumed that the length of the spray-cone is equal to the length of the spray-tower. In this way an 'extreme' mixing pattern is simulated.

Figures 5.1 and 5.2 show the results of the model simulations. Figure 5.1 shows that the mixing patterns profoundly influence drying kinetics, as expected (van der Lijn (1976)), and enzyme inactivation. The highest drying rate as well as inactivation rate is obtained in the 'cocurrent' pattern, the lowest in the 'spray' pattern.

The drying rate differences result from the differences in driving force. In the 'cocurrent'
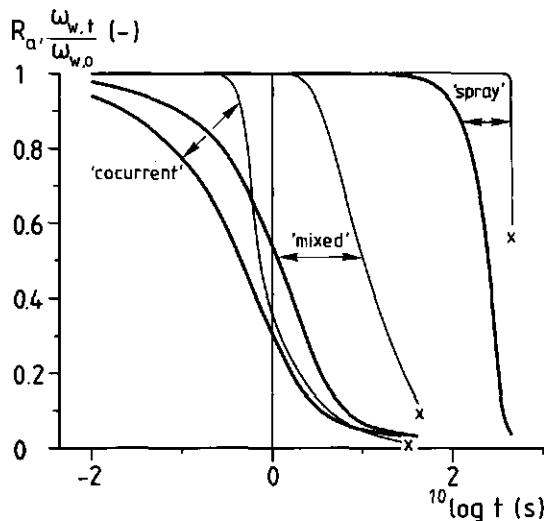
Figure 5.1   Enzyme inactivation and drying kinetics for different spray-air mixing patterns. The changes in time are given of the average water concentration and residual enzyme activity. Initial conditions: see table 5.1; ——————: drying kinetics; ——————: residual enzyme activity; ×: final residual enzyme activity.
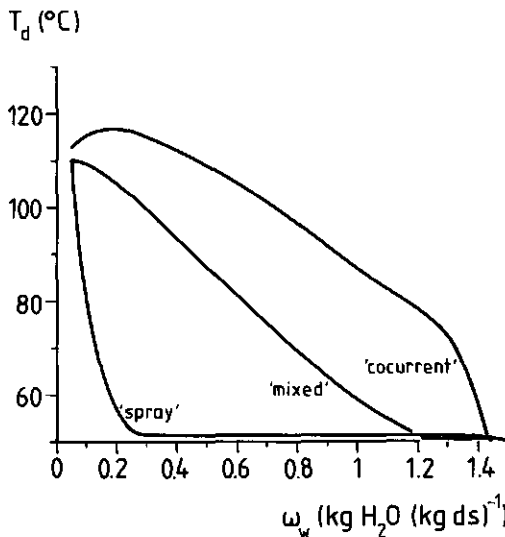
Figure 5.2 Droplet temperature-average water concentration histories for different spray-air mixing patterns. Initial conditions: see table 5.1.

pattern the average driving force is higher than in the 'mixed' pattern, in the 'spray' pattern the reversed situation exists. During drying in the 'cocurrent' pattern the air temperature and humidity changes from inlet to outlet conditions, while in the 'mixed' pattern the air temperature and humidity are always at outlet conditions. In the 'spray' pattern only a limited amount of air at inlet conditions is 'available' at the onset of the drying process. The air temperature in the spray decreases strongly and approaches the adiabatic saturation temperature (51 °C). The droplet is almost in equilibrium with the air in the 'spray'. The rate of admixing of drying air at inlet conditions determines the drying rate. Finally the air temperature and humidity in the 'spray' approach the outlet conditions.

Figure 5.2 shows that at each average water concentration the droplet temperature in the cocurrent case is higher than in the mixed 'case', for the 'spray' case the situation is reversed. In the 'spray' case the droplet temperature is during a large part of the drying process at the wet-bulb temperature.

The residual enzyme activity differences are caused by the fact that the inactivation rate is more sensitive to droplet temperature changes than the water diffusion coefficient. The activation energy of the inactivation reaction ($E_a \approx 200 - 500 \, \text{kJ mol}^{-1}$) is for all water

concentrations higher than the activation energy of the water diffusion coefficient ($E_a \approx 25 - 100 \, \text{kJ} \, \text{mol}^{-1}$). Consequently the enzyme inactivation increases more strongly than the drying time decreases at increasing droplet temperatures, and vice versa. And since the average droplet temperature in the 'cocurrent' pattern is higher than in the 'mixed' pattern, is the residual enzyme activity in the 'cocurrent' pattern lower than in the 'mixed' pattern. For the 'spray' pattern the same reasoning explains the results.

The calculated outlet residual enzyme activities of the 'cocurrent' and 'spray' pattern can be obtained by changing the outlet temperatures in the 'mixed' pattern with +6 °C and -9 °C, respectively. This temperature range is in the same order of magnitude as the outlet temperature ranges considered during design and optimisation of spray-dryers. Consequently, optimisation of spray-dryers regarding product quality using drying models, is only possible if detailed information about the spray-mixing behaviour is available.

In figure 5.3 the change in time of the 'average' inactivation constant k_e is plotted. The 'average' inactivation constants are calculated using the average water concentration. In figure 5.3 it is indicated when the residual enzymes activities are 90 and 50 % respectively. As can be seen from figure 5.3 not only the values of the inactivation constants differ, but
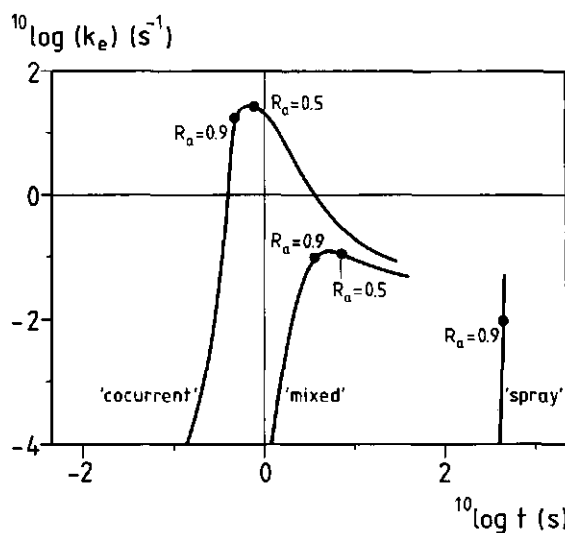
**Figure 5.3**   The change in time of the 'average' inactivation constant k_e for different spray-air mixing patterns. Initial conditions: see table 5.1.

also their change in time. In the 'cocurrent' pattern a rapid increase of the inactivation constant is followed by a decrease. The increase is caused by the rapid droplet temperature increase which completely dominates the decrease due to the water concentration decrease. The final decrease of k_e is caused by the decrease of the droplet temperature and water concentration during the final part of the drying process. In the 'mixed' pattern the inactivation constant remains, after a rapid increase, more or less constant. The increase in droplet temperature is offset by the decrease in moisture content. The inactivation constant in the 'spray' pattern obtains its maximum value when the final water concentration is reached. The temperature increase dominates the moisture content decrease. As a result of these differences the enzyme inactivation takes place in different drying stadiums as well as at different water concentration ranges, dependent on the mixing pattern prevalent.

Interpreting the figures 5.2 and 5.3 one must keep in mind that the use of average water concentrations and 'average' inactivation constants is somewhat misleading. During drying water concentration profiles develop and in connection to that inactivation constant profiles, in such a way that the inactivation constant at the surface of the droplet is lower than in the droplet centre. Consequently the residual enzyme activity is higher at the droplet surface than in the droplet centre, see the figures 3.1 and 3.9.

The simulation results show that the prevalent spray-air mixing pattern influences the residual enzyme activity. As a result the design and control of this mixing pattern is of great importance, among other things, for the resulting (bio-) chemical product quality.

5.3 SIGNIFICANCE OF MEASURED INACTIVATION CONSTANTS FOR SPRAY-DRYING CALCULATIONS

The experimental method used in this thesis for the measurement of the inactivation constant sets an upper limit to the value of the inactivation constant which can be determined. This maximal value of the inactivation constant $k_{e,\max}$ can be estimated as follows. The method assumes that on the time scale of an inactivation kinetics experiment the temperature in the inactivation cell equals the temperature of the external heating medium. The estimation of the maximal value of the inactivation constant is therefore based on the next two considerations:

- the minimal practicable layer thickness in an inactivation cell (see figure 3.2) is 1 mm. The time for 99% temperature equilibration of a water layer of 1 mm thickness is 3 s, assuming that internal conductive heat transfer is rate limiting.

- the characteristic time of the inactivation reaction τ_r ($\tau_r = 1/k_e$) must be 5 times larger than the time for 99% temperature equilibration, to avoid that considerable inactivation (> 10%) already takes place during temperature equilibration.

These two starting points result in a minimum value for τ_r of 15 s and a maximal inactivation constant $k_{e,\text{max}}$ of 0.07 s^{-1}.

In figure 5.4 the inactivation constants calculated in the spray-drying simulations, as discussed in paragraph 5.2, for the thermo-unstable α-amylase are compared with the measured inactivation constants as well as with the maximal inactivation constant. As shown in figure 5.4 the enzyme inactivation occurs in all mixing patterns at temperature-concentration combinations not covered by the inactivation kinetics experiments. Consequently the calculated residual enzyme activities are entirely based on extrapolations to higher temperatures and lower water concentrations of the measured inactivation constants. In the 'cocurrent' pattern the maximal calculated inactivation constant is 30 s^{-1}. Moreover almost all inactivation constants for the relevant temperature-concentration
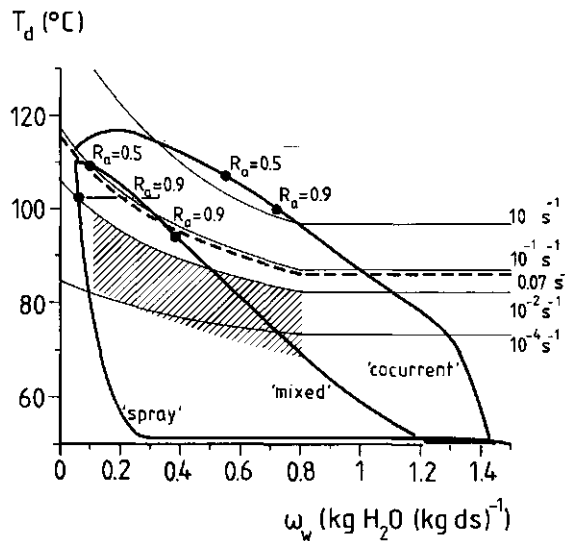
Figure 5.4   Inactivation constants and droplet temperature-water concentration histories. Initial conditions: see table 5.1; ——————: lines of constant values of the inactivation constant; — —: maximal inactivation constant $k_{e,\text{max}} = 0.07\,\text{s}^{-1}$; ——————— : droplet temperature-average water concentration history; see figure 5.2; ▨: range of experimental conditions used in the inactivation kinetics experiments of the thermo-unstable α-amylase. On the droplet 'temperature-water concentration' graphs it is indicated when the residual enzyme activities are 50 and 90 %, respectively.

combinations are higher than the estimated maximal inactivation constant of 0.07 s^{-1} (dotted line). This means that with the given experimental method no solution is available for this extrapolation problem.

To measure inactivation constants at higher temperatures than possible with the method used in this thesis, methodologies must be developed and applied which can estimate inactivation constants from inactivation kinetics experiments in which the characteristic time of the overall inactivation reaction equals the time of 99 % temperature equilibration within the inactivation cells. The methodology must include: a model which calculates the overall inactivation in an inactivation cell using a heat transfer model combined with an inactivation kinetics model and a non-linear optimisation method to estimate the parameters in the inactivation kinetics model, given experimental data.

Figures like figure 5.4 can be useful in evaluating inactivation kinetics experiments already performed and in planning subsequent experiments. It stresses the use of a cyclic method of collecting kinetic data. In such a method calculations based on a limited set of inactivation kinetics data are used to identify critical temperature-water concentration combinations and subsequently the appropriate inactivation kinetics experiments and experimental methodology.

5.4 SEGREGATION DURING SPRAY-DRYING

To examine the occurrence of segregation during spray-drying, model simulations are performed under 'spray-drying' like conditions using the estimated Maxwell-Stefan (MS) diffusion coefficients. In figure 5.5 the results of a model simulation are shown.

The calculated water concentration profiles show a similar behaviour as found in drying kinetics calculations using models as described in chapter 2. Very steep profiles at the onset of the drying process (penetration period), followed by a flattening of the profiles (regular regime period). The surface water concentration decreases very rapidly from the initial water concentration till the final moisture content (0 kg H_2O(kg ds)$^{-1}$ is this simulation), caused by the fact that internal mass transfer is the rate controlling mechanism. As can seen from the calculated ratio profiles, the extent to which segregation occurs under spray-drying conditions is less than that found for the simulated drying experiments (see figure 4.8b), the segregation at the surface is 0.94 kg p(kg s)$^{-1}$ and the 'penetration depth' is ≈ 15 μm. The penetration depth coincides with the steep water concentration profiles in the first stage of the drying process. After a drying time of about 3.5 s the ratio profile is 'fixed'.

water concentration
(kg H_2O (kg p)$^{-1}$)
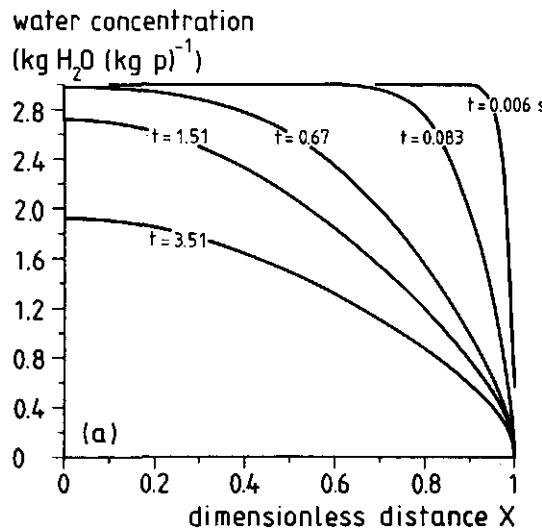
a   Water concentration profiles.
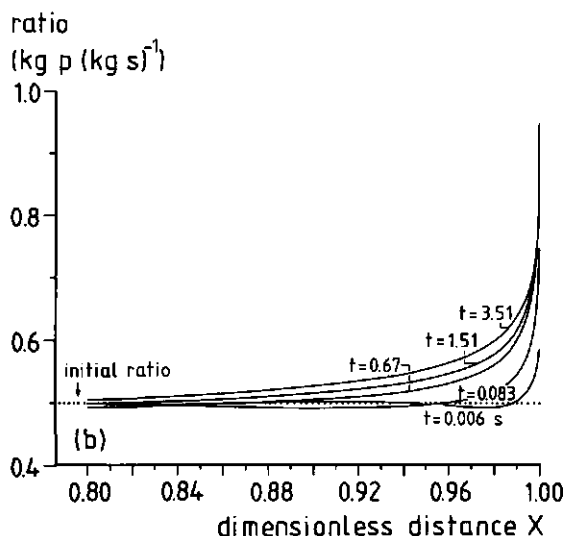
ratio
(kg p (kg s)$^{-1}$)

b   Ratio profiles.

Figure 5.5   Segregation during spray-drying. The initial layer thickness is 50 μm, the initial moisture content is 3 kg H_2O(kg ds)$^{-1}$, the initial ratio is 0.5 kg p(kg s)$^{-1}$ and the external mass transfer coefficient is 1 ms^{-1}. Physical data table 4.1.

The difference in ratio profiles between the drying experiments with the slabs and the 'spray-drying' model simulation is not caused by the different time scales, because the Fourier times are comparable. The main reason for the differences in ratio profiles is the difference in initial dry solids content (50 % on total basis (model simulation) versus 15.9 % (drying experiment)), or more precisely the differences in diffusion velocities due to the water concentration dependency of the MS diffusion coefficients. The value of D_{sp}^{MS} decreases much stronger with increasing solids content than the water mobility (D_{ws}^{MS} and D_{wp}^{MS}). As a consequence the characteristic time of the segregation process increases faster than the characteristic time of the drying process with increasing initial solids content. The 'overall' degree of segregation will therefore be limited at higher initial solid contents, as can be seen from table 5.2 also. The results shown in the figure 5.5 and table 5.2 indicate that segregation does occur during spray-drying, but the extent is dependent on the initial moisture content. The importance for the product quality will depend on the dry solids components involved and the applications aimed at, but effects are possible given the results in table 5.2.

Table 5.2.   Calculated surface ratios at different initial moisture contents. The surface ratio is given at an average moisture content of 0.2 kg H_2O(kg ds)$^{-1}$. The initial ratio is 0.5 kg p(kg s)$^{-1}$. Data see figure 5.5.

Initial moisture content (kg H_2O(kg ds)$^{-1}$)	Surface ratio (kg p(kg s)$^{-1}$)
4	1.41
2.33	1.27
1.5	1.08
1	0.94
0.67	0.81
0.43	0.68

5.5 CONCLUSIONS

The prevalent spray-air mixing pattern profoundly influences the residual enzyme activity. Dependent on the mixing pattern, the change in time of the inactivation constant is different and as a result the enzyme inactivation takes place at different water concentrations. General statements about the drying stage in which the inactivation of enzymes takes place are not possible. Calculations using 'idealised' mixing patterns can only be used to make first estimates of the influence of process conditions on residual enzyme activities.

The method used in the inactivation kinetics experiments is not appropriate to predict quality changes in drying processes in which the characteristic drying times are less than 15 s, like in spray-drying processes. The application of cyclic kinetic data collection methods, in which inactivation kinetics experiments are alternated by model simulations, makes the data collection more efficient and results in more accurate predictions.

Model simulations revealed that during spray-drying segregation will occur in the food model system, although to a lesser extent as found for the slab drying experiments. The calculated surface ratios of the dry solids components are dependent on the initial solids content. The extent of segregation can be controlled by applying different initial dry solids contents.

NOMENCLATURE

a	fitting parameter	-
a_w	water activity	-
$[B]$	matrix of MS diffusion coefficients	$m^2 s^{-1}$
Bi	Biot number	-
b	fitting parameter	-
C	concentration	$kg\ m^{-3}$, $mol\ m^{-3}$
C_t	molar density	$mol\ m^{-3}$
c	fitting parameter	-
C_d	drag coefficient	-
c_p	specific heat	$J\ kg^{-1}\ K$
D	diffusion coefficient	$m^2 s^{-1}$
$[E]$	matrix of transformed Maxwell-Stefan diffusion coefficients	$m^2 s^{-1}$
e	fitting parameter	-
d	diameter	m
d	fitting parameter	-
da	dry air	
ds	dry solids	
E_a	activation energy	$J\ mol^{-1}$
$E_{a,w}$	activation energy diffusion coefficient	$J\ mol^{-1}$
f	frequency	Hz
g	gravity constant	$m\ s^{-2}$
H	water concentration gas phase	$kg\ H_2O\ (kg\ da)^{-1}$
j_w	drying flux	$kg\ H_2O\ m^{-2}\ s^{-1}$
k_e	inactivation constant	s^{-1}
k_g	external mass transfer coefficient	$m\ s^{-1}$
k_∞	pre-exponential factor	s^{-1}
m	mass fraction	-
n	molar flux in stationary co-ordinate system	$mol\ m^{-2}\ s^{-1}$
Nu	Nusselt number	-
p	sodium caseinate	-

$[P]$	concentration transformation matrix	-
Pr	Prandtl number	-
R	general gas law constant	$J\ mol^{-1}\ K^{-1}$
R_a	residual enzyme activity	-
R_d	droplet radius	m
R_e	external radius	m
Re	Reynolds number	-
r	space co-ordinate	m
s	sucrose	-
Sc	Schmidt number	-
Sh	Sherwood number	-
T	temperature	°C, K
t	time	s
u	transformed concentration	-, $mol\ m^{-3}$
V	partial volume	$m^3\ kg^{-1}$, $m^3\ mol^{-1}$
v	velocity	$m\ s^{-1}$
X	dimensionless distance	-
x	mole fraction	-

- Greek

α_g	external heat transfer coefficient	$J\ s^{-1}\ m^{-2}\ K^{-1}$
$[\Gamma]$	matrix of thermodynamic factors	-
γ	thermodynamic activity coefficient	-
ΔH_v	heat of evaporation	$J\ kg^{-1}$
μ	chemical potential	$J\ mol^{-1}$
ρ	concentration gas phase	$kg\ m^{-3}$, $mol\ m^{-3}$
ρ	mass density	$kg\ m^{-3}$
σ	transformed space co-ordinate	kg, m
τ	characteristic time	s
Φ_m	mass flow	$kg\ s^{-1}$
ω_w	water concentration	$kg\ H_2O\ (kg\ ds)^{-1}$

- *Superscript*

i	interface
MS	Maxwell-Stefan
∞	at infinite dilute aqueous solution

- *Subscript*

0	initial
0	at zero moisture content
b	bulk phase
d	droplet
d	drying
ds	dry solids
e	enzyme
eff	effective
g	gas phase
h	heat transfer
i	interface
j	jet velocity
n	nozzle orifice
n	component n
m	maltodextrin
m	component m
max	maximal
p	sodium caseinate (protein)
r	reaction
s	sucrose
T	temperature
t	time
w	water
∞	at infinite dilute aqueous solution

REFERENCES

Alexander, K. (1983). Factors governing surface morphology in the spray drying of foods. PhD thesis, University of California, Berkeley.

Arrowsmith, A. and Foster, P.J. (1973). The motion of a stream of monosized liquid drops in air. Chem. Eng. J., 5, 243-50.

Bird, R.B. , Stewart, W.E. and Lightfoot, E.N. (1960). Transport phenomena, John Wiley & Sons Inc., New York.

Büttiker, R. (1978). Erzuegung von gleich grossen tropfen mit suspendierten und gelösten feststoff und deren trocknung im freien fall. PhD thesis, ETH Zürich, Switzerland.

Chandrasekaran, S.K. and King, C.J. (1972a). Multicomponent diffusion and vapour-liquid equilibria of dilute organic components in aqueous sugar solutions. AIChE J., 18, 513-20.

Chandrasekaran, S.K. and King, C.J. (1972b). Volatiles retention during drying of food liquids, AIChE J., 18, 520-6.

Charlesworth, P.H. and Marshall, W.R. (1960). Evaporation from drops containing dissolved solids. Part I and II. AIChE J., 6, 9-23.

Coumans, W.J. (1987). Power law diffusion in drying processes. PhD thesis, Technical University Eindhoven, The Netherlands.

Crowley, J.M. (1968). Lateral instability of a stream of charged droplets. Physics of Fluids, 11, 1372-74.

Cussler, E.J. (1976). Multicomponent Diffusion. Chemical Engineering Monographs, Vol 3, Elsevier, Amsterdam.

Daemen, A.L.H. (1981). The destruction of enzymes and bacteria during spray-drying of milk and whey. 1. The thermoresistance of some enzymes and bacteria in milk and whey with various total solids contents. Neth. Milk Dairy J., 35, 133-44.

Daemen, A.L.H. (1983). The destruction of enzymes and bacteria during spray-drying of milk and whey. 3. Analysis of the drying process according to the stages in which the destruction occurs. Neth. Milk Dairy J., 37, 213-28.

Daemen, A.L.H. and van der Stege, H.J. (1982). The destruction of enzymes and bacteria during spray-drying of milk and whey. 2. The effect of the drying conditions. Neth. Milk Dairy J., 36, 211-29.

Dunlop, P.J. and Gosting, L.J. (1957). Interacting flows in diffusion of the system raffinose-urea-water. J. Phys. Chem., 61, 1619-22.

Dunlop, P.J. and Gosting, L.J. (1964). Diffusion coefficients for one composition of the system water-sucrose-glycine. J. Phys. Chem., 68, 3874-76.

Ellerton, H.D. and Dunlop, P.J. (1967). Diffusion and frictional coefficients for four compositions of the system water-sucrose-mannitol at 25 °C. Tests of the Onsager reciprocal relation. J. Phys. Chem., 71, 1291-97.

El-Sayed, T.M. (1987). Development of particle morphology of drying drops. PhD thesis, University of California, Berkeley.

El-Sayed, T.M., Wallack, D.A. and King, C.J. (1990). Changes in particle morphology during drying of drops of carbohydrate solutions and food liquids. 1. Effects of composition and drying conditions. Industrial Engineering and Chemistry Research, 29, 2346-54.

Feather, M.S. and Harris, J.F. (1973). Dehydration reactions of carbohydrates. Adv. Carbohydr. Chem., 28, 161-224.

Ferrari, G., Meerdink, G. and Walstra, P. (1989). Drying kinetics for a single droplet of skim-milk. J. of Food Eng., 10, 215-30.

Flick D., Lenoir Ph., and Gibert, H. (1988). The drying of free falling droplets of concentrated skim-milk. In Proc. Sixth Int. Drying Symp., pp 471-78.

Fogarty, W.M. (1983). Microbial Amylases. In Microbial Enzymes and Biotechnology, ed. W.M. Fogarty, Applied Science Publishers, London, pp. 1-92.

Furuta, T., Tsujimoto, S., Makino, H., Okazaki, M. and Toei, R. (1984). Measurement of diffusion coefficient of water and ethanol in aqueuos maltodextrin solution. J. of Food Eng., 3, 169-86.

Furuta, T., Okazaki, M., and Toei, R. (1985). Flavour retention on drying of a single droplet under various drying conditions. In Drying '85, eds. R. Toei and A.S. Mujumdar, Hemisphere Publ. Corp., New York, pp 338-44.

Goulden, J.D.S. (1964). Analysis of milk fat by infra-red absorption. J. Dairy Res., 31, 273-84.

Greenwald, C.G. (1980). Particle morphology in the spray drying of foods. PhD thesis, University of California, Berkeley.

Hendricks, C.D. and Babil, S. (1972). Generation of uniform, 0.5-10 μm, solid particles. J. of Physics E: Scientific Instruments, 5, 905-10.

Hulst, A.C., Tramper, J., van 't Riet, K. and Westerbeek, J.M.M. (1985). A new technique for the production of immobilized biocatalysts in large quantities. Biotechnol. Bioeng., 27, 870-76.

Hunik, J.H. and Tramper, J. (1993). Large-scale production of κ-carrageenan droplets for gel bead production. Biotechn. Prog., 9, 186-92.

Iglesias, H.A. and Chirife, J. (1982). Handbook of Food Isotherms. Academic Press, New York.

Kerkhof, P.J.A.M. (1975). A quantitative study on the effect of process variables on the retention of volatile trace components in drying. PhD thesis, Technical University Eindhoven, The Netherlands.

Kerkhof, P.J.A.M. (1985), personal communication.

Kerkhof, P.J.A.M. and Coumans, W.J. (1990). Drying of foods: transferring inside insights to outside outlooks. Paper presented at the 7th Int. Drying Symp., Praque.

Kerkhof, P.J.A.M. and Schoeber, W.J.A.H. (1974). Theoretical modelling of the drying behaviour of droplets in spray-driers. In Advances in Preconcentration and Dehydration of Foods, ed. A. Spicer, Applied Science Publishers, London, pp. 349-97.

Krishna, R. and Taylor, R. (1986). Multicomponent mass transfer: theory and applications. In Handbook of heat and mass transfer, ed. N.P. Chereminisoff, Vol. 2, Gulf Publishing Corp., Houston, pp 260-424.

Lapidus, L. and Pinder, G.F. (1982). Numerical solution of partial differential equations in science and engineering. Wiley-Interscience, New York, pp 149-62.

Lefebvre, A.H. (1988). Atomization and sprays. Hemisphere Publishing Corporation, New York.

Lijn, J. van der (1976). Simulation of heat and mass transfer in spray-drying. PhD thesis, Wageningen Agricultural University, The Netherlands.

Liou, J.K. (1982). An approximate method for nonlinear diffusion applied to enzyme inactivation during drying. PhD thesis, Wageningen Agricultural University, The Netherlands.

Livesly, D.M., Gillespie, R.F., Veoman, M.L., Oakley, D.E., Elhaus, B., Ranpuria, C.K., Taylor, T. and Wood, W. (1992). Development and validation of a computational model for spray-gas mixing in spray-dryers. In Drying '92, ed. A.S. Mujumdar, Elsevier, Amsterdam, pp 407-16.

Loncin, M. (1980). Diffusion phenomena in solids. In Conference Proc. 2nd Int. Congress on Eng. and Food, eds. P. Linko *et al.*, Applied Science Publishers, London, pp 354-63.

Luikov, A. (1968). Analytical heat diffusion theory. Academic Press, London.

Luyben, K.Ch.A.M., Liou, J.K., and Bruin, S. (1982). Enzyme degradation during drying. Biotechnol. and Bioeng., 24, 533-52.

Luyben, K.Ch.A.M., Olieman, J.J. and Bruin, S. (1980). Concentration dependent diffusion coefficients derived from experimental drying curves. In Proc. 2nd Int. Symp. on Drying, Montreal, pp 233-43.

Menting, L.C. (1970) Diffusion coefficient of water and organic volatiles in carbohydrate-water systems. J. Food Technol., 5, 111-26.

Press, W.H., Flannery, B.P., Teukolsky, S.A. and Vetterling, W.T. (1989). Numerical recipes in pascal. Cambridge Univ. Press.

Ranz, W.E. and Marshall, W.R. (1952). Evaporation from drops. Part I and II. Chem. Eng. Progr., 48, 141-6, 173-80.

Riede, T.T. and Schlünder E.U. (1988). Evaporation and pervaporation of a binary mixture from an inert carrier liquid. Chem. Eng. Technol., 11, 384-91.

Sano, Y. and Keey, R.B. (1982). The drying of a spherical particle containing colloidal material into a hollow sphere. Chem. Eng. Sci., 37, 881-9.

Schoeber, W.J.A.M. (1976). Regular regimes in sorption processes. PhD thesis, Technical University Eindhoven, The Netherlands.

Toei, R., Okazaki M. and Furuta, T. (1978). Drying of a non-supported droplet. In Proc. 1st Int. Drying Symp., Montreal, pp 53-8.

Tong, D.H. and Lund, D.B. (1990). The effective moisture diffusivity in porous materials as a function of temperature and moisture content. Biotechnol. Prog., 6, 67-75.

Tomazic, S.J. and Klibanov, A.M. (1988a). Mechanisms of irreversible thermal inactivation of bacillus α-amylase. J. Biol. Chem., 263, 3086-91.

Tomazic, S.J. and Klibanov, A.M. (1988b). Why is one bacillus α-amylase more resistant against irreversible thermo-inactivation than another? J. Biol. Chem., 263, 3092-6.

Toor, H.L. (1964). Solution of the linearized equations of multicomponent mass transfer: I. AIChE J., 10, 448-55.

Toor, H.L. (1964). Solution of the linearized equations of multicomponent mass transfer: II. Matrix methods. AIChE J., 10, 460-65.

Trommelen, A.M. and Crosby, E.J. (1970). Evaporation and drying of drops in superheated vapors. AIChE J., 16, 857-67.

Verhey, J.P.G. (1973). Vacuole formation in spray powder particles. 3. Atomization and droplet drying. Neth. Milk Dairy J., 27, 3-18.

Verhey, J.P.G. (1972). Vacuole formation in spray powder particles. 2. Location and prevention of air incorporation. Neth. Milk Dairy J., 26, 203-24.

Violet, M. and Meunier, J. (1989). Kinetic study of the irreversible thermal denaturation of *Bacillus licheniformis* α-amylase. Biochem. J., 263, 665-70.

Wallack, D.A. (1988). Stickiness and morphological development during drying of drops. PhD thesis, University of California, Berkeley.

Wallack, D.A., El-Sayed, T.M. and King, C.J. (1990). Changes in particle morphology during drying of drops of carbohydrate solutions and food liquids. 2. Effects on drying rate. Industrial Engineering and Chemistry Research, 29, 2354-57.

Walstra, P. and Jennes, R. (1984). Dairy Chemistry and Physics. John Wiley, New York, pp 304.

Wesselingh, J.A. and Krishna, R. (1990). Mass transfer. Ellis Horwood, Chichester, England.

Wijlhuizen, A.E., Kerkhof, P.J.A.M. and Bruin, S. (1979). Theoretical study of the inactivation of phosphatase during spray-drying of skim-milk. Chem. Eng. Sci., 34, 651-60.

Yamamoto, S., Agawa, M., Nakano, H. and Sano, Y. (1985). Enzyme inactivation during drying of a single droplet. In drying '85, eds. R. Toei and A.S. Mujumdar. Hemisphere, Washington, pp 330-7.

Yamamoto, S. and Sano, Y. (1992). Drying of enzymes: the enzyme retention during drying of a single droplet. Chem. Eng. Sci., 47, 177-83.

Zimmerman, K. (1987). Einflussparameter und mathematisch modellierung der schonende trocknung von starterkulturen. Fortschr.-Ber., VDI Reihe 14, Nr. 36, VDI, Dusseldorf.

SUMMARY

The spray-drying of liquid foods is an important unit operation in the food industry. In spray-dryers the fluid is atomised and brought into contact with hot air. Spray-dryers are mostly operated in the food industry in the co-current mode to avoid heat deterioration of the drying product. 'Overall' dryer models are still in the first stage of development, despite the importance of spray-drying. These models can be used to improve design and performance of the dryer. Essential parts of such 'overall' models are models that predict the drying kinetics of droplets and the final product quality.

In recent years a model has been developed which describes the drying kinetics of liquid food droplets. The model is based on the effective diffusion coefficient concept and it assumes that a liquid food can be considered as a binary system, with water and dry solids as the two components. This drying model can be integrated with a reaction kinetics model to predict the (bio-) chemical product quality. To validate the drying model experimental conditions are used in literature which are very different from conditions during spray-drying.

The aims of the research described in this thesis are: (1) to validate the existing droplet drying kinetics model under spray-drying conditions, (2) to investigate the possibility to predict a (bio-) chemical product quality change during spray-drying, and (3) to examine the validity of the assumption that a drying liquid food droplet can be considered as a binary system. In that case segregation of the dissolved dry solids components does not occur. To reach these goals the droplet drying kinetics model has to be extended to include reaction rates and multicomponent diffusion.

A specially designed drying apparatus has been developed to perform droplet drying experiments under spray-drying conditions. This equipment consists of two main parts: a resonance nozzle and a drying tower. The resonance nozzle is capable of producing small equally sized (uniform) droplets. The drying tower is designed in such a way that the drying conditions are uniform and comparable with spray-drying conditions.

The droplet drying experiments are performed on two levels, on the level of 'large' suspended droplets $(d_d \approx 1\,\text{cm})$ and on the level of 'small' free falling droplets $(d_d \approx 0.02\,\text{cm})$. The experiments with the free falling droplets are performed in the drying tower. The droplet drying kinetics experiments are performed with maltodextrin solutions and skim-milk.

The inactivation of the enzyme α-amylase during drying is studied as an example of a biochemical product quality parameter. The activity of enzymes can be reduced significantly during drying. Maltodextrin is used as support material. To predict the inactivation of α-amylase during drying, the thermal inactivation kinetics is determined at different water concentrations. The inactivation kinetics of two α-amylases, which differ in thermostability, is determined because of the large difference in the characteristic drying times of the droplet drying experiments. The inactivation rate decreases at low water concentrations. The inactivation kinetics can be described by a simple first order Arrhenius-type model.

In the suspended droplet experiments the change in time of the water concentration and the droplet temperature as well as the residual α-amylase activity is measured. The measured values are compared with model simulations, and a good agreement is found.

In the free falling droplets experiments the change of the water concentration as well as of the residual α-amylase activity is measured as function of the falling distance. Comparison of model simulations with experimental data reveals that the drying rate as well as the inactivation rate is overestimated. In the model simulations it is assumed that the air condition inside the spray equals the air condition outside the spray. Air temperature measurements show that this assumption is not valid. Simulations with an adapted droplet drying model result in an improved description of the drying rate as well as of the inactivation rate.

Slab drying experiments with a ternary food model system (water, sucrose and sodium caseinate) are performed to test the assumption that liquid foods can be considered as binary systems. The concentration profiles of the different components are measured and it is determined that segregation of the solutes can occur during drying. The ratio of the sodium caseinate and sucrose concentrations near the surface increases, in the centre of the slab the ratio decreases. This phenomenon is caused by the large difference in the diffusivities of both solutes. To describe this segregation a ternary drying model is developed. This model is based on the generalised Maxwell-Stefan equations. A good agreement is found between model simulations and experimental data. The diffusion coefficients used in the model simulations are estimated from the drying experiments.

To examine the effect of the droplet spray-air mixing pattern in a spray-dryer on the residual enzyme activity, model simulations are performed using different 'idealised' spray-air mixing patterns. The results reveal that the residual enzyme activity is strongly influenced by the prevalent spray-air mixing pattern in the spray-dryer. Model simulations using the ternary drying model show that also during spray-drying segregation of solutes can be expected, however, the extent is strongly influenced by the initial dry solids content. A higher initial dry solids content results in less segregation.

SAMENVATTING

Het sproeidrogen van vloeibare levensmiddelen is een belangrijke bewerking in de levensmiddelenindustrie. In een sproeidroger wordt vloeistof verneveld en met hete lucht in contact gebracht. De droger wordt meestal in meestroom bedreven om hittebeschadiging van het produkt te voorkomen. Modellen die het gehele sproeidroogproces beschrijven zijn, ondanks het belang van sproeidrogen, nog in ontwikkeling. Dergelijke modellen kunnen worden toegepast om het ontwerp en de bedrijfsvoering van de droger te verbeteren. Essentiële onderdelen van een sproeidroogmodel zijn modellen die de droogkinetiek van druppels en de resulterende produktkwaliteit voorspellen.

In het recente verleden is een model ontwikkeld dat de droogkinetiek van druppels beschrijft. Het model veronderstelt dat een vloeibaar levensmiddel kan worden opgevat als een binair systeem met als componenten water en vaste stof. Tevens wordt aangenomen dat het interne watertransport kan worden beschreven met een 'effectieve' diffusiecoëfficiënt. Dit model kan worden geïntegreerd met reactiekinetiek-modellen om de (bio-) chemische produktkwaliteit te voorspellen. In experimenten om het droogkinetiekmodel te verifiëren zijn in de literatuur omstandigheden gebruikt die sterk verschillen van de condities tijdens sproeidrogen.

De doeleinden van het in dit proefschrift beschreven onderzoek zijn: (1) valideren van het bestaande droogkinetiekmodel voor druppels onder sproeidroog-omstandigheden, (2) nagaan of het mogelijk is om de verandering van (bio-) chemische produktkwaliteit tijdens sproeidrogen te voorspellen, en (3) onderzoeken of de veronderstelling terecht is dat een drogend vloeibaar levensmiddel opgevat kan worden als een binair systeem; ontmenging van de vaste-stof-componenten zal dan niet plaatsvinden. Om deze doeleinden te bereiken moet het droogkinetiekmodel worden uitgebreid met zowel reactiekinetiekmodellen als multicomponentdiffusie.

Er is een droogapparaat ontwikkeld om droogexperimenten te kunnen uitvoeren met druppels onder sproeidroog-omstandigheden. Het apparaat bestaat uit een tweetal hoofdonderdelen: een resonantie-verstuiver en een droogtoren. De resonantie-verstuiver is in staat om kleine druppels van gelijke grootte te produceren. De droogtoren is zodanig ontworpen dat de droogcondities overal gelijk zijn en te vergelijken zijn met de condities bij sproeidrogen.

De droogexperimenten met de druppels zijn zowel uitgevoerd met 'grote' druppels (diameter is 1 cm) als met 'kleine' druppels (diameter is 0.02 cm). De experimenten met de 'kleine' druppels zijn uitgevoerd in de droogtoren. Maltodextrine oplossingen en magere melk zijn gebruikt als modelmateriaal.

De activiteit van het enzym α-amylase is gebruikt als voorbeeld van een biochemische kwaliteitsparameter. De activiteit van enzymen kan sterk afnemen tijdens drogen. Maltodextrine is gebruikt als dragermateriaal. Om de restactiviteit van α-amylase na drogen te kunnen voorspellen, is de thermische inactiveringskinetiek bepaald bij verschillende vochtgehalten. De inactiveringssnelheid neemt af bij lage waterconcentraties. De inactiveringskinetiek kan worden beschreven door een eerste-orde-model. De temperatuur- en vochtafhankelijkheid van de inactiveringsconstante is gemodelleerd met behulp van een Arrhenius-achtige vergelijking.

In de experimenten met de 'grote' druppels zijn tijdens het droogproces het watergehalte, de druppeltemperatuur en de resterende α-amylase-activiteit gemeten. De gemeten waarden zijn vergeleken met modelsimulaties, en een goede overeenstemming is gevonden.

In de experimenten met de 'kleine' druppels is de waterconcentratie en de resterende α-amylase-activiteit gemeten bij verschillende valafstanden. Vergelijking van modelsimulaties met experimentele waarden laat zien dat zowel de droog- als de inactiveringsnelheid wordt overschat. In de modelsimulaties wordt verondersteld dat de luchtcondities in de druppelnevel gelijk zijn aan de luchtcondities buiten de druppelnevel. Metingen van de luchttemperatuur laten zien dat die aanname niet terecht is. Simulaties met een aangepast droogmodel geven een betere beschrijving van zowel de droogkinetiek als de enzym-inactivering.

Droogexperimenten met laagjes, bestaande uit een waterige oplossing van saccharose en natriumcaseïnaat, zijn uitgevoerd om na te gaan of vloeibare levensmiddelen beschouwd kunnen worden als binaire systemen. De concentratieprofielen van de verschillende componenten zijn gemeten en het blijkt dat ontmenging van vaste-stof-componenten kan optreden tijdens drogen. De verhouding tussen de natriumcaseïnaat- en saccharoseconcentratie neemt toe aan het oppervlak, en neemt af in het midden van de laag. Dit verschijnsel wordt veroorzaakt doordat de diffusiecoëfficiënten van beide componenten sterk verschillen. Er is een ternair droogmodel ontwikkeld om deze ontmenging te beschrijven. Het model is gebaseerd op de algemene Maxwell-Stefan-vergelijkingen. Het model blijkt in staat te zijn om de experimentele concentratieprofielen goed te beschrijven. De in het model gebruikte diffusiecoëfficiënten zijn geschat met behulp van de resultaten van de droogexperimenten.

Gegeven het ontwerp van een sproeitoren zal de druppelnevel na verstuiving op een bepaalde wijze worden opgemend met de drooglucht. De invloed daarvan op de enzymactiviteit na sproeidrogen is door het uitvoeren van modelsimulaties nagegaan. De resultaten laten zien dat de restactiviteit sterk wordt beïnvloed door het type mengpatroon. Modelsimulaties met het ternaire droogmodel geven aan dat ontmenging ook kan optreden tijdens sproeidrogen. De mate van ontmenging is echter afhankelijk van het beginvochtgehalte; hoe lager het beginvochtgehalte, des te minder ontmenging.

Curriculum vitae

Gerrit Meerdink werd op 2 november 1954 te Winterswijk geboren. Hij behaalde in 1972 het diploma HBS-B. In hetzelfde jaar begon hij aan zijn studie Chemische Technologie aan de Universiteit Twente. Deze studie werd in 1979 met het afleggen van het ingenieursexamen afgerond. Vanaf 1 augustus 1980 tot en met september 1982 was hij werkzaam bij de Vakgroep Proces- en milieubeheer van de Universiteit Twente. Op 1 januari 1983 trad hij in dienst bij de Sectie Proceskunde van de Landbouwuniversiteit Wageningen, eerst als promovendus en vanaf 1986 als universitair docent.